Fault Diagnostics and Fault Tolerant Control of Microgrid

Ebrahim Shahzad

Registration No.84-FET/PhDEE/S15

Supervisor

Dr. Adnan Umar Khan

Department of Electrical and Computer Engineering,

Faculty of Engineering and Technology,

International Islamic University,

Islamabad, Pakistan.

Microgrid - Engineering
Fault Diagnostics
Fault Tolerant computing - Programming
Software engineering

CERTIFICATE OF APPROVAL

Title of Thesis:" Fault Diagnostics and Fault Tolerant Control of Microgrid"

Name of Student: Ebrahim Shehzad

Registration No: 84-FET/PHDEE/S15

Accepted by the Department of Electrical Engineering, Faculty of Engineering and Technology, International Islamic University, Islamabad, in partial fulfillment of the requirements for the Doctor of Philosophy degree in Electronic Engineering.

Viva voce committee:

Dr. Adnan Umar Khan (Supervisor)
Assistant Professor,
DECE,FET, IIUI

Prof. Dr. Muhammad Amir (Internal)
Assistant Professor,
DECE, FET, IIUI.

Dr. Noaman Ahmed Khan (External -I)
Associate Professor/Chairman,
DECE,Sir Syed CASE, Institute of Technology,
Islamabad.

Dr. Hammad Omer (External -II)
Associate Professor
DECE, COMSATS University, Islamabad.

Dr. Shahid Ikram (Chairman)
Chairman, DECE, FET, IIUI.

Prof. Dr. Nadeem Ahmed Shaikh (Dean)
Professor /Dean
FET, IIUI.

August 25, 2023

Declaration

I, *Ebrahim Shahzad* declare that this thesis titled "Fault Diagnostics and Fault Tolerant Control of Microgrid" and the work presented in it are my own and has been generated by me as a result of my own original research.

I confirm that:

1. This work was done wholly or mainly while in candidature for a Ph.D. degree at IIUI

2. Where any part of this thesis has previously been submitted for a degree or any other qualification at IIUI or any other institution, this has been clearly stated

3. Where I have consulted the published work of others, this is always clearly attributed

4. Where I have quoted from the work of others, the source is always given. With the exception of such quotations, this thesis is entirely my own work

5. I have acknowledged all main sources of help

6. Where the thesis is based on work done by myself jointly with others, I have made clear exactly what was done by others and what I have contributed myself

Ebrahim Shahzad,

84-FET/PhDEE/S15

Copyright Notice

- Copyright in the text of this thesis rests with the student author. Copies (by any process) either in full or of extracts, may be made only in accordance with instructions given by the author and lodged in the Library of FET, IIUI. Details may be obtained by the Librarian. This page must form part of any such copies made. Further copies (by any process) may not be made without the permission (in writing) of the author.

- The ownership of any intellectual property rights that may be described in this thesis is vested in FET, IIUI, subject to any prior agreement to the contrary, and may not be made available for use by third parties without the written permission of FET, which will prescribe the terms and conditions of any such agreement.

- Further information on the conditions under which disclosures and exploitation may take place is available from the Library of FET, IIUI, Islamabad.

List of publications

Journal papers

1. **Shahzad, E.**, Khan, A. U., Iqbal, M., Saeed, A., Hafeez, G., Waseem, A., ... Ullah, Z. (2022). Sensor Fault-Tolerant Control of Microgrid Using Robust Sliding-Mode Observer. Sensors, 22(7), 2524.

2. **Shahzad, E.**, Khan, A. U., Iqbal, M., Albalawi, F., Khan, M. A., Saeed, A., Ghoneim, S. S. (2022). Fault Diagnostics and Tolerance Analysis of a Microgrid System Using Hamilton–Jacobi–Isaacs Equation and Game Theoretic Estimations in Sliding Mode Observers. Sensors, 22(4), 1597.

This thesis is dedicated to *my beloved Prophet Muhammad (saw),*

my parents and my teachers

Abstract

This study investigates sensor fault diagnostics and fault-tolerant control (based on observer-based fault estimation) for a voltage source converter-based microgrid (model) using a sliding-mode observer. It provides the diagnosis of multiple faults (i.e., magnitude, phase, and harmonics) occurring simultaneously or individually in current/potential transformers. A modified algorithm based on convex optimization is used to determine the gains of the sliding-mode observer. The algorithm utilizes the feasibility optimization or trace minimization of Ricatti equation-based modification of H-Infinity (H_∞) constrained linear matrix inequalities, which are obtained from negative/semi-negative definitely constrained vector Lyapunov equation. The stability and finite-time reachability of the observers are presented for the considered faulty and perturbed microgrid system using the Lyapunov theory.

Further, the work is extended for robustness and sensitivity analysis for sensor fault diagnosis and fault-tolerant control. It uses robust control parameters such as minimum sensitivity parameter ($H-$), maximum robustness attenuation parameter (H_∞), and both

criteria considered together ($H-/H_{\infty}$), being incorporated in the sliding mode observer theory, using the game theoretic saddle point estimation, achieved through convex optimization of constrained LMIs. The approach used works in a way that the mentioned robust control parameters are embedded in Hamilton–Jacobi–Isaacs-Equation (HJIE) by determination of the inequality version of HJIE through the respective cost functional. It gives linear matrix inequalities (LMIs), which are optimized using iterative convex optimization algorithms to give optimal sliding mode observer gains enhanced with robustness to maximal preset values of disturbances and sensitivity to detection of minimal preset values of faults.

Moreover, the fault and disturbance estimation method is modified and improved with some corrections in previous works. The stability analysis for the extended diagnostic analysis approach is presented by negative definiteness of the same inequality version of HJIE.

A proportional-integral (PI) based control is utilized for the conventional regulations required for frequency and voltage sags occurring in a microgrid. However, the same control block features fault-tolerant control (FTC) functionality, which is attained by reconstructed sensors' (transformers') faults using the sliding-mode observer, being fed to the control block after correction. Simulation-based analysis is performed by presenting the results of state/output estimation, state/output estimation errors, fault reconstruction, estimated disturbances, and fault-tolerant control performance. Simulations

are performed for sinusoidal, constant, linearly increasing, intermittent, saw-tooth, and random sorts of often occurring sensor faults. The comparison analysis is performed in terms of observer gains being estimated by previously used techniques as compared to the proposed modified approach. It also includes the comparison of the voltage-frequency control implemented with and without the incorporation of the used observer-based fault estimation and corrections, in the control block. The faults here are considered for voltage/current sensor transformers, but the approach works for a wide range of sensors.

Keywords: *microgrids, fault-tolerant control, fault diagnosis and estimation, sliding mode observers (SMO), current/potential transformer (C.T/P.T, H_∞ and $H-$ parameters, Hamilton–Jacobi–Isaacs/Bellman-Equation (HJIE or HJBE); PI control, Lyapunov stability, robust control: game theory, linear matrix inequalities*

Acknowledgments

All praise be to Allah, and peace and mercy of Allah on Prophet Muhammad (saw). I pay my humble gratitude to my respected (late) professor Dr. I. M. Qureshi with whom I stayed as a research student from 2011-2021. He was like a father and a moral and spiritual mentor for all his students. He inspired me the most as a teacher in my educational career and he has a deep impact on my various teaching methodologies. He gave us a diverse insight into so many research subjects, and I can say that, whatever I have learned regarding research, I have learned from him. Even before three months of his death, he arranged some core lectures of control theory for our research group and other interested students, which I believe, would benefit us for quite a long time. I am very thankful to my supervisor, Dr. Adnan Umar Khan, who gave me enough room to speak out my research problems even for hours and then always sent me a solution. I would say that whenever I got stuck at some point, he called me himself and gave me a new start with a motivation and way out. Dr. Adnan Umar Khan helped me in the proper understanding of the considered power system, that is, the microgrid and its all

associated things. I am also very thankful to Dr. Muhammad Iqbal Khan, who also co-advised this work. His insight into control theory and listening to research problems and pieces of advice also led me towards some innovative works. Dr. Abdul Basit has guided me with the best possible advice and helped throughout this period in the research tasks and methodologies. Dr Jawwad Ali Shah helped me morally and also arranged research funding from the University of Malaysia for which I am very much thankful to him. I have had a long journey with my research buddy and dearest friend Ahmad Saeed, who is a key member of the research group working on Power Control and we have always stayed together. He has not only helped me to solve and understand my research problems but was always there for me by all his means, providing me with vent for psychological catharsis and emotional support in research and other life problems. My friend and brother Dr Khalid Ibrahim always showed very positive and sincere concerns in giving good pieces of advice and very beneficial guidance to get our works published in reputable journals. I am thankful to Dr Athar Waseem and Dr Atiq Ullah Khan from Hi-Tech University Taxila for helping us in getting the research funding from the University of Taif. My friend and brother Cdr Zunnurain Baig have also accompanied me in the research journey, and being one of my best friends stayed available for all sorts of support. I have learned a lot from the soft and purely research-oriented learning trend of Brother Ahmad Saleem in my Ph.D. research lab. I have learned so many things from Brother Umar Naseer in the FET faculty with his very deep understanding

of human sciences besides his scientific knowledge. Mr Imran Iftkhar in the chairman's office had always been very supportive and friendly in all official and clerical works. Dr Wasim Khan also supported me emotionally with his very soft nature. Mr Laeeq Aslam Sandhu not only helped me in my research work but to life took me out of so many conflicting thoughts and set good practical tasks to be achieved in ractical tasks to be achieved in the future works. I have no words to express my immense gratitude to my grandmother, parents, and brothers who have supported me in very difficult situations by all means. I would say that I could achieve this goal only due to their sincere prayers and endless support. My wife also had a hard time with all my hectic routines and I confess and apologize to my wife and children who have suffered the most.

Contents

List of Figures

List of Tables

List of Abbreviations and Symbols

Abbreviations

BMI	Bi-linear Matrix Inequality
CT	Current Transformer
DE	Differential Equation
DG	Distributed Generator
FAR	False Alarm Ratio
FDR	False Detection Ratio
FD	Fault Detection/Diagnostics
FDI	Fault-Diagnostics-Isolation
FE	Fault Estimation

FTC	Fault-Tolerant Control
GA	Genetic Algorithm
HJIE	Hamilton-Jacobi-Issacs Equation
ILMI	Iterative Linear Matrix Inequalities
inf/sup	Infemum/Supremum
LCL	Inductor Capacitor Inductor
LHP/RHP	Left/Right Half Plane
LMI	Linear Matrix Inequality
LPV	Linear Parameter Varying
LQG	Linear Quadratic Gaussian
LQR	Linear Quadratic Regulator
LQR	Linear Quadratic Regulator
LTV	Linear Time Varying
LTI	Linear Time Varying
MG	Microgrid
MPC	Model Predictive Control

MRAC	Model Reference Adaptive Control
NMI	Non-linear Matrix Inequality
PD	Positive Definite
PI	Proportional-Integral
PID	Proportional-Integral-Differentiator
PLL	Phase Locked Loop
PSO	Particle Swarm Optimization
PT	Potential Transformer
PV	Photo-voltaic
RSMO	Robust Sliding Mode Observer
SMC	Sliding Mode Control
SMO	Sliding Mode Observer
SVPWM	Space Vector Pulse width Modulation
UPS	Un-interrupted Power Supply
VSC	Voltage Source Converter
WES	Wind Energy System

Symbols

α	H-Infinity Coefficient Fault upper bound (in Chapter 5)
α	H-Infinity Coefficient / Fault upper bound (in Chapter 6)
β	Estimatd Fault Scaling factor
β'	H- Coefficient
ξ	Disturbance
ξ_o	Disturbance upper bound
f	Fault
f_o	Fault upper bound
$H-$	H- Norm
$H\infty$	H-Infinity Norm
$\sigma(.)$	Sliding surface
S_f	Estimated fault Scaling factor
T_R	Reachability Time
ψ	Discontinuous Term of Sliding-Mode Observer
$\omega_p LL$	Phase Locked Loop Frequency

γ	Discontinuous Term gain
λ_{min}	Minimum Eigen Value

CHAPTER 1

Introduction

1.1 Smart Grids/Green and Bidirectional Energy

The distributed renewable energy sources featured with bi-directional power transmission can/will now potentially replace the energy produced by fossils being green and environment-friendly energy. These non-conventional sources belong to the natural cycles and there is no alarm or fear of these resources being depleted out. They will not only convene the consumers in monetary terms but will also ensure better-controlled power availability to domestic/industrial sectors in general. Moreover, the conventional consumer side will more dynamically serve as both the consumers and producers at the same time. The consumers' side primarily will be on required power demand when there is a shortfall on its end, and contrarily, if there is an availability of surplus energy, it can either be provided to the utility grid or other consumers or may be consumed in

heating requirements. In this way, different consumers in different distributed infrastructures can compensate for the shortfall directly connected to each other or through the utility grid. All the modules are parts of a bigger smart grid infrastructure/system. The concept diagram is shown in Figure 1.1 [1]. [1]

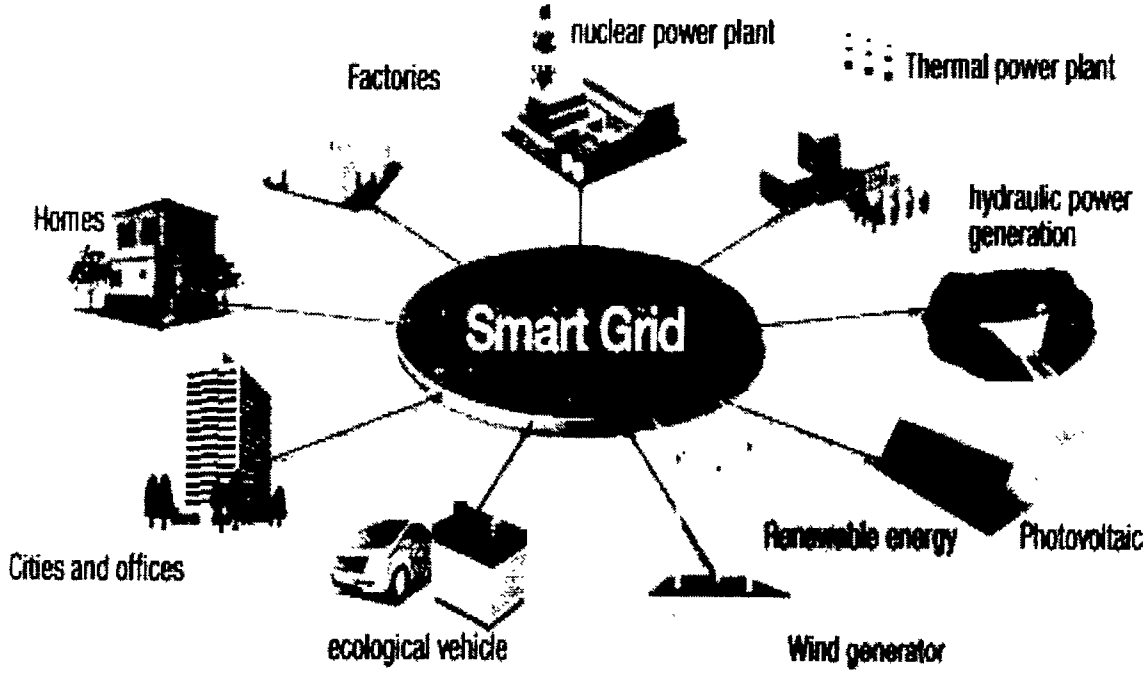

Figure 1.1: Smart Grid Concept Diagram [1]

1.2 Background and Problem Statement

The AC and DC microgrids are emerging and next-generation distributed power sources, however, the systems are still vulnerable to uncertainties due to various natural factors. It is always required for the physical systems to provide reliable working in extreme conditions, staying robust to faults, disturbances, and uncertainties and being conducive

[1]The introductory chapter is a general overview of the dissertation

in fault-tolerance. This work has mainly benefited from the mathematical infrastructure of [2] and extended the works of Edwards [3], Dhahri [4], and Tan [5], however, problem and approach is inspired by a conference paper in 2016 [6], which considers voltage/current transformer fault in VSC based AC microgrid, using the sliding mode observers.The microgrids are connected in multi-terminal networks which are required to be thoroughly analyzed for system integration, dynamic behavior, fault behavior, and power-flow control [7]. The Smart Grid consists of flexible "Micro Grids", which turn into a "Super Grid" with Power/Energy Highways and are suitable for secure and sustainable access to renewable energy resources such as solar, hydro, and wind. This study considers the dynamic behavior of microgrids in the fault conditions. The considered faults (in this study) are sensor faults occurring in a microgrid, which will cause sensing of faulty readings, and hence would disturb the control mechanism as a whole due to tracking of faulty readings by the converter, which will cause voltage and frequency sags and possibly various other faults such as overloads, short circuits and total system failure/shutdown. The considered sensors are current/potential transformers, which undergo saturation very often, causing hysteresis/impedance loading, etc. The faults appear as a composite effect of magnitude faults, frequency shifts, and harmonics, which is through a multiplicative effect but may be considered as additive faults and disturbances in the system output values.

1.3 Research Objectives

1) Grid-tied inverter constituting an AC microgrid, is considered to give optimized performance, in the presence of a sensor (current/potential transformer faults), which works for both the islanded and grid-tied modes. It is required to provide its working as a fault-tolerant module connected in the assembly of smart (micro/super) HVAC grids. 2) The task is to design novel robust observers for faults' diagnostics for stable working of voltage source converter-based microgrid. The task will require a reliable mathematical model of microgrids. A supervisory fault-tolerant controller along with the conventional voltage-frequency regulation will also be designed on the grid level, taking the real-time data from various modules and local controllers to perform reliable online fault-tolerant actions. 3) The systems observers and controllers will be tested on MATLAB SIMULINK Power-Sim Tool Box.

1.4 Contribution of the Thesis

In the article I [8] which is the base work, the study focuses on designing a sensor FTC mechanism applicable at both the primary and secondary levels with reference to hierarchical MG control [9] strategy. The FTC strategy uses the robust sliding-mode observer (RSMO) theory to be utilized for the detection and estimation of sensor faults

of a distributed MG unit operating in an autonomous mode of operation, using a reliably simulated and experimentally verified mathematical model of the MG. The considered system has one current transformer (C.T) and a potential transformer (P.T), but it is easily scalable for multiple and redundant sensor sources (transformers), which can be utilized for enhanced security and reliability. The online fault estimation-based fault tolerance approach is quite general and can be extended to many types of systems by choosing the suitable observer/controller parameters discussed in this paper. The main contributions of this study are:

- We have presented an improved method, as it is capable of dealing with either one or both faulty sensors (transformers) with sinusoidal additive faults (composite of magnitude, phase, and harmonics). Earlier work was performed only for magnitude faults in the current transformer in [6].

- Algorithm for determination of SMO gains is modified and improved by using Ricatti-equation-based modification of H_∞ enhanced LMIs, i.e., the combination of approaches represented by Edwards [5], [4], which enhances the robustness of SMO in fault diagnosis and reconstruction. The method for the mentioned approach is discussed in Theorem 5.2. The comparisons for results produced with SMO gains determined by proposed technique to those determined by earlier/base works (being used in this study), are also presented.

- Fault estimation procedure is modified and contains some factors which were mistakenly missing in reduced order state error equations of earlier works such as [3]. The method also incorporates a numerical solution of the DE for reduced order state error estimation. The mentioned approach is worked in Corollary 7.1.

- Disturbances being unknown inputs are also accurately estimated for all fault types considered in the system. The modified fault estimation method gives very accurate disturbance/unknown inputs estimation as shown in Corollary 7.1.

- Lyapunov stability analysis of SMO with considered additive faults and disturbances for the considered microgrid system is presented, as shown in Proposition 1.

- Reachability of sliding mode in finite time is proved along with determination of reachability time, for the considered faulty and perturbed microgrid system, as shown in Theorem 3.

- Along with voltage-frequency regulation using PI control and SVPWM in earlier studies, FTC is an additional feature in the same control mechanism by using the corrections in faulty sensor outputs achieved through the estimated faults and disturbances by using SMO.

- The system is simulated for various fault types of practical importance, particularly with reference to C.T/P.T and generally for any type of sensors, i.e., a sinusoidal,

linearly increasing, constant, square pulse, and random type faults with additive sinusoidal harmonics in the form of disturbances.

In article II [10]:

1. The major contribution of the paper is to incorporate estimation of game theoretic saddle points similar in nature to robust control parameters ($H_\infty, H-$), using their respective cost functionals and inequality version of HJIE in SMO theory, through Lyapunov theory and convex optimization of consequent LMIs, which also ensures stability. The concept is applied on the VSC-based microgrid model.

   In comparison to earlier works, they have used an approach of using robust control parameters and game theory for ordinary Luenberger Observers, whereas this study has incorporated the mentioned approach in sliding mode observers having a Luenberger gain for output estimation error term along with another switch term gain, which ensures more robustness along with suitability for switching electronic systems. Moreover, this work has incorporated game theoretic saddle points through convex optimization of LMIs, unlike earlier works.

2. The approach works mainly for sensor faults of microgrids and particularly for multiple faults occurring simultaneously in their sensor current and potential transformers. The approach works very well for many other types of faults such as square pulse (intermittent), ramp faults (i.e., incipient nature), constant faults,

etc., but the results are not included in the paper.

3. The inequality version of HJIE (i.e., Hamiltonian as the inequality constraint), which ensures stability in terms of the Lyapunov function (with its negative definiteness) along with giving constrained LMIs. The stability analysis through a cost functional constrained inequality version of HJIE and hence determination of corresponding LMIs are convex optimized to determine the respective SMO gain. The gains are determined for $(H-)$, (H_∞) and then taking both the constraints together i.e. $(H - /H_\infty)$, which are included as theorems as a major contribution of this work.

4. The fault/disturbance estimation by SMO theory, is used for correction of faulty sensor outputs to be supplied to the $P_r - Q_c$ control block, hence acting additionally as a fault-tolerant control. This part uses the work of the base paper of the authors of this study, to in [8]

1.5 Significance of Research

The fault-tolerant working of individual units will ensure uninterrupted and reliable power supplies for industrial, domestic, and critically necessary consumer sectors. This work mainly focuses on one unit of VSC-based AC microgrid which utilizes LCL filters, PI /droop/SVPWM control blocks for voltage-frequency regulations, being operable in

autonomous and islanded modes. The observers are utilized specifically for the reconstruction of CT/PT faults, but the scheme is not only convertible and extendable to various other actuator and system faults but also to a wide variety of linear and non-linear engineering systems with suitable tuning of parameters and minor changes in used SMOs. The SMOs are quite suitably used for the said applications due to their inherent non-linearity and robustness characteristics. The input power source is a DC source because the output voltages of many renewable energy sources are DC. Since the output voltages of many renewable energy sources are DC, such as photovoltaic cells and fuel cells, which are also heading towards DC-microgrid systems.

1.6 List of Chapters

Chapter 1: Introduction

Chapter 2: Literature Review

Chapter 3: System Modelling

Chapter 4: Sliding Mode Observers (Preliminaries)

Chapter 5: Robust Fault Detection and Stability Analysis

Chapter 6: Sensitivity of Fault Detection, Robustness to Disturbance, and Stability Analysis using HJIE and Game Theoretic Parameters

Chapter 7: Finite Time Reachability and Fault Estimation

Chapter 8: Part I: Voltage-Frequency Control Enhanced with Fault-Tolerant Control. Part II: Procedural Algorithms

Chapter 9: Results and Discussions

Chapter 10: Conclusions and Future Directions

Explanation of the Adopted Sequence of the Chapters of the Dissertation:

Chapter 1 comprises of general introduction, followed by a literature review and various other necessarily connected research areas in chapter 2. Chapter 3 explains the microgrid system model and stable filter required for the observer design. Chapter 4 elucidates the basics and preliminaries of sliding-mode observer design based on the system model explained in chapter 3. Chapter 5 has given one methodology to design H_∞ constrained sliding-mode observer gains through optimization of LMIs attained from Lyapunov stability analysis of the sliding-mode observers to be designed. The designed gains are to be used in the SMO explained in Chapter 4. Chapter 6 gives a further and more equipped methodology to design the gains of sliding-mode observer constrained with conditions of sensitivity of fault detection while also being robust to disturbances. This approach also uses Lyapunov stability theory in HJI equations to derive the game theoretic inspired $H-$ and H_∞ constrained LMIs, which are optimized to derive the respective sliding-mode observer gains, which are again used in the SMO presented in chapter 4. This chapter is the main contribution of the paper [10]. Chapter 7 has demon-

strated a Lyapunov stability-based methodology for the estimation/reconstruction of faults and disturbances along with the finite time reachability of the used sliding-mode observer. Chapters 5 and 7 are the main contributions of the paper [8]. Chapter 8 has given the voltage-frequency control for the microgrid after the due corrections of the faulty currents/voltages sensed by C.T/P.T, by using the reconstructed faults and disturbances. This chapter is also the part of both the articles. The detailed and complete block diagram along with both the design procedure algorithms specifically based on the methodologies used in chapters 5 and 6 respectively are also given in this chapter. The results based on both algorithms are given in two separate sections of chapter 9. Chapter 10 gives conclusions and future directions in 2 separate sections. The whole procedure is applied on the microgrid system as an application and example in the above-defined sequence of the procedure.

CHAPTER 2

Literature Review

[1] The dissertation surveys the literature considered in the research/ study to find the recent trends and research trends. The literature studies are done for general research trends and problems in smart grids, the HVAC/HVDC systems, applications and problems of converters/inverters utilized in modern and emerging distribution/transmission structures, and different AC/DC microgrid structures, the microgrid modeling, generally occurring sensor/actuator/system faults, particularly the faults of current and potential transformers, hierarchical centralized/distributed controls, approaches of fault-tolerant control in practice, sliding-mode observers utilized for fault-diagnosis, $H-$ and H_∞ based parameters for enhancing the robustness to disturbances and faults along with providing sensitivity of fault detection, and utilization of Hamilton-Jacobi-Isaacs equation (HJIE) and estimations based on game theory for the above-mentioned tasks.

[1]This chapter contains the literature review contents of both papers [8], [10], along with the overview of the research area, specifically for the research work carried out in this dissertation.

2.1 HVAC/HVDC and Power Converters

The HVAC transmission/grid infrastructures are also soon to be replaced/upgraded with HVDC ones, providing much lesser line losses in the single phase instead of at least 3 times increased losses in the HVAC transmission/grid systems. The emerging HVDC transmission systems are/can be networked underground and under the seas providing various other environmental and space-related trade-offs. The advancement in power electronic devices and subsequently the DC-DC converters, inverters, and rectifiers serve the roles of transformers, isolation providers, and various AC-DC-AC nearly lossless conversions. The converters have made possible the conversion of AC power produced by fluctuating winds, run-of-river, and conventional hydropower plants to DC being transmitted through HVDC networks. A super grid is a wide area transmission network, which makes it possible to transmit electricity at great distances and is also referred to as a "mega grid". The amount of necessary energy storage, in conventional backup power plants can be reduced. These grids have become an attractive and realistic option in the near future with growing and advancing reliable power electronics. Due to the importance of reliability and availability, such a grid will necessarily be a meshed multi-terminal structure [11–16].

2.2 Microgrids

A microgrid (MG) consists of a cluster of loads and distributed generators (DG) that operate as a single controllable system [17]. MGs may operate in both autonomous and grid-connected modes, whereas stability and effective control are issues of concern for both modes of operation of dynamic microgrids [18]. The energy distribution is being adjusted from both the demand and supply sides through microgrids while the transmission losses are reduced due to the proximity of renewable sources to the load. The scale and span of the microgrid is similar to low-voltage distribution, where the underground cables are used to connect low-voltage loads to the microgrid. Microgrids also include energy storage through battery systems and heat treatment i.e. the utilization of excess energy in water heating applications or simply being wasted. The requirement of distribution and transmission circuits is reduced. Microgrid employs the theoretical foundation of distributed generation. In the case of microgrid faults, the distributed generator is isolated to avoid the propagation of faults to important loads. The Microgrid is an intelligent option to improve the effectiveness of the power system, especially the distribution system, as the evolution of the old distribution system is not fast. It is required for microgrids to function robustly against faults and disturbances for the reliable working of micro power plants and uninterrupted power delivery to end users [19].

2.2.1 Trends in AC Microgrids

Distributed electrical power generation by various renewable and non-conventional micro-sources provides diverse options for configuring modern electrical grids. The designs of new generation distribution grids depend upon the areas, possibly available power sources, and power requirements of that area and community; hence they are less dependent on the centralized grids, in terms of handling loads. However, the communication layers and big data handling and processing will be encumbered more magnanimously than before. The interconnection of DGs to the utility grid through power electronic converters has raised concerns about the safe operation and protection of equipment, as power management is required at micro levels as well as for large unified networks. The reliable, properly controlled/regulated, and uninterrupted power supply, therefore, requires all the layers of the system, subsequent controls, and communication layers to be more consistent, resilient, and fault-tolerant [18], [19].

2.2.2 Some AC/DC/Hybrid Microgrid Topologies

The three-terminal distribution grid connecting DC microgrid is shown in Figure 2.1 [20], a three 3 wire DC distribution system configuration is shown in Figure 2.2 [21] a hybrid (AC/DC) microgrid is shown in Figures 2.3 [19] and a ring-shaped DC distribution system is shown in Figure 2.4 [21].

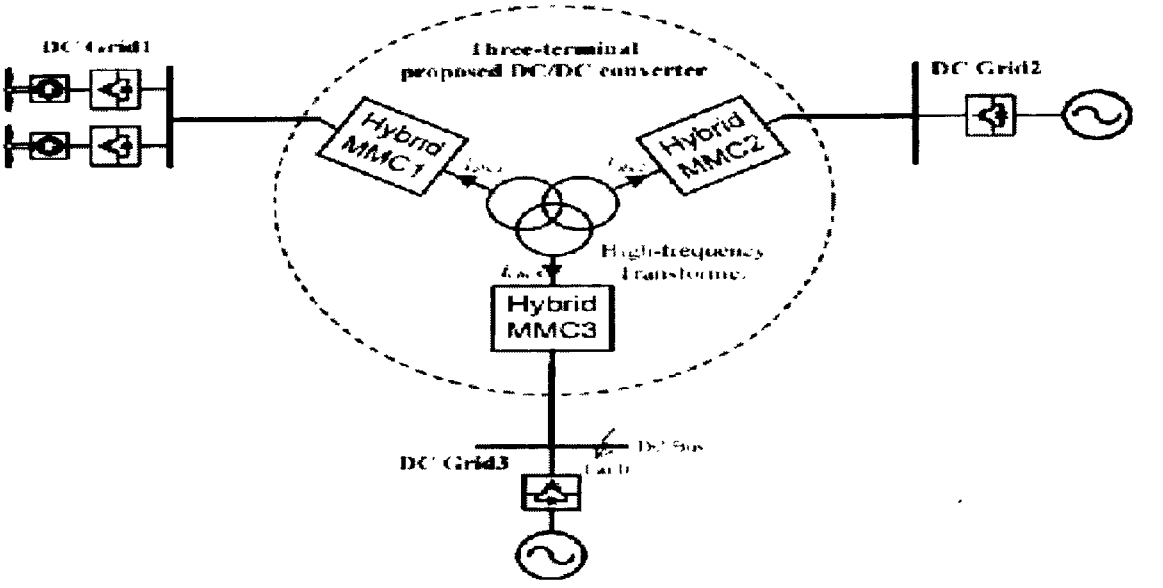

Figure 2.1: Three Terminal Distribution Grid [20]

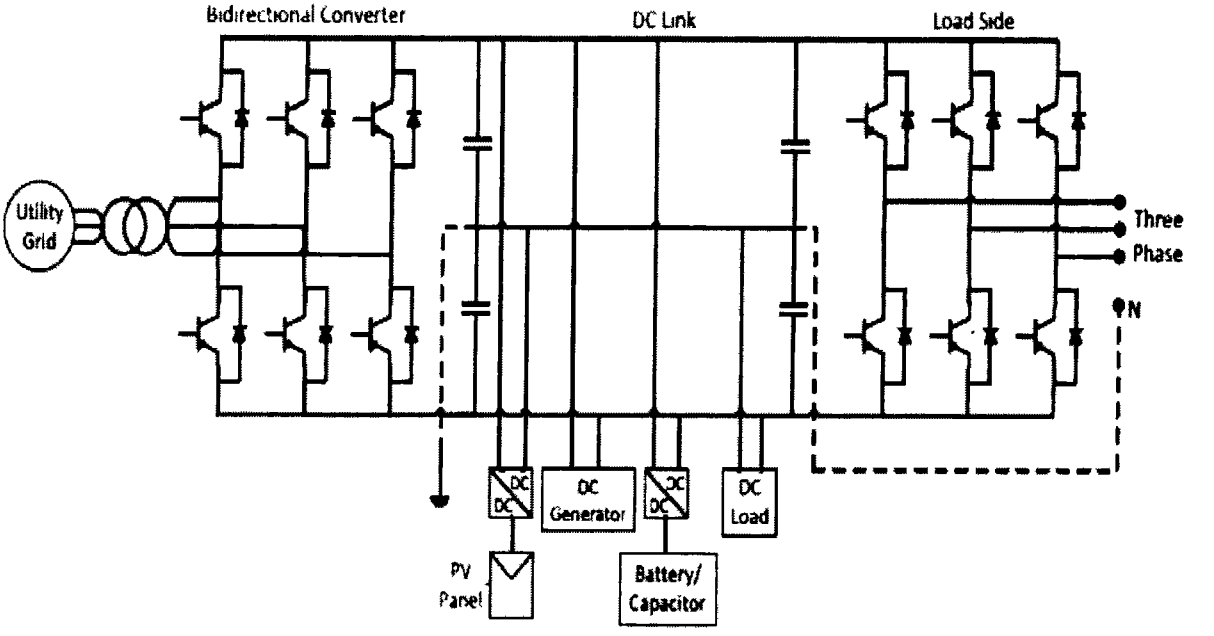

Figure 2.2: Three Wire DC distribution system configuration [21]

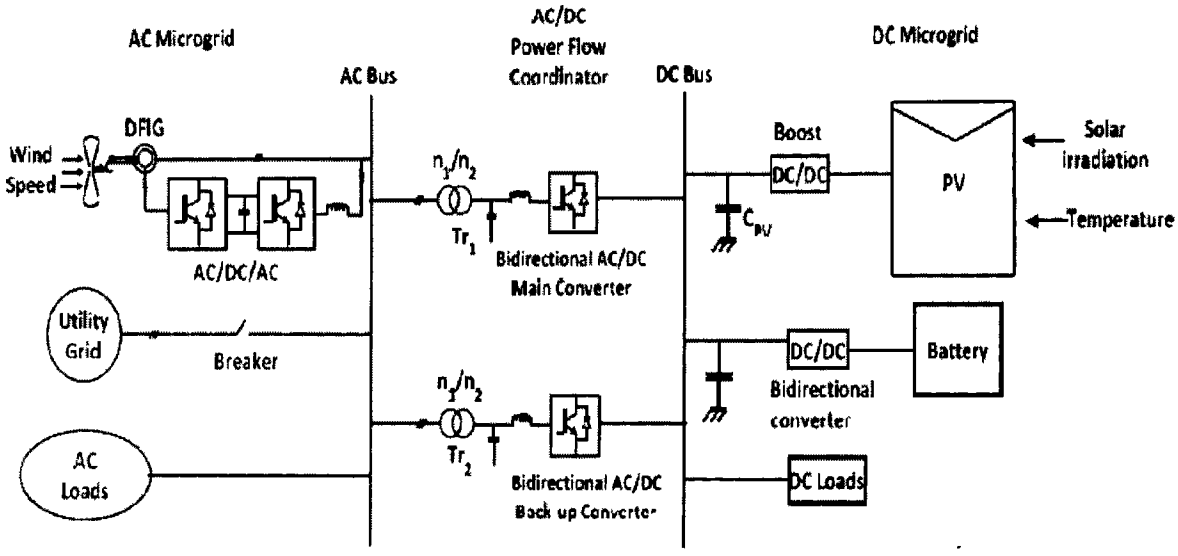

Figure 2.3: Hybrid Microgrid Model [19]

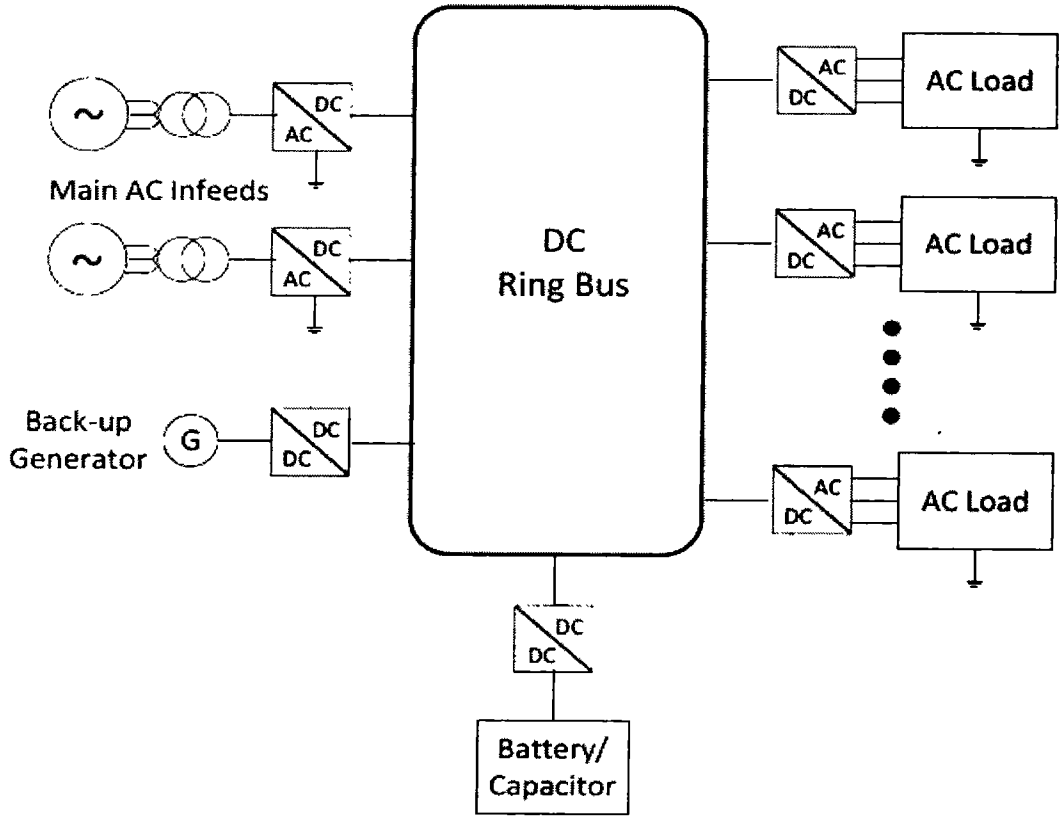

Figure 2.4: Ring-Shaped DC Distribution System Configuration [21]

2.2.3 Need of a Microgrid Model

The microgrids are modeled in several ways depending on designs, magnanimity, and requirements of analysis. The individual units are modeled by small signal models, however, the huge grid networks are modeled by linear programming inspired by the HJB equation of optimal control, knowledge-based models such as using fuzzy logic, data training-based models using Neural Networks and Complex Neural Networks, etc. The complex networks are also an emerging approach to model, and analyse the grids [22], [23]. However, often for the specific requirements of primary control design at a single converter or microgrid level a state space model is required to design the linear observers to replicate the system. In other words, the systems at the very basic (converter/inverter/filters) level are preferable to be modeled by state-space models. The non-linear models can be linearized in certain operating ranges or specifically at each operating point.

A properly simulated and experimentally tested small-signal linearized model of the MG is required for reliable testing of the observer-based FTC techniques used in this work. The FTC approach enhances the safety and reliability of the entire system by generating alarms for fault magnitudes within certain thresholds. Moreover, it will maintain the operation close to normal instead of immediate shutdowns and prevent possible losses, along with providing maintenance opportunities by shifting the power

switches to redundant generator sources using the hierarchical MG control strategy [9],[24]. This work is specifically focused on the FTC of microgrids, particularly with reference to sensor faults, as the control of power systems relies on sensor measurements. The sensors fail, have bad or broken connectivity, cause communication malfunction, etc., which will not only the control mechanism but also the power system. In general terms, reliability enhancement, local voltage support, correction of voltage/frequency sags, and uninterruptible power supply (UPS) are major issues of focus in this work [25]. The small-signal modeling of MGs can be studied in detail in [24, 26–32].

2.3 Faults and Failures

If we classify faults in the chronology of manufacturing, some faults occur in the initial phase of design, then the manufacturing phase can introduce some faults, and finally assembly phase adds some faults. Another aspect covers the operating faults like during normal or abnormal operations. Since the operator is a human, he can also introduce faults. Fault and failure can be differentiated as, the fault is a temporary abnormality, whereas the failure is a more permanent inability of the system. However, both can be detected in a similar way. All the faults, uncertainties, failures, noises, and disturbances can be included in the set of unknown external inputs. FDIA is an acronym for fault detection, isolation, and analysis, and this includes the kind, location, size, and time of detected and isolated fault [33].

2.4 General Fault Types

Incipient Faults: These occur after intervals and are relatively easier to detect due to the regular patterns though the regularity occurs in fault.

Abrupt Faults: These faults occur suddenly like spikes, though detected easily but can affect severely badly.

Intermittent Faults: These faults are developed gradually and are difficult to detect particularly when they are at lower magnitudes.

Sensor Faults: The faults occurring in the plant sensing equipment such as the current/ potential transformers which are used as grid current and voltage sensing are considered in this study.

Actuator Faults: The faults in actuators such as those occurring in pumps or valves in hydraulic systems, motors, batteries of converters, and rods of nuclear reactors are some examples.

Component Faults: The faults occurring in components such as capacitors, resistors, inductors, transistors, springs, masses, etc. are component faults.

2.4.1 Current and Potential Transformer Faults

The work, technique, and scope are general for many types of sensors and their respective connectivity configurations. But here system has specifically considered the

current/voltage transformers of microgrids being faulty and perturbed. It considers faults/disturbances occurring in C.T/P.T, which arise from saturation causing increased core magnetization current and resulting in reduced secondary current than required to switches and relays. The C.T saturation is caused by the DC offset of fault current on the primary side, prior to fault remnant flux and cumulative impedance burden of the secondary side resulting from relay coils and even wires. The C.T. sensor is like a ring on the wire, which measures current through magnetic flux and flux density, hence acts as a current sensor, whereas the P.T. is a 1:1 transformer that is used to measure the voltage. Both the current/voltage sensors are installed on the LCL filter to measure the input/output currents and voltages. The common technical terms are Hysteresis, Saturation, and Eddy currents, etc [34], [35],[36]. The inaccurate C.T/P.T output will result in inaccurate SVPWM signals and VSC currents/voltages, which will then not be able to track the desired active and reactive powers. The faults occurring in C.T/P.T are composite natured inclusive of magnitude, phase, and harmonics where normally previous works have considered only magnitude faults for the sake of simplicity [6].

2.4.2 Importance of FD and FTC in Physical Systems

Reliability and safety are indispensable and important in all modern technologies and engineering applications. But they become even more critical for sensitive and high-risk systems, such as failures and power shutdowns in aerospace and nuclear engineering

installations can be very drastic. When a system is fault-tolerant it tries to behave in a normal way even if with lower performance rather than complete system failure. The uncertain systems can be transformed into switched systems for the purpose of modeling and subsequent fault detection. We can model input output pair in the form of a straight line with a constant slope and if the operating deviates from that straight line, it is considered a fault. We can also understand the concept of fault through three tank systems with leakage or leakages in the tanks and inter-tank connections [37].

2.5 Several FD Approaches

Hardware redundancy is used in more critical/risk-intolerant systems such as flight control systems. This type of fault detection is very reliable and easy. But it involves space and maintenance costs. In the plausibility test, we can use binary logic to verify if the values are compatible with each other. In signal-based detection, we can divide it into time and frequency domains. In this technique, we get the best results in a steady state. Model-based detection is a substitute for hardware redundancy. Parity-based and observer-based approaches are similar. Making the choice of a single approach is challenging considering all scenarios. Some approaches are more effective in electrical or mechanical systems compared to chemical and industrial systems. We can also combine different approaches to achieve more reliable [33].

1. Ideally, If there is no modeling error and disturbance, it's a fault-free case, the residual will be zero and the estimations converge to the measurements.

2. A non-zero residual signal after the transients indicates the occurrence of faults.

3. As the Modeling errors and disturbances exist inevitably; a threshold is required to be designed to distinguish the non-zero residual signal, driven by either fault or by modeling error/disturbance Then criteria are in terms of a higher fault detection rate (FDR), lower false alarm rate (FAR,) or an optimal trade-off.

Faults may occur in Sensors, Actuators, and Components. So generally diagnosis is: 1) Fault detection: Detection of the occurrence of faults, 2) Fault isolation: Localization (classification) of different faults, 3) Fault analysis or identification: Determination of the type, magnitude, and cause of fault.

Desired Characteristics for FDI: 1) Detection of incipient and abrupt faults, 2) Detection of sensor, component, and actuator faults, 3) Fault Detection in a closed loop, 4) Supervised transient states of process [33], [2], [38].

2.5.1 Signal Based Fault Detection

It uses magnitudes of functions of time, trends of derivatives, statistical parameters such as mean and variance, correlation coefficients, power spectral densities, etc. of the signals under consideration being measured.

$$Y_{min} \leq y(t) \leq Y_{max} \implies Faultless(System)$$

$$Y_{min} \geq y(t) \geq Y_{max} \implies Faulty(System)$$

2.5.2 Model Based Fault Detection

1. Compare the behavior of the actual process to that of the nominal fault-free model of the process driven by the same input. Its stages are:

   i) Residual Generation

   ii) Residual evaluation.

   The objective of residual generation is to produce a signal by comparing the measurements with their estimates; and to inspect the residual signal for possible presence of faults.

2. The model can be an Analytical Model represented by the set of differential equations or it can be a Knowledge-Based Model represented by, for example, Neural Networks, Petri Nets, expert systems, Fuzzy Rules, etc.

3. Knowledge-based model approaches do not need full analytical modeling and, therefore, are more suitable in information-poor systems or in situations where the mathematical model of the process is difficult to obtain or is too complex. E.g. Chemical processes which are difficult to model analytically [33], [2], [38].

Hammouri [39] provides sufficient conditions for fault detection, provided for non-linear affine models along with circumstances in which observers with high gains can be used for residual generation for uniformly observable systems.

Zhang [40] uses a detection filter with a bunch of estimators with different thresholds for fault isolation in a dynamic non-linear system with uncertainty. The paper also works on the determination of different adaptive thresholds, fault isolation conditions, and analytical results for the time required for fault isolation.

Maciejowski [41] gives a detailed non-linear reference model for a crashed aircraft being controlled by model predictive control (MPC) controller and pilot controls being modeled by another MPC controller at a low sampling rate to give such a fault detection and isolation (FDI) mechanism, which could have avoided the plane crash in 1862.

Shi [42] presents H_∞ based FTC for actuator and sensor faults occurring in a wind energy system. It considers variable wind speed being modeled with stochastic affine models and uses linear quadratic regulator (LQR)-based state feedback control.

2.5.3 Observer Based Approach

1. Measurements from the process are compared to estimates made by an observer in observer-based techniques, and this comparison generates the residual signal (a filter). It should be recognized that observers employed for FD and control reasons are two different things. The observers required for control are state observers,

meaning that they estimate unmeasured states. On the other hand, the observers required for FD are output observers, meaning that they produce estimates of the measurements.

2. It is desirable for the residual signal to be resilient to unknown inputs. The idea is to use the knowledge of the unknown input distribution matrix to entirely decouple the state estimation from unknown inputs (disturbances). Relative to the unknown inputs, states are independent as well as residual. The Eigen-Structure approach, which also decouples residual from unknown inputs, is a robust method for residual generation. Compared to unknown input observers, the existence conditions for the Eigen-Structure assignment approach are more lenient. For this, the residual signal is made independent of unknown inputs rather than decoupling state estimations from unknown inputs.

3. The fault's impact on the residual is dissociated if it is located in the same area as the disturbances and cannot be seen. Hence, Design observers that lessen the impact of unknown inputs and enhance the impact of faults on the residual signal should be used instead of entirely decoupling unknown inputs. [33], [2], [38].

Pertew [43] creates a dynamic observer for Lipchitz non-linear systems that simultaneously detects and estimates the fault by using an objective function through LMIs to converge the residual vector to the fault vector. Instead of utilizing a traditional con-

stant gain structure, the problem leverages convex optimization of the objective function by employing the appropriate weights to minimize the influence of fault on estimating error. Ding [44] works on a fault detection observer approach with a significant focus on minimal order fault detection filters and associated necessary algorithms for the process, where the system is totally decoupled from unknown inputs. Zhang [45] utilizes a tried-and-true factorization technique to work on an observer-based fault detection with residual norm-based minimization on "false alarm rate" (FAR) for given "false detection rate" (FDR).

2.5.4 Suitability of Sliding-Mode Observers (SMO) for Considered Application

Sliding-mode observer (SMO) being resilient and robust to noises and disturbances, is different from ordinary Luenberger observers because of the nonlinear switch discontinuous term, which is properly processed for fault diagnostics (detection, isolation, and estimation). They are used for both linear/nonlinear systems with additive faults and are capable of handling a large class of perturbations, parametric variations, uncertainties, and unmodeled dynamics. Moreover, it provides compensation for observer mismatches while replicating the system, along with ensuring stability and reachability in finite time [46, 47].

The study uses the sliding-mode observers for fault diagnosis, so a literature survey

for using the SMO for the said purpose is as under. Walcot and Zak [48] used feedback output error linearly in observers, along with a Lyapunov-based stability analysis. The faults can be determined from the deviation of the system trajectory from the sliding surface, but it cannot determine which sensor or actuator is faulty. The basic requirement of fault detection is to detect faults, along with location identification, as mentioned in [49, 50]. The difference between the system and observer outputs generates residual signals, which are processed further with static and dynamic thresholds for better diagnostics, reconfiguration of the system/observer, and fault reconstruction. Residual-based methods were reviewed by [51, 52]. SMO-based methods have also been proposed by [53, 54]. Utkin [55] in his proposed observer used a discontinuous term with a suitably scaled gain, which requires software to solve the synthesis problem.

Edwards [56] extended the work by using both discontinuous and linear terms as feedback in SMO, which is transformed into canonical forms by suitable transformations constrained by conditions on invariant zeros of the system. The methods for computing the required gains of the observer are given, which provides an explicit solution, but all degrees of freedom are not exploited. The work was carried out by [57] using an output term injected with an appropriate gain for fault magnitude determination in the localized sensor/actuator while maintaining the sliding motion. Tan [5] used sliding-mode observer (SMO) with linear matrix inequality (LMI) based convex optimization algorithms to exploit more degrees of freedom for observer gains and establish a rela-

tionship between the sub-optimal observer and the linear part of the SMO using the linear quadratic Gaussian (LQG) theory. The paper also presented a modified algorithm for pole placement and clustering to place eigenvalues of the linear SMO part in a certain region to attain improved observer performance. The algorithms also involve some design matrices inherent in procedures that can modify the dynamics of the sliding motion. Tan [58] applied the SMO theory to find additive sensor faults by transforming them suitably to act as actuator faults. This work was further extended by [59] for localized additive sensor/actuator fault reconstruction with additive uncertainty in the system. It uses the minimization of the L_2 gain of uncertainty and reconstructed fault, scaling of the output injection signal, and application of LMIs for more design freedom. Although the sliding mode is often not retained in most cases in a very ideal sense in the presence of faults, the estimation is shown to be made possible in these works.

Shin [60] also used the idea of correcting the sensor/actuator faults by using the estimated fault, but the technique could not be termed as strictly active or passive. Edwards and Tan [3, 58] use sliding mode observers for fault detection and isolation (FDI) of uncertain linear systems, by output error injection and fault correction through fault detection and estimation while maintaining closed-loop performance.

Yan [61] uses a sliding mode observer-based technique for a non-linear aircraft system where the uncertainty being the function of the state variables has a non-linear bound.

Yan [62] addresses fault estimation for bounded specific classed perturbed non-linear systems using the output error injection approach in sliding mode observers (SMOs), where fault can be estimated online to any accuracy and observer parameters are determined by LMIs, and tested for robotic arm. Aldeen [63] estimated the states, faults, and disturbances/unknown inputs for nonlinear systems by designing an SMO.

Dhahri [4] initially presented a fault reconstruction methodology for matched faults and uncertainties, which is not very practical because of the very nature of uncertainties; hence, the method is not valid for a good range of practical systems. They further extended the work by determining the SMO gains by feasibility optimization of LMIs attained through Lyapunov stability criteria. It minimizes the H_∞ criteria (ratio of residual to disturbance), and the reduced effect of disturbance on fault reconstruction improves the fault estimation, along with validation of the work for unmatched uncertainties/ faults. This study proved the stability and reachability of the sliding-mode observer and evaluated the reachability time by using a suitable mathematical estimation.

Alwi [64] uses unknown input linear SMOs for sensor faults' estimation, which works even without the requirement or constraint of the stability of an open loop system.

In [6], SMO was applied to sensor faults, that is, for current transformer (C.T) magnitude faults, and used an estimated fault for correction of sensor (C.T) fault. It also uses

feedback pole placement control to track the real and complex powers, and in this way, a compensating sensor (C.T) fault without even replacement or alarm, which can be better termed as a method to design a software-based sensor.

Ning [65] addresses a stochastic system with limited network resources and uses a filter mechanism for fault detection. The system operates on an event-triggered mechanism instead of extensive data coming from sensors to filter. The residual generator is more attenuating to disturbances along with sensitivity to faults compared to conventional FD methods while saving network resources.

2.5.5 Parameter Estimation Based Approach

1. The physical parameters of systems exhibit faults. According to this premise, the system's parameters are continuously calculated online, and if there is a difference between the estimated and actual parameters, it indicates a problem.

2. One benefit of the parameter estimating approach is that several parameters can be estimated with only one input signal and one output signal, providing a complete picture of the internal process quantities. The approach also has the benefit of producing the size of deviations, which is crucial for fault analysis. PE is helpful for identifying component defects, but it can also identify sensor and actuator faults.

3. The fact that excitation is always required in order to estimate the parameters has the drawback that it may cause issues if the process is running at a stationary speed.

4. E.g Methods of least squares (LS), recursive least squares (RLS), extended least squares (ELS), etc.

Threshold Selection An essential component of a fault detection system is the threshold selection. False alarms will occur if the threshold is set too low because some disturbances will cause the residual to exceed the threshold and trigger the alert. Little defects won't be recognized if the threshold is set to a high value.

2.6 Motivation for FTC in Microgrids

A properly simulated and experimentally tested small-signal linearized model of the MG is required for reliable testing of the observer-based FTC techniques used in this work. The FTC approach enhances the safety and reliability of the entire system by generating alarms for fault magnitudes within certain thresholds. Moreover, it will maintain the operation close to normal instead of immediate shutdowns and prevent possible losses, along with providing maintenance opportunities by shifting the power switches to redundant generator sources using the hierarchical MG control strategy.

A study [66] discusses various intelligent methods for designing and controlling small-

and large-scale MGs operating in parallel or in isolation. The increasing complexity of MG systems with various combinations of active and passive elements requires individual converter units to act in a fault-tolerant manner for better efficiency and reliability in generation, distribution, and transmission.

MPC is proposed for the voltage-frequency regulation of standalone wind-diesel hybrid MG, which consists of a diesel generator, PV sources, and battery storage. It employs an additional FTC module that uses MRAC and a PID controller tuned by the GA for reconfiguration under fault conditions [67].

The wind-diesel hybrid standalone MG is controlled in a fault-tolerant manner using MRAC-LPV along with a PID controller tuned by GA for frequency regulation to maintain a constant speed. Voltage regulation is achieved by classic MRAC, and the entire system is tested for several fault cases, such as sudden load connection, three-phase faults, and diesel engine actuator faults with various magnitudes. The FTC unit activates the fault condition, whereas the PI control serves as a baseline controller that enhances the reliability of the automated system as a whole [68],[69]. A paper provides an FTC operation for wind power generative systems using terminal sliding mode control (SMC) for the rotor side and provides supporting control to series grid-side converters, which are controlled primarily by fuzzy and posicast-based approaches. As a whole, it targets handling various types of voltage sags, including deep ones [70]. A paper proposes a lower-order observer for a linear system with bounded varying pa-

rameters available online, which first determines the unknown states and then the fault estimates. These estimates are used to decide the mitigation strategy using the adaptive thresholds, along with the prevention of false alarms, and these estimates are also used to compensate for the effects of faults. The system acts as a first-order filter with less complexity and cost while preventing the effects of disturbances and measurement noise [71]. A neural network (auto-encoders) and particle swarm optimization (PSO) based evaluation and restoration of faulty or failed sensors was proposed in [72].

An adaptive-fuzzy-PID robust sliding control is proposed for an uncertain class of nonlinear systems, particularly focusing on aircraft flight control, is referred to in [73].

The work in [74] designed a sliding control with adaptive gains and an integral surface for robustness against actuator faults of a wind turbine system to maintain the rotor speed, with simulation results. Recent approaches are moving towards consensus/distributed controls of MGs along with trending applications of fuzzy control. A distributed adaptive fuzzy-based control is presented for large-scale systems with sensor and actuator faults [75].

2.6.1 Hierarchical Control

The optimized control strategies are required to be applied in control of AC/DC microgrids in islanded and grid-connected modes. A hierarchical control strategy manages the drawbacks of central control in terms of reliability and provides economic benefits

as well. When central control fails, the functionality of the system can be continued through the primary level of control. The flexibility of the system depends upon energy flow into and out of the microgrid, which is possible in a hierarchical control strategy by establishing communication between control levels. This technique is also multi-modal in terms of operation [76].

Sources and converters form the primary level of control and they often control the system voltages/currents through PI and droop methods. The primary level of control isthe most challenging and is also called zero-level control. The instability of voltage and frequency is caused by the discrepancy between the amount of power at generation and consumption. It is also required to avoid overcurrent in power electronic devices (converters, rectifiers, inverters, etc.) caused by circulating currents. Primary control adds stability to voltage and frequency after the islanding process. The loads applied to the islanded microgrid can be linear or non-linear which involves control of power sharing in terms of both active and reactive power. Then the central controller forms the second level of control which constantly observes the system in terms of its limits. The third level controls the flow of power inside the microgrid and between the microgrid and the main grid. [77], [78].

2.7 Lyapunov Theory for Stability Analysis

This work uses Lyapunov Theory to prove the stability of the proposed Sliding-Mode Observers for the detection and estimation of faults and disturbances. It requires a vector Lyapunov function in terms of the error function of the detector/estimator SMOs. The positive definiteness of the Lyapunov function and the negative/semi-negative definiteness of its time derivative is required to prove the required stability of observers. The negative definiteness is also further extended to prove the reachability of sliding surfaces in finite time to show the real-time working performance of the fault detection and tolerance system.

2.8 LMIs and Convex Optimization

The negative definiteness of vector Lyapunov function gives constrained LMIs which are convex optimized to find the Lyapunov matrix, which is used to find the Sliding-mode Observer gains. The optimization is performed using MATLAB toolbox using 'feasp' function for feasibility optimization and 'mincr' for minimization of the linear objective (Trace being used here) under the LMI constraint. The functions are defined in Appendix C.

Damiano Rotando [79] developed an LMI-based observer/controller to be employed for dynamic cost estimation and control for a saturated-actuator class of non-linear systems

to maintain the cost below an upper bound. The scheme is tested by simulation results on the rotational single-arm-inverted pendulum.

2.9 Criteria of Robustness and Sensitivity (H_∞ and $H-$)

We want the filter to be inclusive of both the characteristics i.e. sensitivity to detection of faults and attenuation of disturbances. $H-$ index and H_∞ norm are used to quantify the worst way in which fault detection is performed. When the residual signal is least sensitive, the gain from that fault should be higher than a constant value. While $H\infty$ based fault gain is less than a constant value because it deals with attenuation. Both fault detection functions deal with both faults and disturbances but not in the desired way. We use multi-objective fault detection to achieve attenuation and amplification at the same time [33], [2], [38].

$H-$

A fault detection filter that ensured a fault sensitivity greater than a specified constant was presented. However, this filter does not provide any information regarding its ability to attenuate disturbances. The filter may also make residual sensitive to disturbances in addition to making residual sensitive to errors. This is definitely not a characteristic that the $H-$ filter wants to have.

$$H_o(G_o.\boldsymbol{f}) = \int (\boldsymbol{r}_K{}^T \boldsymbol{r}_K - \beta \boldsymbol{f}^T \boldsymbol{f}) dt; (\boldsymbol{\xi} = 0) \tag{2.9.1}$$

H_∞

Although it does not provide any information regarding fault sensitivity, the $H\dot{\infty}$ fault detection filter ensures that disturbance attenuation will be larger than a specified constant. In addition to attenuating disturbances, the filter may also lessen the impact of flaws. Better fault detection filters ought to be both disturbance-resistant and fault-sensitive. We can alternatively define the H_∞ disturbance attenuation problem as a two-player, zero-sum differential game with disturbance d and filter gain L as the players, in a manner similar to that of the $H-$ fault sensitivity problem. Hence, specifying the cost functional

$$H_o(G_o, \boldsymbol{\xi}) = \int (\boldsymbol{r_K}^T \boldsymbol{r_K} - \alpha^2 \boldsymbol{\xi}^T \boldsymbol{\xi}) dt; (for) \boldsymbol{f} = 0 \tag{2.9.2}$$

$H-/H_\infty$

1. The goal of the multi-objective index $H-/H_\infty$ based design is to maximize the ratio of β/α rather than maximising or minimizing either variable individually. As a result, an $H-/H_\infty$ based filter may not be the best in terms of the $H-$ index, meaning that another filter gain may exist that provides a larger fault to residual gain than the $H-/H_\infty$ based designed filter gain.

2. The disturbance to residual gain for the former FDF may be smaller than that for the latter FDF and multi-objective index-based FDF, i.e., the two two-player

nonzero-sum differential games with the following two cost functionals discussed above. A similar comparison of *Hinfty*-based FDF and multi-objective index-based FDF can be presented. [33], [2], [38].

Hou [80] uses $H-/H_\infty$ robust fault detection technique, where the $H-$ index enhances the sensitivity of residual w.r.t fault and H_∞ deals with the robustness of disturbances effect on the residual. The observer design is an optimization problem where the necessary conditions for fault detection are embodied in terms of linear matrix inequalities (LMIs), which are solved by an iterative algorithm.

Edelmayer [81] uses H_∞ constraint through a filter transformed into an LMI-based convex feasibility optimization problem, to suppress the effect of disturbances and unknown inputs for robust detection of faults and modes of failure in linear time variant (LTV) systems.

Liu [82] works on using $H-$ and H_∞ norms for worst-case fault sensitivity and robustness to disturbances, respectively, represented in the forms of LMIs as bounded real lemma, along with additionally performing the analysis problem for finite frequency range using weighing filters, which is useful in strictly proper systems.

Liu [83] works on making the outputs least sensitive to inputs through an $H-$ index in terms of LMIs added input observability with new conditions necessary and sufficient for fault detection with worst-case sensitivity of faults.

Wang [84] works on H_∞ H_∞ and $H-H-$ index-based optimization using LMIs to enhance the detection of faults while attenuating disturbances and uncertainties along with working on the threshold required for fault detection.

Wang ([85]) uses $H-$ index for sensitivity to worst-case fault detection while minimizing the effect of worst-case disturbance using H_∞ norm using $H-/H_\infty$ observer-based fault detection. The conditions necessary and sufficient for fault detection filters are solved with iterative LMI algorithms and results are determined for both the finite and infinite frequency ranges.

Wang [86] works on $H-$ and H_∞ criteria for fault detection in linear systems, where the fault detection problem is unconstrained using a pole assignment approach and observer gains are determined by a gradient optimization approach. The paper considers the sensitivity of fault for a finite frequency range. The problem is tested for faults occurring in take-off and vertical landing of air crafts.

Khan [87] has mainly worked on the computation of threshold for faults' detection while formulating an LMI optimization problem for continuous time non-linear systems.

Aliyu [88] uses H_2/H_∞ mixed and finite dimensional filtering such that the conditions are in terms of coupled discrete Hamilton–Jacobi–Isaacs equations. The problem addresses the discrete-time nonlinear affine systems for both the finite and infinite horizon problems.

Li [89] studies the tradeoff for between sensitivity to faults and robustness to disturbances using $H-/H_\infty$ and H_∞/H_∞ optimization problems using iterative linear matrix inequalities (ILMIs) based on a factorization technique, for linear time invariant (LTI) systems in state space form.

Raza [90] considers a switched asynchronous system with disturbances and noises for designing fault detection (FD) filters with mixed $H-/H_\infty$ sensitivity and robustness criteria, along with piecewise Lyapunov function stability. Conditions in terms of LMIs and average dwell time were also investigated. The schemes were tested on buck-boost converters for matched and unmatched durations of switched systems.

Ahmad [91] uses a robust fault detection filters (FDF) design with H_∞ criteria for sensitivity to faults while completely isolating the system from unknown inputs using LMIs for LTI systems.

Kangdi Lu [92] proposed robust PI control for load-frequency control (LFC) of multi-area interconnected scenario, where its parameters are estimated by constrained population extremal optimization. It uses H_∞ determined from LMIs as one constraint whereas the integral-based time absolute error is another constraint. The papers showed the effectiveness of the scheme by its comparison with other PI control methods and an optimized model predictive control (MPC). Kang-Di Lu [93] developed adaptive, resilient event-triggered PI-based LFC which works with energy constraints. Lyapunov's theory

to derive criterion of stability which is tested for various case studies, is proved to be defeating denial of service attacks and reducing the communication burdens.

These Ph.D. dissertations are considered in detail [2, 33, 37, 38] in order to learn the approaches. The book of Yuri and Edwards on sliding mode control and observers is also considered in detail [94].

Chapter Summary: The chapter surveys sequentially all the sufficient parts of the research area as mentioned in the chapter's starting paragraph to find the research gaps while giving the necessary understanding of the research area.

t

CHAPTER 3

System Modelling

3.1 System Modeling

[1]. The system modeling requires modeling of considered microgrid systems to design a suitable observer for the system, which would replicate the actual system for detection, isolation, and estimation of faults.

3.1.1 Mathematical Model of Current/Potential Transformer Faults

The mathematical model of faults and perturbations serves the existence of the actual C.T/P.T faults comprising magnitude, harmonics, and phase existing simultaneously. So, the fault is considered mathematically to be considering magnitude and phase and an additive disturbance being sinusoidal with different frequencies serves as additive

[1]This chapter with slight differences is part of both papers [8], [10]

harmonics. In this way, the complete model of faults is being considered in the system, which are added using a Simulink block to be added in the faultless VSI current/voltage signals. The fault and disturbance mathematical model is defined as:

$$f(t) + \xi(t) = f_o sin(\omega_1 t + \phi_1) + \xi_o sin(\omega_2 t + \phi_2). \tag{3.1.1}$$

3.1.2 Mathematical Model of the Microgrid System

A small signal model of MG is used in this work to determine the workability and efficiency of a fault-tolerant control scheme. The small signal model of MG is claimed to be properly simulated, experimentally verified, and able to be used as a block in large grid networks.

The mathematical model of a voltage source inverter-based microgrid basically comprises non-linear equations, whose linearized version at the operating point is used in this work. The complete microgrid model, as proposed by [26] comprises of inverter equations, LCL filter, droop control equations, PLL, current controller, voltage controller, SVPWM, and real and reactive power calculation, which all together form a non-linear model, and needs to be linearized at the operating point. The LCL filters are placed just after the VSI, as passive filters to manage the current/voltage spikes. The modeling of stray/line inductances, capacitances, and resistances are also considered with LCL filters, i.e., the resistors r_c and r_f are the parasitic resistances of the inductors, a damping

resistor R_d is connected in series with the filter capacitor, however, the capacitor's ESR is not considered, as it can be lumped into R_d. The current and potential transformers are mounted on LCL filter to read the instantaneous current/voltage readings, which are used to calculate the instantaneous values of real and reactive (P_r, Q_c) powers. The inverter model is considered an average model in his work, i.e., without any major inaccuracies, we can assume that the commanded voltage appears at the input of the filter inductor i.e., $\boldsymbol{V}^*_{idq} = \boldsymbol{V}_{idq}$. This approach neglects only the losses in the IGBT and diodes. The LCL part of the whole system mathematically modeled with KCL/KVL along with average VSI model, is considered as a required part of the complete mathematical model to design the SM observer because it is placed right after VSI, and C.T/P.T are also mounted on them to read the instantaneous values of input/output currents/voltages. Therefore, if there is no fault in the sensors (C.T/P.T) of the system, the model and the actual system states/outputs are compromised and are showing no difference. The Simulink-based wired grid model is shown in Figure 3.1, the single-line diagram of microgrid system is presented in Figure 3.2, and the simulink-based grid system model is shown in Figure 3.3.

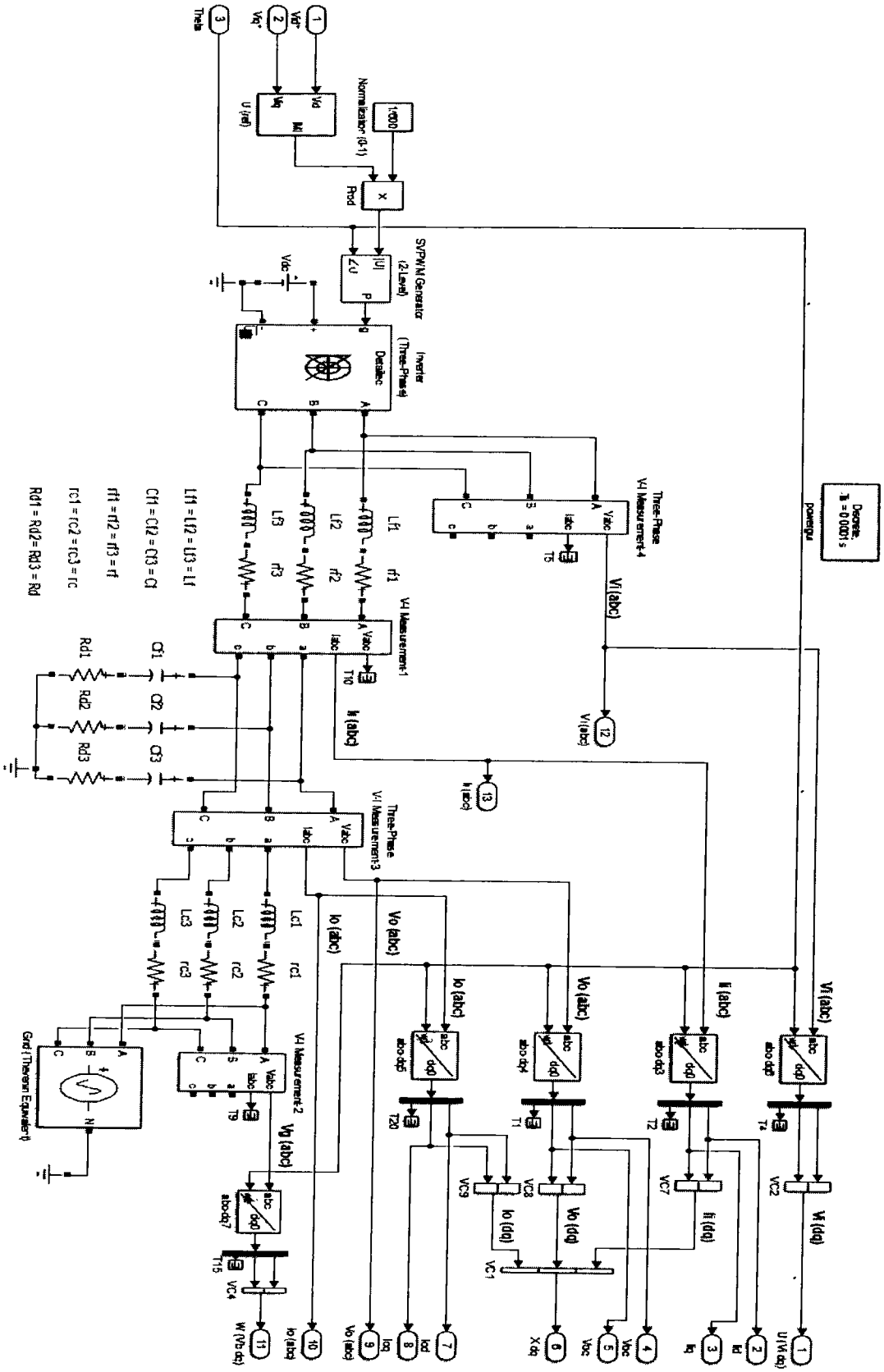

Figure 3.1: Microgrid System Model

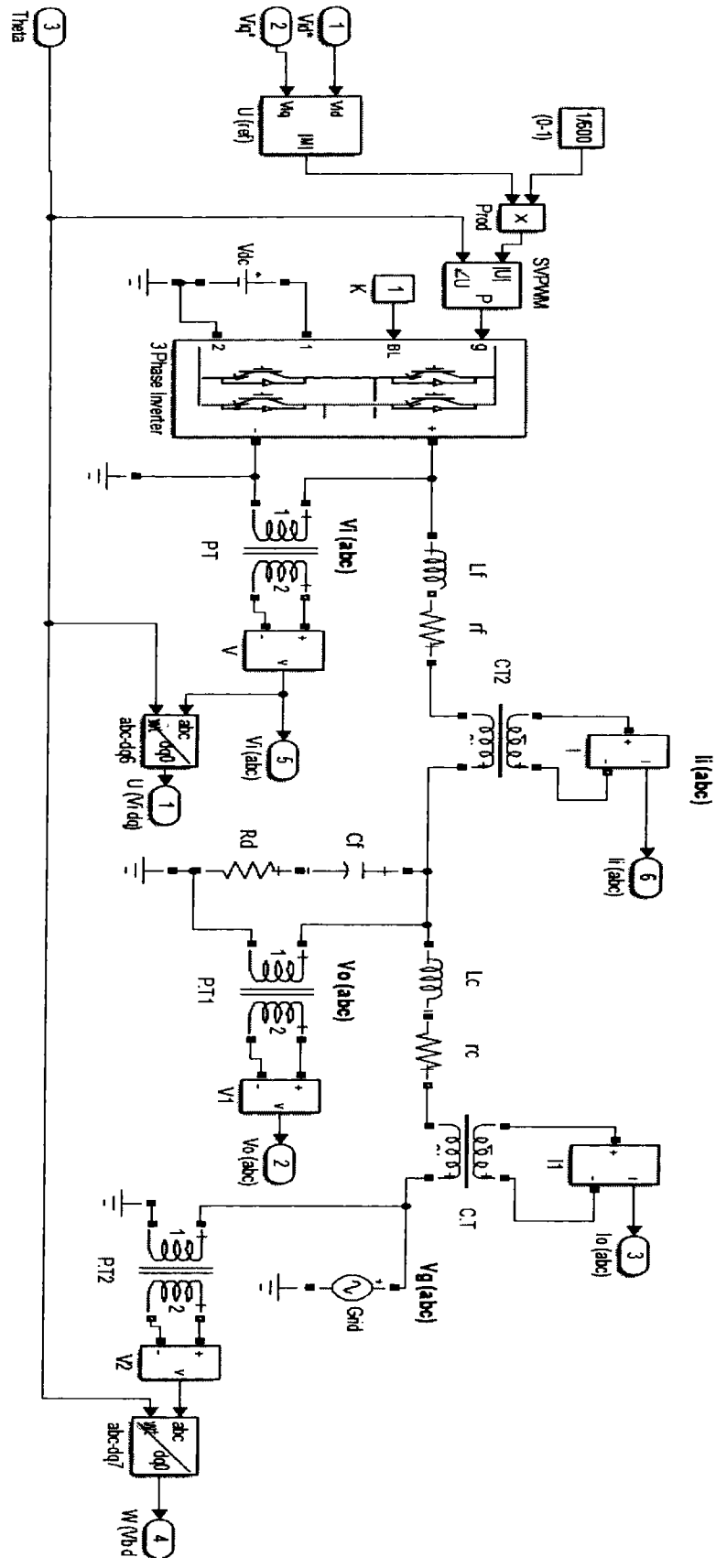

Figure 3.2: Single Line Diagram of Microgrid

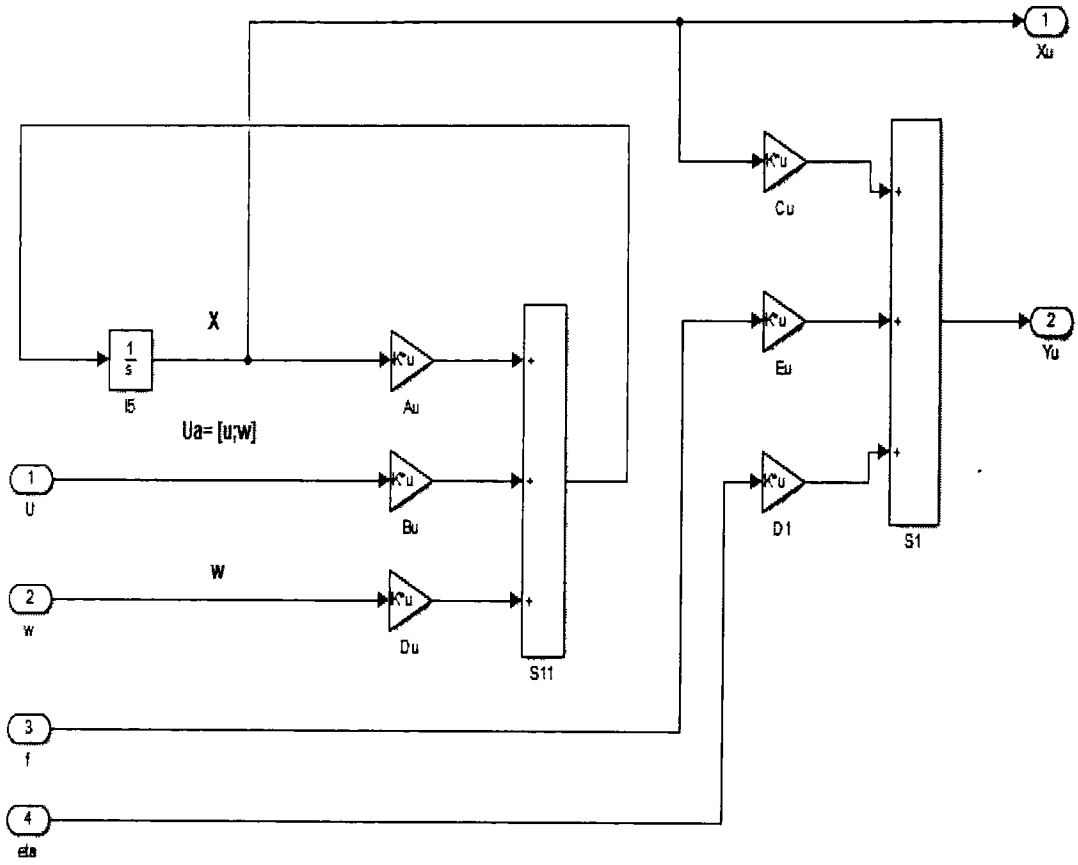

Figure 3.3: Simulink based Diagram of Microgrid

The considered required part of the MG system is a continuous time LTI system, which follows the separable principle, i.e., the controller and observer can work in combination with each other, i.e., the unknown system input/output states required for the control action can be determined using the observer. The pair (A_s, C_s) are observable, C_s is full rank output matrix, the matrices (A_s, C_s, E_s) have no invariant zeros, which is satisfied if outputs are more than inputs, i.e., $(p > m)$. For the considered microgrid case p = 4 and m = 2. The fault and disturbance distribution matrices $E_s = D_s$ are simply the identity matrices in the considered microgrid application.

Separation Principle: For stochastic systems, under some conditions, the optimal state feedback controller can be designed by an optimal state observer which feeds the optimal deterministic controller, such that both the controller and observer can work separately. For the deterministic linear systems, if an observer and a stable state feedback are designed for a linear time-invariant system, then the combined observer and feedback are stable.

Therefore, the linearized mathematical model of considered MG from [26] is given as under.

$$\begin{bmatrix} \dot{i}_i \\ \dot{i}_o \\ \dot{v}_o \end{bmatrix} = \begin{bmatrix} -r_f/L_f & 0 & -1/L_f \\ 0 & r_c/L_c & 1/L_c \\ 1/C_f - r_f R_d/L_f & -(1/C_f - r_c R_d/L_c) & -(R_d/L_f + R_d/L_c) \end{bmatrix} \begin{bmatrix} i_i \\ i_o \\ v_o \end{bmatrix} + \begin{bmatrix} 1/L_f \\ 0 \\ 1/L_f \end{bmatrix} v_i + \begin{bmatrix} 0 \\ -1/L_c \\ R_d/L_c \end{bmatrix} v_g \tag{3.1.2}$$

where v_i is the input (inverter) voltage, v_g is the grid voltage, L_c, L_f, C_f are the LCL filter inductances and capacitances, respectively.

The abc-dq0 transformation is defined as a combination of Clark and Park transformation to convert a three phase voltage/current into effectively a two phase form. Some explanation of the said transformations are given in Appendix A.8.

For any signal $s(t)$

$$\begin{bmatrix} s_d \\ s_q \\ s_0 \end{bmatrix} \triangleq \sqrt{2/3} \begin{bmatrix} cos(\theta) & cos(\theta - \frac{2\pi}{3}) & cos(\theta + \frac{2\pi}{3}) \\ -sin(\theta) & -sin(\theta - \frac{2\pi}{3}) & -sin(\theta + \frac{2\pi}{3}) \\ \sqrt{2}/2 & \sqrt{2}/2 & \sqrt{2}/2 \end{bmatrix} \begin{bmatrix} s_a \\ s_b \\ s_c \end{bmatrix}. \tag{3.1.3}$$

A PLL is required to measure the actual frequency of the system. A dq based PLL was chosen, where the PLL input is the d-axis component of the voltage measured across the filter capacitor. Therefore, the phase is locked, such that $V_{od} = 0$. The grid side voltage angle is measured by PLL in our problem, and then according to convention that angle is used for all abc-dq and vice versa transformations, which is needed in the system.

The system model in Equation (3.1.2) in dq transformed form is

$$A_s = \begin{bmatrix} \frac{-r_f}{L_f} & W_{pLL} & 0 & 0 & \frac{-1}{L_f} & 0 \\ w_{pLL} & \frac{r_f}{L_f} & 0 & 0 & 0 & \frac{-1}{L_f} \\ 0 & 0 & \frac{-r_c}{L_c} & w_{pLL} & \frac{1}{L_c} & 0 \\ 0 & 0 & -w_{pLL} & \frac{-r_c}{L_c} & 0 & \frac{1}{L_c} \\ \frac{1}{C_f} - \frac{r_f R_d}{L_f} & w_{pLL} R_d & \frac{-1}{C_f} + \frac{r_c R_d}{L_c} & -w_{pLL} R_d & -(w_{pLL} + \frac{R_d}{L_f} + \frac{R_d}{L_c}) & 0 \\ -w_{pLL} R_d & \frac{1}{C_f} - \frac{r_f R_d}{L_f} & w_{pLL} R_d & \frac{-1}{C_f} + \frac{r_c R_d}{L_c} & 0 & -(w_{pLL} + \frac{R_d}{L_f} + \frac{R_d}{L_c}) \end{bmatrix},$$

$$B_s = \begin{bmatrix} 1/L_f & 0 \\ 0 & 1/L_f \\ 0 & 0 \\ 0 & 0 \\ R_d/L_f & 0 \\ 0 & R_d/L_f \end{bmatrix}, B_g = \begin{bmatrix} 0 & 0 \\ 0 & 0 \\ -1/L_c & 0 \\ 0 & -1/L_c \\ R_d/L_c & 0 \\ 0 & R_d/L_c \end{bmatrix}, C_s = \begin{bmatrix} 0 & 0 & 1 & 0 & 0 & 0 \\ 0 & 0 & 0 & 1 & 0 & 0 \\ 0 & 0 & 0 & 0 & 1 & 0 \\ 0 & 0 & 0 & 0 & 0 & 1 \end{bmatrix}, E_s = D_s \begin{bmatrix} 1 & 0 & 0 & 0 \\ 0 & 1 & 0 & 0 \\ 0 & 0 & 1 & 0 \\ 0 & 0 & 0 & 1 \end{bmatrix},$$

and the vectors

$$x_s = [I_{id}, I_{iq}, I_{od}, I_{oq}, V_{od}, V_{oq}]^T, u = [V_{id}, V_{iq}]^T, w = [V_{gd}, V_{gq}]^T, f = [f_{i_d}, f_{i_q}, f_{v_d}, f_{v_q}]^T, \xi = [\xi_{i_d}, \xi_{i_q}, \xi_{v_d}, \xi_{i_d}]^T.$$

The dq axis output voltage and current measurements are used to calculate the instantaneous active power ($\boldsymbol{P}_r$) and reactive power ($\boldsymbol{Q}_c$) generated by the inverter.

$$P_r = 3/2(V_{od}I_{od} + V_{oq}I_{oq}) \tag{3.1.4}$$

$$Q_c = 3/2(V_{oq}I_{od}\check{} - V_{od}I_{oq}), \tag{3.1.5}$$

where V_{od}, V_{oq}, I_{od}, I_{oq} are the d and q components of sensor (C.T/P.T) output voltages/currents. Instantaneous powers are then passed through low pass filters with the corner frequency ω_c to obtain the filtered output power.

The general state-space form of the system is:

$$\dot{\boldsymbol{x}}_s = A_s\boldsymbol{x}_s + B_s\boldsymbol{u} + B_g\boldsymbol{w} \tag{3.1.6}$$

$$\boldsymbol{y}_s = C_s\boldsymbol{x}_s + E_s\boldsymbol{f} + D_s\boldsymbol{\xi}. \tag{3.1.7}$$

The dimensions of vectors in a general form are $\boldsymbol{x}_s \in \Re^{n\times 1}, \boldsymbol{x}_h \in \Re^{p\times 1}, \boldsymbol{u} \in \Re^{m\times 1}$, $\boldsymbol{w} \in \Re^{m\times 1}, \boldsymbol{y}_s \in \Re^{p\times 1}, \boldsymbol{f} \in \Re^{q\times 1}, \boldsymbol{\xi} \in \Re^{q\times 1}$, dimensions of system matrix, actuator matrix, grid side dynamics matrix, output matrix and stable filter matrix, respectively, are $A_s \in \Re^{n\times n}$, $B_s \in \Re^{n\times m}$, $B_g \in \Re^{n\times m}$ and $C_s \in \Re^{p\times n}$ i.e., $[0_{p\times(n-p)}, I_{p\times p}]$; whereas dimensions of fault and disturbance distribution matrices with full row and column rank are $E_s \in \Re^{q\times q} = I_{q\times q}$ and $D_s \in \Re^{q\times q} = I_{q\times q}$ respectively, where $n \geq p \geq q$.

Since the norm of generally any vector x is defined by

$$\|\boldsymbol{x}\| \triangleq \sqrt{\boldsymbol{x}^T\boldsymbol{x}}.$$

The boundedness of fault and disturbance magnitudes is shown in terms of the norm as: $\|\boldsymbol{f}\| \leq \alpha$ and $\|\boldsymbol{\xi}\| < \xi_o$ which along with the above-mentioned matrix dimensions are the design requirements.

3.1.3 Stable Filtering and Augmented System

A stable Filter lessens the effect of faults and disturbances on the grid system output variables. The filter first magnifies the undetectably small magnitude faults, using a gain matrix, which is then subtracted from the output state variable. In other words, the stable filter, as used in Equation (3.1.8), is used to make the output least dependent on faults and provide magnification of insignificant small faults. The scaled output state variable with the information of only faulty sensors is augmented with the system states' variable, which itself also involves the output

states, which are unscaled. In this way, stable filtering also gives the isolation of faulty sensors, which is required for the proper diagnosis process. In some cases, a stable filter can be simply a positive definite (PD) stable identity matrix with eigenvalues in the left half plane, or a first-order low-pass filter to suppress the high-frequency noise effects in the output signal, required for some applications. However, according to the used approach in this work, the sensor faults and disturbances appear in the output equation and the actuator faults appear in the state equation. The faulty output variables of interest are also part of state variables, which are replicated on a stable filtered output equation but in the scaled form. So it can also be stated that the method to detect isolated faulty actuator faults is extended for the detection of sensor faults using the SMO Theory. It helps to replicate the techniques used earlier in [3] for actuator faults to be used for sensor faults, appearing in the output equation only.

$$\dot{\boldsymbol{x}}_{\boldsymbol{h}} = -A_h \boldsymbol{x}_{\boldsymbol{h}} + A_h \boldsymbol{y}_{\boldsymbol{s}}, \tag{3.1.8}$$

where $A_h \in \Re^{p \times p}$ is the stable filter matrix or

$$\dot{x}_h = -A_h x_h + A_h C_s \boldsymbol{x}_{\boldsymbol{s}} + A_h E_s \boldsymbol{f} + A_h D_s \boldsymbol{\xi}. \tag{3.1.9}$$

The system model, i.e., the states, are augmented with a stable filtered output for convenience and easy handling in a compact form. The augmented system is

$$\begin{bmatrix} \dot{x}_s \\ \dot{x}_h \end{bmatrix} = \begin{bmatrix} A_s & 0 \\ A_h C_s & -A_h \end{bmatrix} \begin{bmatrix} x_s \\ x_h \end{bmatrix} + \begin{bmatrix} B_s & B_g \\ 0 & 0 \end{bmatrix} \begin{bmatrix} u \\ w \end{bmatrix} + \begin{bmatrix} 0 \\ A_h E_s \end{bmatrix} f + \begin{bmatrix} 0 \\ A_h D_s \end{bmatrix} \xi \tag{3.1.10}$$

$$\dot{\boldsymbol{x}}_c = A_c\boldsymbol{x}_c + B_c\boldsymbol{u}_c + E_c\boldsymbol{f} + D_c\boldsymbol{\xi} \tag{3.1.11}$$

$$\boldsymbol{y}_c = C_c\boldsymbol{x}_c \tag{3.1.12}$$

where $y_c \in \Re^{p\times 1}$

$$\boldsymbol{y}_c = \begin{bmatrix} 0 & I \end{bmatrix} \begin{bmatrix} \boldsymbol{x}_s \\ \\ \boldsymbol{x}_h \end{bmatrix} \tag{3.1.13}$$

where $\boldsymbol{x}_c = \begin{bmatrix} \boldsymbol{x}_s \\ \\ \boldsymbol{x}_h \end{bmatrix}$, $\boldsymbol{u}_c = \begin{bmatrix} \boldsymbol{u} \\ \\ \boldsymbol{w} \end{bmatrix}$, $A_c = \begin{bmatrix} A_s & 0 \\ \\ A_hC_s & -A_h \end{bmatrix}$, $B_c = \begin{bmatrix} B_s & B_g \\ \\ 0 & 0 \end{bmatrix}$, $E_c = \begin{bmatrix} 0 \\ \\ A_hE_s \end{bmatrix}$ and $D_c = \begin{bmatrix} 0 \\ \\ A_hD_s \end{bmatrix}$.

The dimensions of the vectors are $x_h \in \Re^{p\times 1}$, $\boldsymbol{x}_c \in \Re^{n_c\times 1}$, $\boldsymbol{u}_c \in \Re^{2m\times 1}$ whereas the dimensions of augmented system matrices are $A_c \in \Re^{n_c\times n_c}$, $B_c \in \Re^{n_c\times p_c}$, $C_c \in \Re^{p_c\times n_c}$ i.e., $[0_{p_c\times(n_c-p_c)}, I_{p_{cc}}]$, $A_hE_s = E_o \in \Re^{q\times q}$, $A_hD_s = D_o \in \Re^{q\times q}$, where $E_c \in \Re^{n_c\times q_c}$, $D_c \in \Re^{n_c\times q_c}$ are the fault and disturbance distribution matrices, respectively, in the augmented system, such that $E_c = D_c = \begin{bmatrix} 0_{n\times p} \\ \\ I_{p\times p} \end{bmatrix}$ and for the considered augmented MG system $n_c = n + p = 10$, $p_c = p = 4$, $q_c = q = 4$.

The augmented simulink-based system model is given in Figure 3.4.

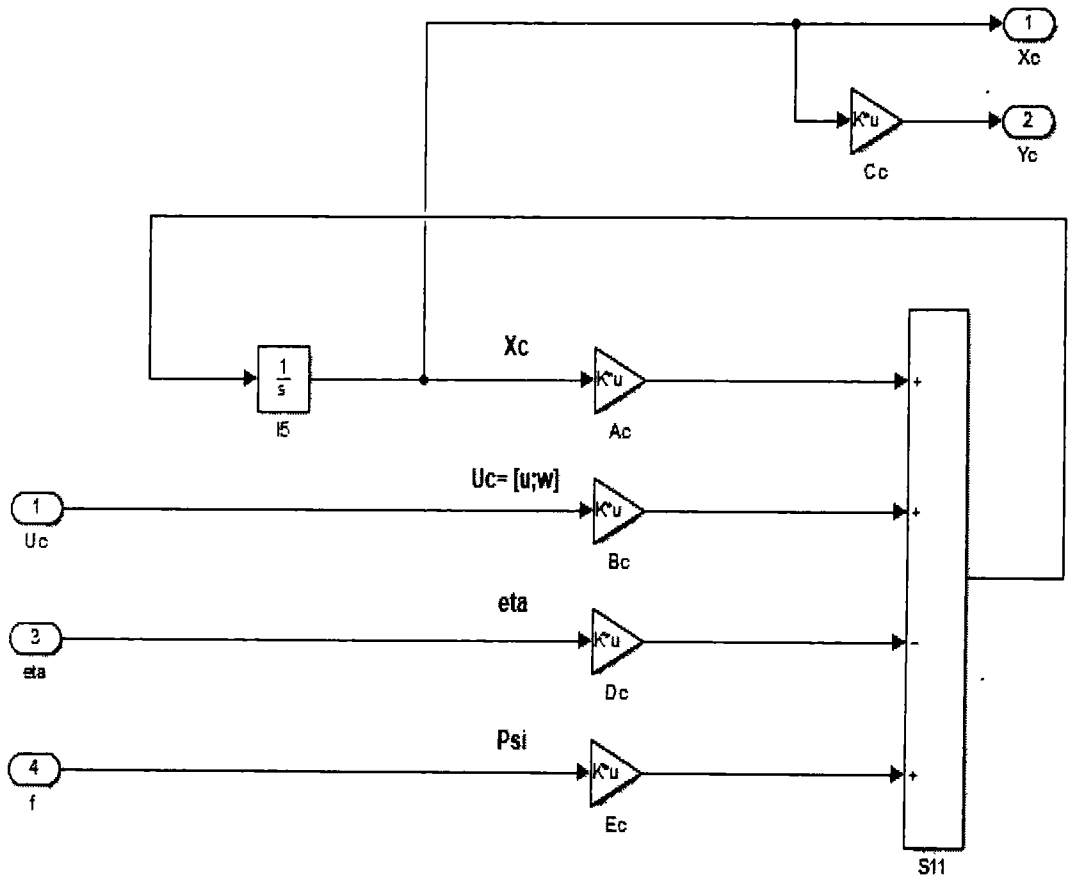

Figure 3.4: Simulink-based augmented system model of Microgrid

As shown by [3] since $rank(C_cE_c) \leq q$, the invariant zeros of $(A_c, E_c, C_c) \subseteq \lambda(A_s)$, so if the open loop system is stable, the system (A_c, E_c, C_c) will be minimum phase. In other words, if the system has more outputs then inputs, i.e., $p \geq q$, then it is expected that the system will not have any invariant zeros.

Summary: The chapter discussed in sufficient detail, the mathematical model for the VSI-based microgrid to be utilized for designing the suitable observer on the system, for system replication, and hence using that for the determination of faults and unknown inputs. The model used is well simulated and tested, to be able to be applied for the mentioned application.

CHAPTER 4

Sliding-Mode Observers

(Preliminaries)

4.1 Fault Diagnosis Using SMOs (Preliminaries)

[1]. The phrase 'fault diagnosis' in literature refers to three main objectives: namely, detection, isolation, and estimation of faults in the system [2]. In most of cases, fault detection is not sufficient, instead, it also requires isolation of the fault location and estimation to manage the corrective mechanism to ensure the system's protection. The mentioned objectives are fulfilled using methods that are categorized into four main classes: signal-based, model-based, parameter estimation-based, and observer-based approaches of fault diagnosis [33, 37, 38, 94].

By concept and application, the observer system gets the same inputs as the system i.e., ($\boldsymbol{u}$ and $\boldsymbol{w}$) with the input distribution matrices (B_s, B_g), system distribution applies on the estimated

[1]This chapter with slight differences is part of both papers [8], [10]

state and Luenberger gain (G_o) applies on stable filtered output estimation error ($\boldsymbol{e_o}$) term along with switch term gains (G_m and γ) also influencing the $\boldsymbol{e_o}$ in a switch mode, and all in combination try to form the observer to replicate the system properly.

Remark 4.1: (Role of Luenberger Gain/How SMO is Different from Ordinary Luenberger Gain Observer) This gain G_o is the main controlling matrix parameter used to manipulate the output estimation error ($\boldsymbol{e_o}$) to manipulate the observer system to replicate the system properly, in order to give a proper estimation of the states/outputs. The first-order SMO filter is different from ordinary Luenberger observer in a way, as it involves a switch discontinuous term (ψ) that is multiplied with another gain G_m, which is also related to Luenberger gain in terms of some common matrices. The switch discontinuous term possesses another constrained internal gain (γ) and both are multiplied with stable filtered output error term ($\boldsymbol{e_o}$). It helps the estimated states to track the actual states in a more effective way in a finite time, which is specifically termed as achieving the sliding mode. In sliding mode, a chattering path is followed (due to the discontinuous term) on the phase plane plot (i.e., the graph between $\boldsymbol{e_o}$ and $\boldsymbol{de_o/dt}$) to approach to zero stable filtered output estimation error. This is done by considering the SMO in terms of the error system and the error surface to be a sliding surface in this SMO with an error surface (variable). The same SMO is used to estimate/ reconstruct the faults after having achieved the sliding surface, i.e., output estimation error to be approaching zero in the finite time, which not only ensures the reachability of error estimator SMO but also the stability of the fault estimation process in the finite time.

Fault Detection and State Error Estimation with SMO

SMO is used for fault diagnostics, i.e., the detection and isolation of faults by estimation of

states/outputs for the considered case, i.e., MG application. The isolation property in a literal sense localizes the faulty sensors in the system; however, for the considered case, isolation and estimation are both performed by the fault estimation SMO. The standard first order SMO is given as proposed by [3, 55, 56], according to which the estimated states of the MG system are by [3, 55, 56], according to which the estimated states of the MG system are

$$\dot{\boldsymbol{x}}_{\boldsymbol{o}} = A_c\boldsymbol{x}_{\boldsymbol{o}} + B_c\boldsymbol{u}_{\boldsymbol{c}} + G_o\boldsymbol{e}_{\boldsymbol{o}} + G_m\boldsymbol{\psi}, \tag{4.1.1}$$

where $\boldsymbol{x}_{\boldsymbol{o}} = \begin{bmatrix} \boldsymbol{x}_{\boldsymbol{s}}{}^* \\ \boldsymbol{x}_{\boldsymbol{h}}{}^* \end{bmatrix} \in \Re^{n_c \times 1}$ is the estimated state vector, which is an augmented vector of estimated system states $\boldsymbol{x}_{\boldsymbol{s}}{}^* \in \Re^{n \times 1}$ and estimated stable filtered output $x_h^* \in \Re^{p \times 1}$. The matrix $G_o \in \Re^{n_c \times p_c}$ is the SMO Luenberger gain of output error injection term $\boldsymbol{e}_o \in \Re^{p \times 1}$, which ensures that the stability of the term $(A_o = A_c - G_oC_c)$ and $G_m \in \Re^{n_c \times p_c}$ is the SMO gain of discontinuous switching term (ψ), where both G_o,G_m need to be determined. The proposed form of (ψ) term is $(\psi = -\gamma\frac{P_o\boldsymbol{e}_o}{\|P_o\boldsymbol{e}_o\|})$, where the factor (γ) is appropriately chosen as a constant gain factor depending on the application under consideration and the needs to be determined. The gain G_m is proposed to be of the form $G_m = \begin{bmatrix} -LT^T \\ T^T \end{bmatrix}$, where $T \in \Re^{q \times q}$ is an orthogonal matrix that can be determined by QR factorization, however, the matrices, L and P_o are sub-parts of a PD Lyapunov matrix $P > 0$, which is proposed to be in the form of $P = \begin{bmatrix} P_1 & P_1L \\ L^TP_1 & T^TP_oT + L^TP_1L \end{bmatrix} > 0$, where the matrices $P \in \Re^{n_c \times n_c}, P_1 \in \Re^{n \times n}, P_o \in \Re^{p \times p}, T \in \Re^{p \times p}, L \in \Re^{n \times p}$ are to be determined [5]. The Luenberger gain G_o is actually also determined from the Lyapunov matrix P, as its working will be explained in detail in the next section.

The simulink-based diagram of fault detection sliding-mode observer in Figure 4.1.

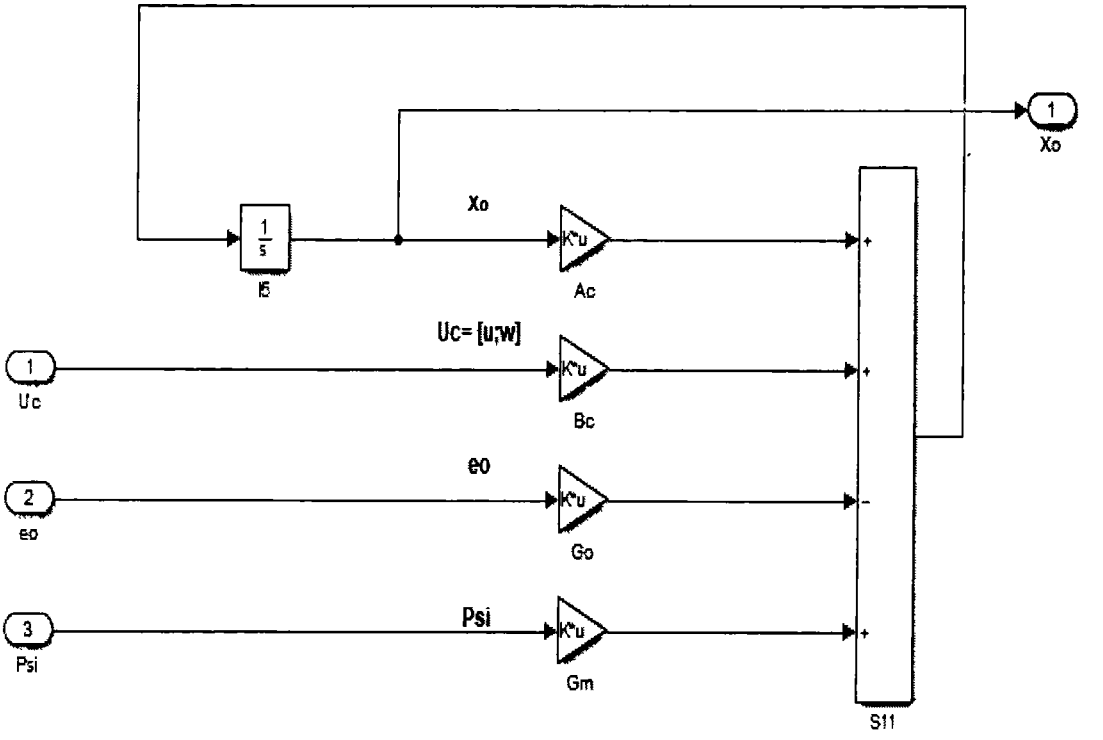

Figure 4.1: Fault Detection Sliding-Mode Observer

The state estimation error is determined by taking the difference of the system states as determined from the mathematical model in (3.1.11) and the estimated states based on SMO in Equation (4.1.1) is

$$\boldsymbol{e_d = e = x_o - x_c}. \tag{4.1.2}$$

The estimated output states of the system are given by

$$\boldsymbol{y_o = C_c x_o}, \tag{4.1.3}$$

whereas the term e_o is the output estimation error

$$\boldsymbol{e_o} = \boldsymbol{y_o} - \boldsymbol{y_c}. \tag{4.1.4}$$

The output estimation error is the residual signal, which can be defined in terms of augmented error term e

$$\boldsymbol{e_o} = \boldsymbol{r(t)} = C_c(\boldsymbol{x_c} - \boldsymbol{x_o}) = C_c\boldsymbol{e} \tag{4.1.5}$$

and

$$A_c = \begin{bmatrix} A_{11} & A_{12} \\ A_{21} & A_{22} \end{bmatrix}, \boldsymbol{x_o} = \begin{bmatrix} \boldsymbol{x_s}^o \\ \boldsymbol{x_h}^o \end{bmatrix}$$

Since $\boldsymbol{e_o}$ is not the actual output error, but rather the (scaled) stable filtered output error, the empirical suggestion is to use the form of ψ in Equation (4.1.6) instead of its normalized (scaled) version for the MG application, i.e.

$$\psi = -\gamma \times P_o\boldsymbol{e_o}. \tag{4.1.6}$$

Remark 4.2: As shown in [3], the observer, as mentioned in Equation (4.1.1), is completely insensitive to faults (f) exits if:

1- $Rank(C_cE_c) = q$;

2- The invariant zeros of the system triple (A_c, E_c, C_c) lie in Left Half Plane (LHP)

Using Equation (4.1.2), the state estimation error SMO is

$$\dot{\boldsymbol{e}} = A_c\boldsymbol{e} - E_c\boldsymbol{f} - D_c\boldsymbol{\xi} - G_o\boldsymbol{e_o} + G_m\psi. \tag{4.1.7}$$

Using Equation (4.1.5) it takes the form

$$\dot{e} = (A_c - G_o C_c)e - E_c f - D_c \xi + G_m \psi, \tag{4.1.8}$$

where, $A_o = A_c - G_o C_c \in \Re^{n_c \times n_c}$, $e \in \Re^{n_c \times 1}$.

The above Equations (4.1.7) or (4.1.8) are also a standard SMO ([55]), being applied on an error system for state error estimation, where the error surface is the sliding surface. The error state is further used for fault estimation. Since the error system is an augmented form of state and the stable filtered output error, i.e.,

$$\begin{bmatrix} \dot{e_s} \\ \dot{e_o} \end{bmatrix} = \begin{bmatrix} A_{11} & A_{12} \\ A_{21} & A_{22} \end{bmatrix} \begin{bmatrix} e_s \\ e_o \end{bmatrix} - \begin{bmatrix} G_1 \\ G_2 \end{bmatrix} e_o - \begin{bmatrix} 0 \\ E_o \end{bmatrix} f - \begin{bmatrix} 0 \\ D_o \end{bmatrix} \xi - \begin{bmatrix} LT^T \\ T^T \end{bmatrix} \psi \tag{4.1.9}$$

where

$$e = \begin{bmatrix} e_s \\ e_o \end{bmatrix}, G_o = \begin{bmatrix} G_1 \\ G_2 \end{bmatrix}, E_c = \begin{bmatrix} 0 \\ E_o \end{bmatrix}, G_m = \begin{bmatrix} LT^T \\ T^T \end{bmatrix}.$$

The dimensions of vectors and matrices in general form are $e_s \in \mathbb{R}^{n \times 1}$, $e_o \in \mathbb{R}^{p \times 1}$, $\psi \in \mathbb{R}^{q \times 1}$, $f \in \mathbb{R}^{q \times 1}$, $\xi \in \mathbb{R}^{q \times 1}$, $A_{11} \in \mathbb{R}^{n \times n}$, $A_{12} \in \mathbb{R}^{n \times p}$, $A_{21} \in \mathbb{R}^{p \times n}$, $A_{11} \in \mathbb{R}^{p \times p}$, $D_o \in \mathbb{R}^{q \times q}$, $E_o \in \mathbb{R}^{q \times q}$, $G_o \in \mathbb{R}^{n_c \times p}$,$G_1 \in \mathbb{SR}^{n \times p}$, $G_2 \in \mathbb{R}^{p \times p}$, $L \in \mathbb{R}^{n \times p}$, $T \in \mathbb{R}^{q \times q}$ whereas for the MG system considered $n = 6, p = 4, q = 4, m = 2, n_c = n + p = 10, m_c = m = 2, p_c = p = 4, q_c = q = 4$.

The simulink-based diagram of fault estimation sliding-mode observer in Figure 4.2.

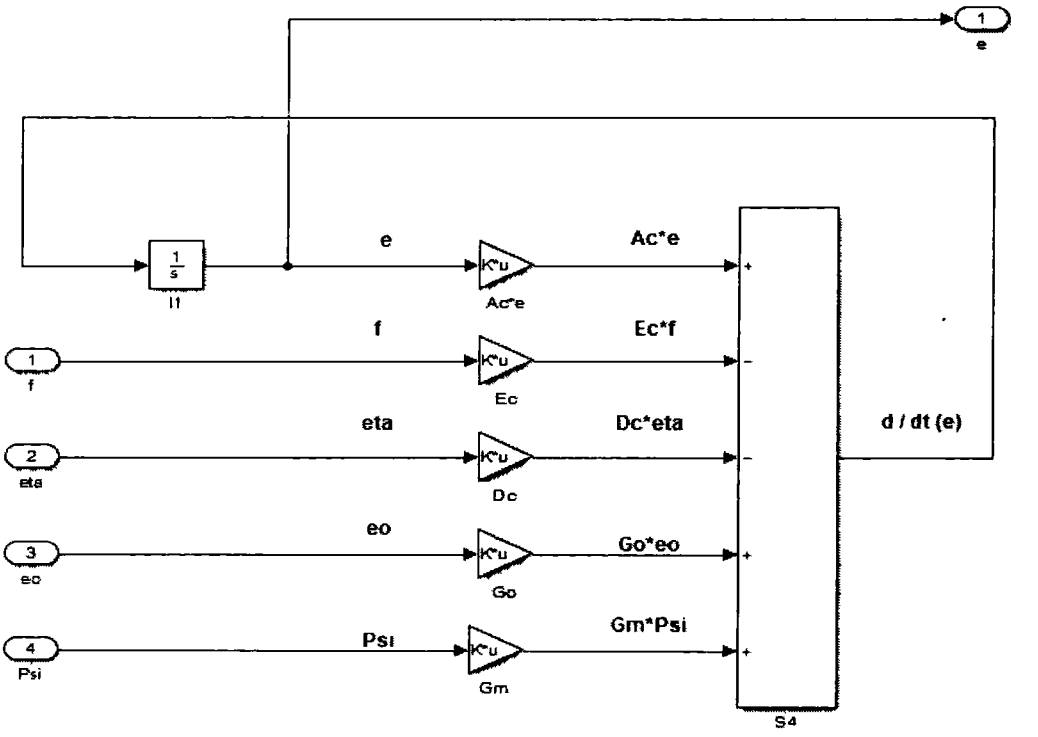

Figure 4.2: Fault Estimation/Reconstruction Sliding-Mode Observer

Summarizing Remark: The chapter presents preliminaries of SMO being used for fault diagnostics i.e. detection and estimation of faults. It also discusses the conditions of applicability and utilization of SMO for the said tasks, while explaining its difference from ordinary Luenberger Observers. The next chapters are focused on the stability analysis of the proposed observers for the MG system, as well as the determination of gains of fault detection and fault estimation observers.

CHAPTER 5

Robust Fault Detection and Stability Analysis

5.1 Determination of Sliding Mode Observer Gains through Stability Analysis

[1] A lemma for the existence of the sliding mode is given, before the Lyapunov-based stability analysis of the proposed fault detection/ estimation SMOs for the considered MG system.

Lemma 5.1: If $\sigma(e)$ defines the sliding surface, then for the Lyapunov function

$$V = e^T P e = e^T P^{1/2} P^{1/2} e = \|\sqrt{P}e\|^2, \tag{5.1.1}$$

which implies that $\sqrt{V} = \|\sqrt{P}e\|$, $\sigma(e) = \sqrt{P}e$, and $\|\sigma\|_2 = \|\sqrt{P}e\|_2$ defines the distance from

[1] This chapter is the main contribution of the paper II referred in [8]

the sliding surface $\sigma(e) = 0$. The sliding surface is reached if

$$\frac{dV}{dt} = \frac{dV}{d\sigma}\frac{d\sigma}{dt} = \sigma^T \dot{\sigma} < 0 \tag{5.1.2}$$

in the neighborhood of surface $\sigma(e) = 0$ and

$$\dot{\sigma} = \frac{d\sigma}{de_o}\dot{e}. \tag{5.1.3}$$

Remark 5.1: The Lemma 5.1 can be studied in detail in [94], as it is the pivotal concept of SMO-based FTC techniques used in this work.

Proposition 5.1: If (G_o) is SMO gain for the output error estimation term (e_o), G_m the SMO gain of the discontinuous control term (ψ) is proposed to be of the form $G_m = \begin{bmatrix} -LT^T \\ T^T \end{bmatrix}$, the constant gain (γ) in the (ψ) term is constrained as $(\gamma \geq \eta_o - \|E_o\|\alpha)$ where $(\eta > 0)$ and P is a PD matrix, i.e., $(P > 0)$ of the form

$$P = \begin{bmatrix} P_1 & P_1 L \\ L^T P_1 & T^T P_o T + L^T P_1 L \end{bmatrix} > 0$$

which satisfies $(PA_o + A_o^T P < 0)$, then the estimation error $e(t)$ stays bounded and hence asymptotically stable.

Proof. Let V define the Lyapunov function for an augmented error system. The stability of the equilibrium requires the Lyapunov function to be positive definite, and its time derivative to be

negative or semi-negative-definite.

$$V(e) = e^T P e \tag{5.1.4}$$

$$\dot{V}(e) = \dot{e}^T P e + e^T P \dot{e} \tag{5.1.5}$$

Using $\dot{e}$ from Equation (4.1.8)

$$\dot{V}(e) = e^T (A_c - G_o C_c)^T P e + e^T P (A_c - G_o C_c) e - 2e^T P E_c f - 2e^T P D_c \xi + 2e^T P G_m \psi. \tag{5.1.6}$$

Using the definition of G_m as given in the statement of the proposition, and dropping the negative definite Lyapunov term because $Z = A_o^T P + P A_o < 0$, where $A_o = A_c - G_o C_c$, the remaining terms are still negative, and the time derivative of the Lyapunov function becomes an inequality, which is always easier to handle in terms of parametric independence.

$$\dot{V}(e) \leq -2e^T P E_c f - 2e^T P D_c \xi + 2e^T P G_m \psi \tag{5.1.7}$$

Using the definitions of (ψ, G_m, $PG_o = C_o^T P_o$, $PE_c = C_o^T P_o E_o$, and $e^T C_o^T = e_o$),

$$\dot{V}(e) \leq -2{e_o}^T C_o^T P_o E_o f - 2{e_o}^T C_o^T P_o D_o \xi - 2\gamma \| P_o e_o \|. \tag{5.1.8}$$

Taking norm and upper bounds $\|f\| < \alpha$, $\|\xi\| < \xi_o$

$$\dot{V}(e) \leq -2\|e_o\|[\gamma \|P_o C_o\| + \|P_o C_o E_o\| \alpha + \|P_o C_o D_o\| \xi_o]. \tag{5.1.9}$$

Let if $\gamma\|P_oC_o\| + \|P_oC_oE_o\|\alpha + \|P_oC_oD_o\|\xi_o \geq \eta_o\|P_oC_o\|$,

$$\gamma \geq \eta_o - \|E_o\|\alpha - \|D_o\|\xi_o. \tag{5.1.10}$$

Using the constraint on γ from equation(5.1.10) in Equation (5.1.9).

$$\dot{V}(e) \leq -2\eta_o\|e_o\|. \tag{5.1.11}$$

Because the Thau inequality ([95]) for the Lyapunov equation for any PD matrix P_o is defined for any vector x as [4, 94],

$$x^T P_o^{-1} x \geq \lambda_{min}(P_o^{-1})\|x\|_2^2.$$

The Lyapunov function in terms of the error function can be represented in the inequality form as: $(e^T Ze > \lambda_{min}(Z)\|e\|^2)$. Using the Thau inequality and Equation (5.1.11), the inequality version of Equation (5.1.6) becomes:

$$\dot{V}(e) \leq \lambda_{min}(Z)\|e\|^2 - 2\eta_o\|e_o\|, \tag{5.1.12}$$

which proves the stability (i.e., negative definiteness) of the time derivative of the Lyapunov function.

Since $\|x\| > \sqrt{\lambda_{min}(P^{-1})}\|x\|_2$ and can be seen in [94],[4].

$$\dot{V}(e) \leq \lambda_{min}(Z)\|e\|^2 - 2\eta_o\sqrt{\lambda_{min}(P_o^{-1})\|\sqrt{P_o}e_o\|} \tag{5.1.13}$$

$$\dot{V}(e) \leq \lambda_{min}(Z)\lambda_{min}(P^{-1})\|e\|^2 - 2\eta_o\sqrt{\lambda_{min}(P_o^{-1})}\|\sqrt{P_o}e_o\| \tag{5.1.14}$$

□

The equations (5.1.11) and its representation in terms of (5.1.14) show the asymptotic stability of the considered observer system.

Remark 5.2: Proposition 1 is analytical proof, particularly for the considered microgrid system with faulty and perturbed sensors using the same steps as performed by Yuri and Edwards in Proposition 3.1 [94], whereas the Thau inequality and observer can be studied in more detail in [95].

Theorem 5.1: Let $Z = A_oP + PA_o < 0$ such that $P > 0$ and the constant gain of the discontinuous switch term γ is constrained by $\gamma \geq \eta_o - \|E_o\|\alpha$, then the augmented error system (state error and stable filtered output error) dynamics defined by Equation (3.1.9) remains bounded, such that the error magnitude remains bounded within the set $X = \{\mathbf{e}|\|e\| \leq \frac{2\xi_o\|PD_c\|}{\lambda_{min}(Z)}\}$, and the Lyapunov function in vector form gives the constraint in the form of LMI $L_{i1} = \begin{bmatrix} A_o{}^TP + P(A_o) & PD_c \\ -D_c^TP & 0 \end{bmatrix} < 0$, where $A_o = A_c - G_oC_c$, the LMI is further modified by general algebraic Ricatti equation with additional control parameters to give LMI $L_{i2} = \begin{bmatrix} A_c{}^TP + PA - C_c^TF_1{}^{-1}C_c & Y \\ Y^T & F_1{}^{-1} \end{bmatrix} < 0$, and the iterative feasibility optimization or minimization of linear objective (i.e., trace) under LMI constraint L_{i2} gives the SMO gain for output estimation error term to be $G_o = P^{-1}C^TF_1{}^{-1}$, such that Y is constrained to $Y = C_c{}^TF_1{}^{-1^T} > 0$, where $(F_1 > 0)$.

Proof. Considering the Lyapunov function from Equation (5.1.6)

$$\dot{V}(e) = e^T(A_c - G_oC_c)Pe + e^TP(A_c - G_oC_c)e - 2e^TPE_cf - 2e^TPD_c\xi + 2e^TPG_m\psi,$$

Considering switch and fault terms from the above equation, i.e., Equation 5.1.6), let

$$T_{sf} = -2e^TPE_cf + 2e^TPG_m\psi \tag{5.1.15}$$

$T_{sf} = -2e^TPE_cf + 2e^TPG_m(-\gamma\frac{P_oe_o}{\|P_oe_o\|})$.

(Since $PG_o = C_o^TP_o$ and $PE_c = C_o^TP_oE_o$)

$T_{sf} = -2e^TC_o^TP_oE_of - 2\gamma\|C_oP_oe_o\|$,

Taking the norm, we use the Cauchy–Schwartz inequality and bounded fault with $\|f\| \leq \alpha$,

$T_{sf} = -2\|e_o\|(\|C_oP_oE_o\|\alpha + \|C_oP_o\|\gamma)$.

Because it is desired that the above term stays more negative $T_{sf} < 0$, for the negative definiteness of the time derivative of Lyapunov function in Equation (5.1.6), which is satisfied if

$\|P_oC_oE_o\|\alpha + \|P_oC_o\|\gamma > \eta_o\|P_oc_o\| \Rightarrow \gamma \geq \eta_o - \|E_o\|\alpha$. □

Furthermore, since $(A_o = A_c - G_oC_c)$, and if $(Z = A_oP + PA_o < 0)$ where $(P > 0)$, so dropping the negative T_{sf} terms, the Lyapunov function is still negative

$$\dot{V}(e) \leq e^T(A_c - G_oC_c)Pe + e^TP(A_c - G_oC_c)e - 2e^TPD_c\xi. \tag{5.1.16}$$

To show stability in terms of viable set form,

$$\dot{V}(e) \leq \lambda_{min}(Z)\|e\|^2 - 2\xi_o\|PD_c\|\|e\|. \tag{5.1.17}$$

$$\dot{V}(e) \leq \|e\|(\lambda_{min}(Z)\|e\| - 2\xi_o\|PD_c\|). \tag{5.1.18}$$

If $(\|e\|^2 > \frac{2\xi_o\|PD_c\|}{\lambda_{min}(Z)})$, we obtain $\dot{V} < 0$, which ensures that the error magnitude remains bounded for the set

$$X = \{\mathbf{e}|\|e\| \geq \frac{2\xi_o\|PD_c\|}{\lambda_{min}(Z)}\}$$

Using Equation (5.1.16) and expressing in terms of the vector quadratic function, LMIs can be determined.

$$\dot{V}(e) \leq \begin{bmatrix} e^T & \xi^T \end{bmatrix} \begin{bmatrix} A_oP + PA_o & PD_c \\ -D_c^TP & 0 \end{bmatrix} \begin{bmatrix} e \\ \xi \end{bmatrix} \tag{5.1.19}$$

The constraint is true if the matrix in the vector quadratic function is negative definite i.e.,

$$L_{i1} = \begin{bmatrix} A_oP + PA_o & PD_c \\ -D_c^TP & 0 \end{bmatrix} < 0. \tag{5.1.20}$$

The LMI in Equation (5.1.20) can be solved for the trace minimization-based algorithm given by [5] to determine the optimized gains of the SMO. However, for the LMIs to be optimized with trace minimization without the H_∞ constraint for the determination of traditional SMO gains,

it needs some modification. Applying the Schur complement to the LMI in Equation (5.1.20),

$$(A_c - G_o C_c)^T P + P(A_c - G_o C_c) \leq 0. \tag{5.1.21}$$

Because the LMI is not feasible in the actual form mentioned by L_{t1} in Equation (5.1.20) with a trace-minimization-based optimization algorithm, some modifications are required. By adding/subtracting the term $(C_c^T {F_1}^{-1} C_c)$ and two more Lyapunov stable terms in above Lyapunov equation to form a balanced algebraic Ricatti equation, i.e., $(Y F_1 Y^T)$ and (PWP) in the inequality, where $(Y = PG_o)$.

$$A_c^T P + P A_c - Y C_c - {C_c}^T Y^T + {C_c}^T {F_1}^{-1} C_c - C_c {F_1}^{-1} C_c + Y F_1 Y^T + P W^{-1} P \leq 0 \tag{5.1.22}$$

$${A_c}^T P + P A_c - C_c^T (Y^T - F_1^{-1} C_c) - Y(C_c - F_1 Y^T) - {C_c}^T {F_1}^{-1} C - Y F_1 Y^T + P W^{-1} P \leq 0 \tag{5.1.23}$$

Using/constraining $C_c - F_1 Y^T = 0$, which is equivalent to $Y^T - {F_1}^{-1} C_c = 0$ gives the Luenberger SMO gain

$$G_o = P^{-1} C_c^T {F_1}^{-1}. \tag{5.1.24}$$

Parameters such as the Lyapunov matrix P and matrix F are missing and need to be determined. Using the constraint $C_c - F_1 Y^T = 0$, Equation (5.1.23) becomes:

$${A_c}^T P + P A_c - C_c^T {F_1}^{-1} C_c + P W^{-1} P \leq 0. \tag{5.1.25}$$

Applying Schur complement on LMI in Equation (5.1.25), and the constraint $F_1^{-1} C_c = Y^T$,

$$L_{i2} = \begin{bmatrix} A_c P + P A_c - C_c^T Y^T & P \\ P & -W \end{bmatrix} < 0. \tag{5.1.26}$$

Remark 5.3: The LMI L_{i2} is optimized by using iterative convex feasibility optimization or alternatively trace minimization, as explained by an algorithm in ([5]), to determine the unknown parameters such as Lyapunov matrix P and matrix F, which are used to determine Luenberger gain G_o of SMO. Moreover, the discontinuous term gain, $G_m = \begin{bmatrix} -LT^T \\ T^T \end{bmatrix}$ as discussed in Proposition 1 can also be determined, as the parameter matrix L is also determined from the part P_{12} of Lyapunov matrix P by the relation ($L = P_{11}^{-1} P_{12}$), where the orthogonal matrix T is can be determined by QR factorization.

The next subsection discusses the H_∞ enhanced trace minimization of LMIs to attain the robustness of the SMO for fault estimation with disturbance rejection.

5.1.1 H_∞ Optimized Robust Sliding Mode Observer Gains (Using LMIs)

H_∞ is a robust control criterion that may have several meanings with reference to context; however, in this work, it is desired that the fault detection and estimation be ensured with robustness against disturbances, whereas the H_∞ gain will ensure an upper bound of the disturbance voltage/current that will be suppressed to ensure the fault detection/estimation task. The method of incorporating H_∞ criteria may also have different approaches; however, this study uses a game-theoretic basis [2]. The criteria are incorporated in the Lyapunov function to derive the LMIs that are convex optimized (using the LMI-optimization toolbox in Matlab) for the determination of the SMO gains.

Definition 5.1: H_∞ based disturbance attenuation problem can be put into the formulation as a two-player-zero-sum differential game with disturbance ξ and Luenberger observer gain G_o are two players, respectively, where the SMO gains G_o, G_m are required to be designed to minimize the game /cost functional.

Lemma 5.2: The maximum robustness attenuation problem

$$H_\infty = sup_{[\xi \neq 0, f=0]} \frac{\|r_H\|_{2,[0.t1]}}{\|\xi\|_{2,[0,t1]}} \leq \alpha \tag{5.1.27}$$

for the system given in Equation (3.1.6), is satisfied, if the cost functional

$$f_H(G_o, G_m, \xi) = \int ({r_H}^T r_H - \alpha \xi^T \xi) dt, (for) f = 0. \tag{5.1.28}$$

is smaller than or equal to zero for any possible disturbance, where (α) is the (H_∞) parameter and $(r_H = Hr(t) = He_o = HC_c e)$ is the output estimation error. The problem is now viewed as a two-player-zero-sum differential game with the above-defined cost function in Equation (5.1.28), where the minimizing player minimizes the functional through (G_o, G_m) and the maximizing player tries to maximize the function through ξ. The details can be seen in Problem 3.1 in [2].

Theorem 5.2: Let $Z = A_o P + P A_o < 0$, where $P > 0$, and if $(H > 0)$, then the augmented error system dynamics defined by Equation (4.1.7) remains asymptotically stable, and if the Lyapunov function in vector form is enhanced with H_∞ constraint, the disturbance attenuation

gives the constraint in the form of LMI

$$L_{i3} = \begin{bmatrix} A_o P + P A_o + C_c^T H^T H C_c & -P D_c \\ -D_c^T P & -\alpha I \end{bmatrix} < 0.$$

which is further modified by the Riccati equation with additional control parameters to give constraint LMI

$$L_{i4} = \begin{bmatrix} {A_c}^T P + P A_c - C_c^T Y^T & P D_c \\ D_c^T P & -\alpha^{-1} \end{bmatrix} < 0,$$

and the iterative minimization of linear objective (i.e., trace) under LMI constraint L_{i4} gives the Luenberger gain of output error estimation term as $G_o = P^{-1} C^T F'^{-1}$, where $Y = P G_o > 0$ is constrained to $Y = {C_c}^T F > 0$ and $W = P \bar{D} P$.

Proof: Because V is a PD Lyapunov function, the negative definiteness of its derivative determines the stability of the system. If the H_∞ criterion is used to enhance the robustness of the traditional SMO, the criterion in terms of the norm is defined by

$$\|r_H(t)\| \leq \alpha \|\xi(t)\|. \tag{5.1.29}$$

Because the LMI solver constraints for feasible optimization require the residual to be of the form

$$r_H(t) \triangleq H r(t), \tag{5.1.30}$$

where the output estimation error, i.e., residual is defined by,

$$r(t) = e_o = y_o - y_c = C_c e$$

and H is a scaling matrix. The Lyapunov function in inequality form in Equation (5.1.16) is added with the $H\infty$ criterion according to Lemma 5.2 as follows:

$$\dot{V} + {r_H}^T r_H - \alpha \xi^T \xi \leq 0 \tag{5.1.31}$$

$$\dot{V}(e) \leq e^T[(A_c - G_o C_c)P + P(A_c - G_o C_c)]e + e^T C_c^T H^T H C_c e - 2e^T P D_c \xi - \alpha \xi^T \xi \tag{5.1.32}$$

where

$$H^T H = F' = \begin{bmatrix} 0 \\ \\ F \end{bmatrix}. \tag{5.1.33}$$

The matrix $F \in \mathbb{R}^{p*p}$ is a subpart of matrix H, which provides a control on the residual signal for stability purposes. However, as discussed above, in the definition of $r_H(t)$, it is suggested by the LMI solver to meet the conditions of feasible optimization.

and if

$$H = \begin{bmatrix} H_1 \\ \\ H_2 \end{bmatrix}, {r_H}^T r_H = e^T {C_c}^T H^T H C_c e = e^T C_c F' C_c e, \tag{5.1.34}$$

where $H \in \mathbb{R}^{n_c * p_c}, H_1 \in \mathbb{R}^{n*p}, H_2 = F \in \mathbb{R}^{p*p}$,

$$\dot{V}(e) \leq \begin{bmatrix} e^T & \xi^T \end{bmatrix} \begin{bmatrix} A_o P + P A_o + C_c^T F' C_a & -P D_c \\ \\ -D_c^T P & -\alpha I \end{bmatrix} \begin{bmatrix} e \\ \\ \xi \end{bmatrix}. \tag{5.1.35}$$

The LMI, which can be solved for feasibility or trace minimization-based optimization, to determine the optimized parameters of the matrix is

$$L_{i3} = \begin{bmatrix} A_o P + P A_o + C_c^T F' C_c & -P D_c \\ -D_c^T P & -\alpha I \end{bmatrix} < 0. \tag{5.1.36}$$

The Schur complement can be applied to convert any bi-linearity to linearity. Applying Schur complement on LMI in Equation (5.1.36),

$$(A_c - G_o C_c)^T P + P(A_c - G_o C_c) + C_c^T F'^{-1} C_c + PD(\alpha^{-1} I) D^T P \leq 0. \tag{5.1.37}$$

Using $(Y = PG_o)$ and adding subtracting the term $(YF'^{-1}Y^T)$,

$$A_c{}^T P + PA - C_c(Y - C_c^T F') - Y^T(C_c^T - YF'^{-1}) + YF'^{-1}Y^T + P\bar{D}P \leq 0, \tag{5.1.38}$$

where $\bar{D} = D_c(\alpha I) D_c^T$.

Setting $(Y - C_c^T F' = 0)$ which is equivalent to $(C_c^T - YF'^{-1} = 0)$ gives,

$$G_o = P^{-1} C_c^T F'^{-1}, \tag{5.1.39}$$

and the inequality in 5.1.38 reduces to,

$$A_c{}^T P + PA_c - YF'^{-1}Y^T + W \leq 0 \tag{5.1.40}$$

where $W = P\bar{D}P$.

Using Schur complement on inequality and $C^T = YF'^{-1}$,

$$L_{i4} = \begin{bmatrix} {A_c}^T P + P A_c - C^T Y^T & P D_c \\ D_c^T P & -\alpha I \end{bmatrix} < 0. \tag{5.1.41}$$

Remark 5.4: Trace minimization based optimization of Ricatti equation-motivated modification of LMIs, for determination of SMO gains is presented by [5], and $H\infty$ based feasibility optimization of LMIs for determination of SMO gains is used by [4]. However, this work combines the application of both, i.e., to carry out the feasibility or the linear objective (i.e., trace) minimization-based iterative convex optimization of Ricatti equation-based modification of $H\infty$ enhanced LMIs, which can work or maybe tested on generally any system, and particularly here being applied on MG under consideration.

Summary: The modified gains are used for fault detection and estimation SMOs presented in chapter 4, followed by a detailed and modified fault-estimation process in chapter 7, along with the reduced order sliding motion with finite time reachability.

CHAPTER 6

Sensitivity of Fault Detection, Robustness to Disturbance and Stability Analysis using HJIE and Game Theoretic Parameters

6.1 Stability Analysis and Determination of Robust to Disturbance/Fault Sensitive SMO Gains

[1] **Lemma 6.1:** For general stability analysis of SMOs, using Proposition (1) from [8], if (G_o) is the gain of SMO for output estimation error injection term $(\boldsymbol{e_o})$, G_m the SMO gain of discontinuous control term (ψ) is proposed to be of the form $G_m = \begin{bmatrix} -LT^T \\ T^T \end{bmatrix}$, the constant gain (γ) of (ψ) term is constrained as $(\gamma \geq \eta_o - \|E_o\|\alpha')$ where $(\eta > 0)$ and P is a positive definite matrix, i.e., $(P > 0)$ of the form

$$P = \begin{bmatrix} P_1 & P_1 L \\ L^T P_1 & T^T P_o T + L^T P_1 L \end{bmatrix} > 0,$$

which satisfies $(PA_o + A_o^T P < 0)$, then the estimation error $\boldsymbol{e}(t)$ is asymptotically stable.

Remark 6.1: The Lyapunov matrix (P) is basically manipulating the energy of the error estimation system, i.e., $\boldsymbol{e}^T\boldsymbol{e}$, as P is used as the scaling matrix in the Lyapunov function. i.e., $V = \boldsymbol{e}^T P \boldsymbol{e}$, which requires to be proved positive definite, i.e., the one with Eigen-values in the left half plane ensuring stability. Similarly, the first derivative needs to be proved to be negative or semi-negative definite according to Lyapunov theory to prove its stability. The equation for the derivative of the Lyapunov function i.e. dV/dt is mathematically manipulated to make the equation instead an inequality to prove its negative definiteness to achieve freedom of controllable parameters. This can be done by dropping some of the terms for simplification by attaining the respective conditions from the dropped terms and by ensuring that the rest of the terms are

[1] This chapter is the main contribution of the paper II referred in [10]

still negative. The vector algebraic inequality is then transformed to LMIs, which are convex optimized using the MATLAB toolbox to determine the unknown design Lyapunov matrix P (with a higher degree of freedom being in the inequality form of Lyapunov equation fromwhich it is determined). It is important due to the reason that the gains of SMO (G_o and G_m) are determined from the Lyapunov matrix (P), which ensures the proper state/output/error/fault/disturbance estimation by achieving the sliding mode required for the suitable estimation process. The convex optimization tools and solvers are mentioned in Appendix A.5.

Now we have to analyze the system using the criteria of robustness to disturbance H_∞, the criteria of sensitivity to faults $H-$, and the compromised criteria $H-/H_\infty$ for fault diagnosis and tolerance analysis. The theory depends more on Game Theoretic estimation being utilized in Hamilton–Jacobi–Isaacs-Equation (HJIE) and to convert the equalities to inequalities for better handling and more design freedom.

6.1.1 H_∞ Robustness Analysis

Lemma 6.2: According to Problem 3.1 in [2], for the system defined in Equation (3.1.11), the maximum robustness attenuation problem

$$H_\infty = sup_{[\boldsymbol{f}=0,\boldsymbol{\xi}\neq 0]} \frac{\|\boldsymbol{r_K}\|_{2,[0,t]}}{\|\boldsymbol{\xi}\|_{2,[0,t]}} \leq \alpha' \tag{6.1.1}$$

is satisfied, if the cost functional

$$H_o(G_o, \boldsymbol{\xi}) = \int (\boldsymbol{r_K}^T \boldsymbol{r}_K - \alpha'^2 \boldsymbol{\xi}^T \boldsymbol{\xi}) dt; (for) \boldsymbol{f} = 0 \tag{6.1.2}$$

is smaller than or equal to zero for any possible disturbance, where (α') is (H_∞) parameter and residual signal $(\boldsymbol{r}_K = K\boldsymbol{r}(t) = KC_e\boldsymbol{e})$ in this case is state estimation error. The problem is now viewed/explained as two player zero-sum differential game with the above-defined cost functional in Equation (6.1.2), where the maximizing player tries to maximize the functional through ξ and the minimizing player minimizes the functional through (G_o, G_m) [37]. Then, using the concepts of dynamic game theory, the cost function in Equation (6.1.2) gives the pair of strategies (G_o^*, ξ^*), providing a saddle-point solution

$$H_o(G_o, \xi^*) \leq H_o(G_o^*, \xi^*) \leq H_o(G_o^*, \xi). \tag{6.1.3}$$

Definition 6.1: (Saddle Point) In mathematics, a minimax point or saddle point is a point on the surface of the graph of a function where the slopes (derivatives) in the orthogonal directions are all zero (a critical point), but which is not a local extremum of the function. The saddle point of the problem is taken in terms of cost functionals. Its mathematical details are shifted in the Appendix A.6.

Lemma 6.3: Considering the cost functional of disturbance attenuation problem from Equation (6.1.2), constraining $(H_o(G_o, \xi) < 0)$ and using the definition, for any general state x^*

$$\frac{dV_1(\boldsymbol{x}^*, t)}{dt} = \frac{\partial V_1(\boldsymbol{x}^*, t)}{\partial t} + \frac{\partial V_1(\boldsymbol{x}^*, t)}{\partial \boldsymbol{x}^*}\frac{\partial \boldsymbol{x}^*}{\partial t}.$$

The inequality version of HJI equation , as mentioned in Equation (A.6.1) in Appendix A.6, is

$$\frac{-\partial V_1(\boldsymbol{x}^*(t), t)}{\partial t} \geq \frac{\partial V_1(\boldsymbol{x}^*, t)}{\partial \boldsymbol{x}^*}\dot{\boldsymbol{x}}^* + \boldsymbol{r_K}^T\boldsymbol{r_K} - \alpha'^2\boldsymbol{\xi}^T\xi. \tag{6.1.4}$$

Remark 6.2: The derivation for H_∞ constrained inequality version of HJIE is given in Appendix A.6.3 The problem can be studied in detail in [2, 33, 38].

Remark 6.3: Considering Appendix A.5, using the HJIE in Equations (A4) and (A7), the Hamiltonians in Equations (A5) and (A7) and the disturbance attenuation/fault sensitivity constraints in Equations (6.1.2) and (6.1.13), the analytical solution for gain G_o will be dependent on states that are undesired (theoretically by Luenberger linear observer theory). However, the inequality version of HJIE will give more freedom in choosing the Lyapunov function $V_1(e,t)$ and hence more freedom in the design of the sliding mode observer gain G_o being state independent.

Remark 6.4: (Approach of Using HJIE, H_∞, $H-$ and Game Theory in This Study:) The approach used here is to design the observers for linear/non-linear systems based on game theoretic saddle point estimation. The H_∞ and $H-$ parameters deal with the extreme cases in a way that they provide robustness to worst-case disturbances and sensitivity to minimum faults. These parameters in inequality form are similar in nature to the saddle point of the game theory, as described by Equations (6.1.3) and (6.1.14). The H_∞ and $H-$ constraints are also part of the Hamiltonians (in Equations (A.6.2) and (A.6.4) in Appendix A.6) along with the Lyapunov (energy) function. According to the approach used by [2], the Hamiltonian and its derivative w.r.t faults ($\boldsymbol{f}$)/disturbances ($\boldsymbol{\xi}$)/SMO gain (G_o) following the H_∞ and $H-$ constraints can let us determine the optimal values of faults/disturbances, i.e., ($\boldsymbol{f}^*$, $\boldsymbol{\xi}^*$, G_o), by its minimization. However, this work instead uses the approach that the H_∞ constraint in inequality form, inspired by the saddle point, is manipulated to form the inequality version of HJIE, which has the Hamiltonian incorporated in it as well.

The resulting HJIE consists of the faults/disturbances, Lyapunov function, and output estima-

tion error (e_o) as variables. The inequality version of this HJIE not only ensures Lyapunov stability but also gives the LMIs, which are convex and optimized using the MATLAB toolbox to find the optimized SMO gains, which are used to estimate the states/outputs/state errors.

The game theoretic saddle point's approach for incorporating the H_∞ and $H-$ norms also has the application for the considered faulty and perturbed systems due to the reason that faults and disturbances are unknown. In this case, the worst-case fault and disturbance values are used for observer/filter designs for robust residual generation and fault/disturbance estimations. The SMO in reduced order is used to reconstruct faults/disturbances, while following the constraints of fault-detection-sensitivity and rejecting the effects of disturbances through the observer gains. The proof for HJIE and some more details are given in the appendix in Appendix A.3 and A.6.

Theorem 6.1 If V_1 defines the positive definite Lyapunov function which satisfies the HJIE in Equation (6.1.4) constrained with disturbance attenuation problem defined in Equation (6.1.2), then the Lyapunov function in vector form gives LMI

$$L_{RD} = \begin{bmatrix} (A_c - G_oC_c)Q + Q(A_c - G_oC_c) + C_a^T F C_a & -3QE_c & -QD_c \\ -E_c^T Q & 0 & 0 \\ -D_c^T Q & 0 & -\alpha'^2 I \end{bmatrix} \leq 0,$$

which is convex optimized iteratively to give a robust set value of the worst case disturbance SMO gain defined by $G_o = Q^{-1}C_c^T F'^{-1}$.

Proof Consider the general HJIE in Equation (6.1.4) with the cost functional in Equation (6.1.2) to ensure maximum robustness to a worst case disturbance

$$\frac{\partial V_1(\boldsymbol{e}(t),t)}{\partial t} + \frac{\partial V_1(\boldsymbol{e}(t),t)}{\partial e}\dot{\boldsymbol{e}} + \boldsymbol{r_K}^T\boldsymbol{r_K} - \alpha'^2\boldsymbol{\xi}^T\boldsymbol{\xi} \leq 0.$$

Since $(V_1 = e^T Qe)$ and $(\frac{\partial V_1(e,t)}{\partial t} = \dot{V}_1(e,t) = \dot{e^T}Qe + e^T Q\dot{e})$

Using the above given H_∞ constrained HJIE equation,

$$\dot{e^T}Qe + e^T Q\dot{e} + (2\dot{e^T})Qe - \alpha'^2 \xi^T \xi + e^T C_c^T K^T K C_c e \leq 0, \tag{6.1.5}$$

where $K^T K = F' = \begin{bmatrix} 0 \\ F \end{bmatrix}$ and the matrix $F \in \mathbb{R}^{p*p}$ as the subpart of matrix K,

$$\dot{e^T}Qe + 3e^T Q\dot{e} - \alpha'^2 \xi^T \xi + e^T C_c^T F' C_c e \leq 0. \tag{6.1.6}$$

Substituting equations for $\dot{e}$,

$$e^T (A_c - G_o C_c)^T Qe + 3e^T Q(A_c - G_o C_c)e - f^T E_c^T Pe - \xi^T D_c^T Qe + \psi G_n^T Qe$$

$$-3e^T Q E_c f - 3e^T Q D_c \xi + 3e^T Q G_n \psi + e^T C_c^T F' C_c e - \alpha'^2 \xi^T \xi \leq 0. \tag{6.1.7}$$

The inequality in vector form gives:

$$\begin{bmatrix} e^T & f^T & \xi^T \end{bmatrix} \begin{bmatrix} (A_c - G_o C_c)Q + Q(A_c - G_o C_c) + C_c^T F' C_c & 3QE_c & -QD_c \\ -E_c^T Q & 0 & 0 \\ -D_c^T Q & 0 & -\alpha'^2 I \end{bmatrix} \begin{bmatrix} e \\ f \\ \xi \end{bmatrix} \leq 0. \tag{6.1.8}$$

The LMI obtained from the vector Lyapunov equation is

$$L_{RD} = \begin{bmatrix} (A_c - G_oC_c)Q + P(A_c - G_oC_c) + C_c^T F' C_c & 3QE_c & -QD_c \\ -E_c^T Q & 0 & 0 \\ -D_c^T Q & 0 & -\alpha'^2 I \end{bmatrix} \leq 0. \quad (6.1.9)$$

As according to the cost functional in Equation (24) $f = 0$, dropping the disturbance terms gives the LMI

$$\begin{bmatrix} (A_c - G_oC_c)Q + Q(A_c - G_oC_c) + C_c^T F' C_c & -QD_c \\ -D_c^T Q & -\alpha'^2 I \end{bmatrix} \leq 0. \quad .(6.1.10)$$

Remark 6.5: The LMIs obtained using the above process are processed further with an algebraic Riccati equation according to Theorem (5.2) in [8] to avoid optimization infeasibility issues with (H_∞) criterion LMIs, specific to the system. The definition and a brief mathematical explanation of the Riccati equation is given in Appendix A.7

The modified LMI is thus given by

$$L_{RDO} = \begin{bmatrix} A_cQ + QA_c - 3YC_c & -QD_c \\ -D_c^T Q & -3\alpha'^2 I \end{bmatrix} \leq 0, \quad (6.1.11)$$

where $Y = QG_o$.

The LMI is solved by iterative convex optimization to determine the robust to disturbance sliding mode observer gains. The tools and solvers used are mentioned in Appendix A.5

6.1.2 $H-$Minimum Fault Sensitivity Analysis

Lemma 6.4: According to Problem 3.2 in [2], for the system defined in Equation (3.1.11), the maximum sensitivity to minimum fault problem

$$inf_{[\xi=0, f\neq 0]} \frac{\|r_K\|_{2,[0,t]}}{\|f\|_{2,[0,t]}} \geq \beta'^2 \tag{6.1.12}$$

is satisfied, if the cost functional

$$H_o(G_o, f) = \int ({r_K}^T r_K - \beta' f^T f) dt; (\xi = 0) \tag{6.1.13}$$

is greater than or equal to zero for each possible fault. This can be viewed as a two-player zero-sum differential game with the cost functional. The maximizing player maximizes the functional through G_o and the minimizing player tries to minimize the functional through f. Then, using the concepts of dynamic game theory, the cost functional in Equation (6.1.13) gives the pair of strategies (H^*, f^*), providing a saddle-point solution, i.e.,

$$H_o(G_o, f^*) \leq H_o(G_o^*, f^*) \leq H_o(G_o^*, f). \tag{6.1.14}$$

Its mathematical detail is also shifted in the appendix A.6.

Lemma 6.5: Considering the cost functional of fault sensitivity problem from Equation (6.1.13), constraining $(H_o(G_o, f) < 0)$ and using the definition, for any general state x^*

$$\frac{dV_2(x^*, t)}{dt} = \frac{\partial V_2(x^*, t)}{\partial t} + \frac{\partial V_2(x^*, t)}{\partial x^*} \frac{\partial x^*}{\partial t}.$$

The inequality version of the HJIE Equation in (6.1.15) is

$$\frac{-\partial V_2(e(t),t)}{\partial t} \leq \frac{\partial V_2(\boldsymbol{e}(t),t)}{\partial \boldsymbol{e}}\dot{\boldsymbol{e}} + \boldsymbol{r_K}^T\boldsymbol{r_K} - \beta'^2\boldsymbol{f}^T\boldsymbol{f}. \tag{6.1.15}$$

Remark 6.6: The mathematical proof for the $H-$ constrained inequality version of HJIE is given in Appendix A.6.4. The problem can be studied in detail in [2, 33, 38].

Theorem 6.2: If V_2 defines the positive definite Lyapunov function that satisfies the HJIE in Equation (6.1.15) constrained with the maximum sensitivity of the minimum set fault problem defined in Equation (6.1.13), then the Lyapunov function in vector form gives LMI

$$L_{SF} = \begin{bmatrix} -(A_c - G_oC_c)P - P(A_c - G_oC_c) - C_c^TF'C_c & 3PE_c & PD_c \\ E_c^TP & \beta'^2I & 0 \\ D_c^TP & 0 & 0 \end{bmatrix} \leq 0,$$

which in a reduced form is convex optimized iteratively to give a sensitive set value of minimum case fault SMO gain defined by $G_o = P^{-1}C_c^TF'^{-1}$.

Proof: Consider the general HJIE in Equation (6.1.15) with the cost functional in Equation (6.1.13) to ensure maximum sensitivity to minimum case fault

$$\frac{-\partial V_2(e(t),t)}{\partial t} \leq \frac{\partial V_2(\boldsymbol{e}(t),t)}{\partial \boldsymbol{e}}\dot{\boldsymbol{e}} + \boldsymbol{r}_K{}^T\boldsymbol{r}_K - \beta'^2\boldsymbol{f}^T\boldsymbol{f},$$

Since $(V_2 = \boldsymbol{e}^T\boldsymbol{P}\boldsymbol{e})$ and $(\frac{\partial V_2(\boldsymbol{e},t)}{\partial t} = \dot{V}_2(\boldsymbol{e},t) = \dot{\boldsymbol{e}^T}\boldsymbol{P}\boldsymbol{e} + \boldsymbol{e}^T\boldsymbol{P}\dot{\boldsymbol{e}})$.

Using the above given $H-$ constrained HJIE equation,

$$\dot{\boldsymbol{e}^T}\boldsymbol{P}\boldsymbol{e} + \boldsymbol{e}^T\boldsymbol{P}\dot{\boldsymbol{e}} \leq (2\dot{\boldsymbol{e}^T})\boldsymbol{P}\boldsymbol{e} - \beta'^2\boldsymbol{f}^T\boldsymbol{f} + \boldsymbol{e}^TC_c^TK^TKC_c\boldsymbol{e}, \tag{6.1.16}$$

$$\dot{\boldsymbol{e}}^T P\boldsymbol{e} + 3\boldsymbol{e}^T P\dot{\boldsymbol{e}} + e^T C_c^T F' C_c e - \beta'^2 \boldsymbol{f}^T \boldsymbol{f} \geq 0, \tag{6 1.17}$$

$$-\dot{\boldsymbol{e}}^T P\boldsymbol{e} - 3\boldsymbol{e}^T P\dot{\boldsymbol{e}} - e^T C_c^T F' C_c e + \beta'^2 \boldsymbol{f}^T \boldsymbol{f} \leq 0. \tag{6.1.18}$$

Substituting equations for $\dot{e}$,

$$3e^T(A_c - G_o C_c)P\boldsymbol{e} + 3\boldsymbol{e}^T P(A_c - G_o C_c)\boldsymbol{e} - \boldsymbol{f}^T E_c^T P\boldsymbol{e} - \boldsymbol{\xi}^T D_c^T P\boldsymbol{e} + \psi G_n^T P\boldsymbol{e} -$$

$$3e^T P E_c \boldsymbol{f} - 3\boldsymbol{e}^T P D_c \boldsymbol{\xi} + 3\boldsymbol{e}^T P G_n \psi + \boldsymbol{e}^T C_c^T F' C_c \boldsymbol{e} - \beta'^2 \boldsymbol{f}^T \boldsymbol{f} \leq 0. \tag{6.1.19}$$

The inequality in vector form gives

$$\begin{bmatrix} \boldsymbol{e}^T & \boldsymbol{f}^T & \boldsymbol{\xi}^T \end{bmatrix} \begin{bmatrix} -(A_c - G_o C_c)P - P(A_c - G_o C_c) - C_c^T F' C_c & 3PE_c & PD_c \\ E_c^T P & \beta'^2 I & 0 \\ D_c^T P & 0 & 0 \end{bmatrix} \begin{bmatrix} \boldsymbol{e} \\ \boldsymbol{f} \\ \boldsymbol{\xi} \end{bmatrix} \leq 0. \tag{6.1.20}$$

The LMI obtained from the vector Lyapunov equation is

$$L_{SF} = \begin{bmatrix} -(A_c - G_o C_c)P - P(A_c - G_o C_c) - C_c^T F' C_c & 3PE_c & PD_c \\ E_c^T P & \beta'^2 I & 0 \\ D_c^T P & 0 & 0 \end{bmatrix} \leq 0. \tag{6.1.21}$$

According to the cost functional in Equation (6.1.13) $\xi = 0$, then dropping the disturbance terms

gives the LMI to be optimized

$$L_{SFO} = \begin{bmatrix} -(A_c - G_oC_c)P - P(A_c - G_oC_c) - C_c^T F' C_c & PE_c \\ E_c^T P & \beta'^2 I \end{bmatrix} \leq 0. \tag{6.1.22}$$

The LMI is solved by iterative convex optimization to determine the fault sensitive sliding mode observer gains

6.1.3 Theorem 6.3: H_- / H_∞ Criteria Based on HJIE for Observer Design

If $V_1 = \boldsymbol{e}^T P \boldsymbol{e}$ and $V_2 = \boldsymbol{e}^T Q \boldsymbol{e}$ define the positive definite Lyapunov functions that satisfy the HJIEs in Equations (6.1.4) and (6.1.15) constrained with disturbance attenuation and minimum sensitivity problems defined in Equations (6.1.2) and (6.1.13), respectively, then the Lyapunov functions in vector form gives LMIs

$$L_{SF} = \begin{bmatrix} -(A_c - G_oC_c)P - P(A_c - G_oC_c) - C_c^T F' C_c & 3PE_c & PD_c \\ E_c^T P & \beta'^2 I & 0 \\ D_c^T P & 0 & 0 \end{bmatrix} \leq 0$$

and $L_{RD} = \begin{bmatrix} (A_c - G_oC_c)Q + Q(A_c - G_oC_c) + C_c^T F' C_c & 3QE_c & -QD_c \\ -E_c^T Q & 0 & 0 \\ -D_c^T Q & 0 & \alpha'^2 I \end{bmatrix} \leq 0.$ which in a modified and reduced form are a convex optimized iteratively as a mixed problem to give a compromised form of SMO gains G_o and G_m, which possesses robustness to worst case disturbance along with sensitivity to minimum fault at the same time. The Luenberger gain G_o is defined

by $G_o = P^{-1}C_c^T F'^{-1}$ in Theorem 6.2.

Proof. Considering the general HJIEs in Equations (6.1.4) and (6.1.15) with cost functions in Equations (6.1.2) and (6.1.13) to ensure maximum robustness to worst case disturbance and sensitivity to minimum fault at the same time

Let, if the Lyapunov functions in terms of positive definite matrices, $(P > 0)$ and $(Q > 0)$ be $V_1 = \boldsymbol{e}^T P \boldsymbol{e}$ and $V_2 = \boldsymbol{e}^T Q \boldsymbol{e}$.

Using the $H-$ constrained HJIE inequality version (6.1.15) and vector form from Equation (6.1.20),

$$-3\boldsymbol{e}^T(A_c - G_o C_c)P\boldsymbol{e} - 3\boldsymbol{e}^T P(A_c - G_o C_c)\boldsymbol{e} + \boldsymbol{f}^T E_c^T P\boldsymbol{e} + \boldsymbol{\xi}^T D_c^T P\boldsymbol{e} - \psi G_n^T P\boldsymbol{e} - 3\boldsymbol{e}^T P E_c \boldsymbol{f} - 3\boldsymbol{e}^T P D_c \boldsymbol{\xi} - 3\boldsymbol{e}^T P G_n \psi - \boldsymbol{e}^T C_c^T F' C_c \boldsymbol{e} + \beta'^2 \boldsymbol{f}^T \boldsymbol{f} \leq 0.$$

$$\begin{bmatrix} \boldsymbol{e}^T & \boldsymbol{f}^T & \boldsymbol{\xi}^T \end{bmatrix} \begin{bmatrix} -(A_c - G_o C_c)P - P(A_c - G_o C_c) - C_c^T F' C_c & 3PE_c & PD_c \\ E_c^T P & \beta'^2 I & 0 \\ D_c^T P & 0 & 0 \end{bmatrix} \begin{bmatrix} \boldsymbol{e} \\ \boldsymbol{f} \\ \boldsymbol{\xi} \end{bmatrix} \leq 0.$$

Using the H_∞ constrained HJIE inequality version (6.1.4) and vector form from Equation (6.1.8),

$$\boldsymbol{e}^T(A_c - G_o C_c)^T Q\boldsymbol{e} + 3\boldsymbol{e}^T Q(A_c - G_o C_c)\boldsymbol{e} - \boldsymbol{f}^T E_c^T P\boldsymbol{e} - \boldsymbol{\xi}^T D_c^T Q\boldsymbol{e} + \psi G_n^T Q\boldsymbol{e} + 3\boldsymbol{e}^T P E_c \boldsymbol{f} - 3\boldsymbol{e}^T P D_c \boldsymbol{\xi} + 3\boldsymbol{e}^T P G_n \psi + \boldsymbol{e}^T C_c^T F' C_c \boldsymbol{e} - \alpha^2 \boldsymbol{\xi}^T \boldsymbol{\xi} \leq 0.$$

$$\begin{bmatrix} \boldsymbol{e}^T & \boldsymbol{f}^T & \boldsymbol{\xi}^T \end{bmatrix} \begin{bmatrix} (A_c - G_o C_c)Q + Q(A_c - G_o C_c) + C_c^T F' C_c & -3QE_c & -QD_c \\ -E_c^T Q & 0 & 0 \\ -D_c^T Q & 0 & -\alpha'^2 I \end{bmatrix} \begin{bmatrix} \boldsymbol{e} \\ \boldsymbol{f} \\ \boldsymbol{\xi} \end{bmatrix} \leq 0.$$

The LMIs obtained for the mixed $H-/H_\infty$ problem are the same as given by Equations (6.1.22)

and (6.1.11) are,

$$L_{SF} = \begin{bmatrix} -(A_c - G_o C_c)P - P(A_c - G_o C_c) - C_c^T F' C_c & 3PE_c & PD_c \\ E_c^T P & \beta'^2 I & 0 \\ D_c^T P & 0 & 0 \end{bmatrix} \leq 0.$$

$$L_{RD} = \begin{bmatrix} (A_c - G_o C_c)Q + Q(A_c - G_o C_c) + C_c^T F' C_c & -3QE_c & -QD_c \\ -E_c^T Q & 0 & 0 \\ -D_c^T Q & 0 & -\alpha'^2 I \end{bmatrix} \leq 0.$$

The LMIs to be optimized in reduced and modified forms are given in Equations (6.1.11) and (6.1.22) to give gains of SMOs following the mixed constraint, i.e., are sensitive to faults and robust to disturbance at the same time. □

Remark 6.7: According to Algorithm 5.1.1. in [33] for the mixed problem with $H - /H_\infty$ constraint, both inequalities are taken either greater than zero or less than zero with signs of terms being reversed for one of the constraints according to the HJIE equation, so that LMI optimization stays possible along with a condition on Lyapunov matrices as $P = Q$.

Remark 6.8: The algorithm used for optimization is in [33], which mainly imposes the condition on Lyapunov matrices P=Q.

Summarizing Remark: The SMO gains, which are robust to disturbances and sensitive to faults are determined by convex optimizations of the respective LMIs presented in Theorems 6.1-6.3 subject to feasibility constraints These gains are used in both the detection and estimation SMOs presented in chapter 4. The next chapter discusses in detail the stability and finite-time

reachability of fault estimation SMO in sliding mode.

CHAPTER 7

Finite Time Reachability and Fault Estimation

7.1 Reduced Order Sliding Motion

[1]. The error system augments state/ stable filtered output error vectors that is,

$$\begin{bmatrix} \dot{e}_s \\ \dot{e}_o \end{bmatrix} = \begin{bmatrix} A_{11} & A_{12} \\ A_{21} & A_{22} \end{bmatrix} \begin{bmatrix} e_s \\ e_o \end{bmatrix} - \begin{bmatrix} G_1 \\ G_2 \end{bmatrix} \epsilon_o - \begin{bmatrix} 0 \\ E_o \end{bmatrix} f - \begin{bmatrix} 0 \\ D_o \end{bmatrix} \xi - \begin{bmatrix} LT^T \\ T^T \end{bmatrix} \psi, \tag{7.1.1}$$

. where, $e = \begin{bmatrix} e_s \\ e_o \end{bmatrix}, G_o = \begin{bmatrix} G_1 \\ G_2 \end{bmatrix}. E_c = \begin{bmatrix} 0 \\ E_o \end{bmatrix}$ and $G_m = \begin{bmatrix} LT^T \\ T^T \end{bmatrix}$

The generalized dimensions of matrices and vectors are $e_o \in \mathbb{R}^{p*1}$, $e_s \in \mathbb{R}^{n*1}$, $\xi \in \mathbb{R}^{q*1}$, $\psi \in \mathbb{R}^{q*1}$, $f \in \mathbb{R}^{q*1}$, $A_{11} \in \mathbb{R}^{n*n}$, $A_{12} \in \mathbb{R}^{n*p}$, $A_{21} \in \mathbb{R}^{p*n}$, $A_{22} \in \mathbb{R}^{p*p}$, $E_o \in \mathbb{R}^{q*q}$, $D_o \in \mathbb{R}^{q*q}$,

[1]This chapter is the main contribution of the paper I [8] and is also referred and used in [10]

$G_o \in \mathbb{R}^{n_o * p}$, $G_1 \in \mathbb{R}^{n*p}$, $G_2 \in \mathbb{R}^{p*p}$, $L \in \mathbb{R}^{n*p}$, $T \in \mathbb{R}^{q*q}$ whereas for the MG system considered

$p = 4, n = 6, m_c = m = 2, m = 2, m_c = m = 2, n_c = n + p = 10, p_c = p = 4, q_c = q = 4.$

A transformation is used to make the state error part of the error system least dependent on faults to retain the sliding motion, along with the attainment of reduced-order sliding motion for fault estimation. Ideally, the fault term in the state error part of the system and the state error term in the output error part should be eliminated; however, such a transformation cannot be designed. Thus, practically and very strictly, the sliding motion may not be retained owing to faults and disturbances, but the transformation not only provides control over the state error part through the gain matrix (L) but also reduces the effect of the state error part in the fault term to a negligible order in terms of magnitude for the considered MG system. However, the reduced-order state estimation error increases with the passage of time, which can be controlled by scalar (δ) and (β) parameters. Applying Transformation

$$T_L = \begin{bmatrix} I_{n-p} & L \\ 0 & T \end{bmatrix}, \tag{7.1.2}$$

where its inverse (which also explains the form of the discontinuous term gain of the SMO) is given by

$$T_L{}^{-1} = \begin{bmatrix} I_{n-p} & -LT^T \\ 0 & T^T \end{bmatrix}. \tag{7.1.3}$$

The transformation obtains the system to attain a reduced-order sliding surface along with fault estimation. The transformation and its inverse also explain the sense of the considered form of the switching term gain G_m in the SMO. The orthogonal matrix T was determined using the

QR transformation method.

$$\bar{A} = T_L A T_L^{-1} = \begin{bmatrix} \bar{A}_{11} & \bar{A}_{12} \\ \bar{A}_{21} & \bar{A}_{22} \end{bmatrix}, \tag{7.1.4}$$

where

$\bar{A}_{11} = A_{11} + LA_{21}$,

$\bar{A}_{21} = TA_{21}$,

$\bar{A}_{12} = (L\bar{A}_{22})T^T - (A_{11} + LA_{21})LT^T + A_{12}$,

$\bar{A}_{22} = TA_{22}T^T - TA_{21}LT^T$,

$$T_L G_o = \begin{bmatrix} G_1 + LG_2 \\ TG_2 \end{bmatrix}, T_L E_o = \begin{bmatrix} LE_o \\ TE_o \end{bmatrix}.$$

$$T_L D_o = \begin{bmatrix} LD_o \\ TD_o \end{bmatrix}, T_L G_m = \begin{bmatrix} 0 \\ I \end{bmatrix}, C_o T_L = \begin{bmatrix} 0 & T \end{bmatrix}. \tag{7.1.5}$$

$$\begin{bmatrix} \dot{e}_s \\ \dot{e}_o \end{bmatrix} = \begin{bmatrix} \bar{A}_{11} & \bar{A}_{12} \\ \bar{A}_{21} & \bar{A}_{22} \end{bmatrix} \begin{bmatrix} e_s \\ e_o \end{bmatrix} - \begin{bmatrix} G_1 + LG_2 \\ TG_2 \end{bmatrix} \begin{bmatrix} 0 \\ e_o \end{bmatrix} - \begin{bmatrix} LE_o \\ TE_o \end{bmatrix} f - \begin{bmatrix} LD_o \\ TD_o \end{bmatrix} \xi - \begin{bmatrix} 0 \\ I \end{bmatrix} \psi \tag{7.1.6}$$

$$\dot{e}_s = \bar{A}_{11} e_s + \bar{A}_{12} e_o - (G_1 + LG_2) e_o - LE_o f - LD_o \xi. \tag{7.1.7}$$

$$\dot{e}_o = \bar{A}_{21} e_s + \bar{A}_{22} e_o + TG_2 e_o - TE_o f - TD_o \xi + \psi. \tag{7.1.8}$$

A reduced-order error system is needed for fault and disturbance estimation if the observer mechanism remains stable along with the reachability of the sliding surface in the finite time. The scalar gain (γ) to be used with he output estimation error term (e_o) in the discontinuous

control law defined by term (ψ) is also determined from the analytical work of the stability analysis.

7.1.1 Reachability and Stability Analysis

The complete stability analysis of SMOs used for fault detection and estimation is shown in terms of the estimation error as a sliding surface. The error vector comprises of the state estimation error and the stable filtered output estimation error in the augmented vector form. A transformation is used in the above section for reduced-order error dynamics, which is particularly needed for fault and disturbance estimations. Therefore, considering the state error stability from the earlier section in Proposition 1, the Lyapunov stability of only the stable filtered output estimation error part is performed again to show the reachability of the sliding surface and hence ensures the estimation of the fault in finite time. The reachability is directly related to stability, and its analytical work is also used to determine the sliding surface reachability time. Before detailed analytical work, a Lemma for the stability and reachability conditions is provided.

Lemma 7.1: If the sliding mode for the surface $\sigma(e)$ is attained in finite time, that is, $\sigma(e) = 0$, then the time derivative of the Lyapunov function dV/dt may follow the inequality

$$\frac{dV}{dt} \leq k(\sqrt{V})^{z} \tag{7.19}$$

must be bounded more strongly, somewhat away from zero. That is, the attraction to the sliding mode will only be asymptotic if it vanishes too quickly The solution of inequality in Equation

(7.1.9) is given by

$$2\sqrt{V(t)} \leq -kV(t) + 2V_0. \tag{7.1.10}$$

Because $\sqrt{V} \geq 0$, then the inequality in Equation (7.1.10) states that V must reach $V = 0$ in finite time. In addition, because V is proportional to the Euclidean norm of the sliding surface $\sigma(e_o)$, that is, $\|\sigma(e_o)\|$, the rate of reaching the sliding surface is bounded away from zero [56, 94].

Theorem 7.1: If the augmented state estimation error system defined by equation (7.1.6) is transformed by matrix $T_L' = \begin{bmatrix} I_{n-p} & L \\ 0 & T \end{bmatrix}$ to induce reduced order sliding motion on estimation SMO,

and if the constraint on Lyapunov design matrix is,

$(Q = P_o T(A_{22} - G_2) + (A_{22}^T - G_2^T)T^T P_o < 0)$,

and if $\sigma(e_o) = \{e_o \,.\, Ce_o = 0\}$ governs the reduced order sliding motion,

such that the magnitudes of fault/ disturbance are bounded, i.e.,

$(\|f\| < \alpha')$ and $(\|\xi\| \leq \xi_o)$,

and if the gain factor (γ) for output error estimation term is bounded by

$\gamma \geq \|T\bar{A}_{21}\|\|e_s\| - \|TE_o\|\alpha' - \|TD_o\|\xi_o + \eta$,

then the fault detector/ estimator SMOs utilized for MG system are ensured to be stable in terms of Lyapunov criteria along with the reachability of the sliding motion in the finite time . The finite time required to reach/hit the sliding surface is given by,

$$T_R \leq \sqrt{\frac{e_o^T P_o e_o}{\lambda_{min}(P_o^{-1})}}.$$

Proof: Let the Lyapunov function for the error system be V_e, where the error vector is augmented by the state estimation error and stable filtered output error for the considered system. Thus, the complete Lyapunov function can be represented as:

$$V_e = V_{e_s} + V_{e_o} = e_s^T P_1 e_s + e_o^T P_o e_o. \tag{7.1.11}$$

Taking the time derivative of the Lyapunov function to prove the stability of the error system based on its negative definiteness.

$$\dot{V}_e = \dot{e}_s^T P_1 e_s + e_s^T P_1 \dot{e}_s + \dot{e}_o^T P_o e_o + e_o^T P_o \dot{e}_o \tag{7.1.12}$$

$$\dot{V}_{e_s} = \dot{e}_s^T P_1 e_s + e_s^T P_1 \dot{e}_s \tag{7.1.13}$$

Substituting the values for $\dot{e}_s$ from Equation (7.1.7), -

$$\dot{V}_{e_s} = e_s^T \bar{A}_{11}^T P_1 e_s + e_o^T \bar{A}_{12}^T P_1 e_s - f^T E_o^T L^T P_1 e_s - \xi^T D_o^T L^T P_1 e_s - e_o^T G_1^T P_1 e_s - e_o^T G_2^T L^T P_1 e_s +$$

$$\dot{e}_s^T P_1 \bar{A}_{11} e_s + e_s^T P_1 \bar{A}_{12} e_o - e_s^T P_1 L E_o f - e_s^T P_1 L D_o \xi - e_s^T P_1 G_1 e_o - e_s^T P_1 L G_2 e_o \tag{7.1.14}$$

The stability of the sliding motion in reduced-order is proved by considering the Lyapunov function on the output part of the error vector only i.e ,

$$\dot{V}_{e_o} = \dot{e}_o^T P e_o + e_o^T P \dot{e}_o. \tag{7.1.15}$$

Substituting the values for $\dot{e}_s$ from Equation (7.1.8),

$$\dot{V}_{e_o} = e_s^T \bar{A}_{21}^T T^T P_o e_o + e_o^T \bar{A}_{22}^T T^T P_o e_o + e_o^T G_2^T T^T P_o e_o - f^T E_o^T T^T P e_o - \xi^T D_o T T^T P_o e_o +$$

$$\psi^T P_o e_o + e_o^T P_o T \bar{A}_{22} e_o + e_o^T P_o T G_2 e_o + e_o^T P_o T G_2 e_o + e_o T P_o T E_o f - e_o^T P_o T D_o \xi + e_o^T P_o \psi. \tag{7.1.16}$$

$$\dot{V}_{e_o} = 2e_o^T P_o T^T \bar{A}_{22} e_o + 2e_o^T P_o T^T G_2 e_o + 2e_o^T P_o T^T G_2 e_o + 2e_o^T P_o E_o f - 2e_o^T P_o D_o \xi + 2e_o^T P_o \psi. \tag{7.1.17}$$

$$\dot{V}_{e_o} = e_o^T [P_o T(\bar{A}_{22} - G_2) + (\bar{A}_{22}^T - G_2^T) T^T P_o] e_o + 2e_o^T P_o T \bar{A}_{21} e_s - 2e_o P_o T E_o f - \tag{7.1.18}$$

$$2e_o^T P_o T D_o \xi + 2e_o^T P_o \psi.$$

If designed suitably,

$$Q = P_o T(A_{22} - G_2) + (A_{22}^T - G_2^T) T^T P_o < 0. \tag{7.1.19}$$

Dropping the negative definite term, the inequality version of Equation (7.1.18) is,

$$\dot{V}_{e_o} < 2e_o^T P_o T \bar{A}_{21} e_s - 2e_o P_o T E_o f - 2e_o^T P_o T D_o \xi + 2e_o^T P_o \psi. \tag{7.1.20}$$

Taking norm of above equation, and using the Cauchy–Schwartz inequality,

$$\dot{V}_{e_o} \leq 2\|e_o\| \|P_o T \bar{A}_{21}\| \|e_s\| - 2\|e_o\| \|P_o T E_o\| \|f\| - 2\|e_o\| \|P_o T D_o\| \|\xi\| - 2\gamma \|P_o e_o\|. \tag{7.1.21}$$

$$\dot{V}_{e_o} \leq 2\|P_o e_o\| [\|T A_{21}\| \|e_s\| - \|T E_o\| \|f\| - \|T D_o\| \|\xi_o\| - \gamma]. \tag{7.1.22}$$

Furthermore, since magnitudes of fault and disturbance are bounded: $\|f(t)\| < \alpha'$ and $\|\xi(t)\| \leq$

$\xi_o < \infty$,

$$\dot{V}_{e_o} \leq 2\|P_o e_o\|[\|T\bar{A}_{21}\|\|e_s\| - \|TE_o\|\alpha' - \|TD_o\|\xi_o - \gamma]. \tag{7.1.23}$$

The derivative of the Lyapunov function is negative definite if

$$\gamma > \|T\bar{A}_{21}\|\|e_s\| - \|TE_o\|\alpha' - \|TD_o\|\xi_o, \tag{7.1.24}$$

where η is a positive constant that ensures Lyapunov stability in terms of V_{e_o}. Using the bound for γ from Equation (7.1.24) in Equation (7.1.23),

$$\dot{V}_{e_o} \leq -2\eta\|P_o e_o\|. \tag{7.1.25}$$

If P is a positive definite matrix, then $\|x\|_2^2 > \lambda_{min}(P^{-1})\|x\|_2^2$ ([95]),

$$\Rightarrow \|e_o\|^2 = e_o^T e_o = e_o^T P_o^{1/2} P_o^{-1} P_o^{1/2} e_o \geq \lambda_{min}(P_o^{-1}\|e_o\|^2.$$

$$\Rightarrow \|e_o\| \geq \sqrt{\lambda_{min}(P_o^{-1})}\sqrt{V_{e_o}}. \tag{7.1.26}$$

where $\|P_o^{1/2} e_o\| = \sqrt{V_{e_o}}$.

Using Lemma 7.1, Equation (7.1.25) shows the stability and finite-time reachability of the sliding motion for the sliding-mode observers. The finite-time reachability governs and ensures the real-time operation of the proposed observers for fault detection and estimation, that is, the sliding surface is ensured to be reached/hit in a finite time. Using Equations (7.1.19), (7.1.20), (7.1.21),

and (7.1.25) in the Lyapunov function in Equation (7.1 18), in the inequality form yields:

$$\dot{V_{e_o}} \leq \lambda_{min}(Q)\|e_o\|^2 - 2\eta\|P_o e_o\|. \tag{7.1.27}$$

Using Equation (7.1.26),

$$\dot{V_{e_o}} \leq \lambda_{min}(Q)\lambda_{min}(P_o^{-1})V_{e_o} - 2\eta\sqrt{\lambda_{min}(P_o^{-1})V_{e_o}}, \tag{7.1.28}$$

$$\dot{V_{e_o}} \leq \frac{\lambda_{min}(Q)}{\lambda_{min}(P_o^{-1})}V_{e_o} - 2\eta\sqrt{\lambda_{min}(P_o^{-1})V_{e_o}}. \tag{7.1.29}$$

For the DE of the form $(\dot{x}(t) \leq -ax(t) - b\sqrt{x(t)})$ ([4]), the time required for $x(t)$ to move from $x_0 = x(t = 0)$ to $x_1 = x(t = 1)$ is

$$T_R \leq \frac{2}{a}ln(\frac{a\sqrt{x_o} + b}{a\sqrt{x_1} + b}) \leq \frac{2}{b}(\sqrt{x_o} - \sqrt{x_1}).$$

The reachability time (T_R) is given by

$$T_R \leq \frac{1}{\eta}(\frac{V_o(e_o(t_o)) - V_o(e_o(t_o + T_R))}{\lambda_{min}(P_o^{-1})}) \leq \sqrt{\frac{e_o^T P_o e_o}{\lambda_{min}(P_o^{-1})}}, \tag{7.1.30}$$

where

$$V_o(e_o(t_o + T_R)) = e_o^T(t_o + T_R)P_o e_o(t_o + T_R) = 0.$$

Because the stability and finite-time reachability of the sliding-mode observers is shown and the gain of the output error injection term is determined, the estimation of faults and disturbances

can proceed with the results determined in previous sections.

7.1.2 Reconstructed Fault and Estimated Disturbance

This subsection describes the analytical work of faults and disturbance reconstruction based on the results obtained in the previous sections

Corollary 7.1: Considering the MG system/ observer in Equation (3.1.11) and Equation (4.1.1) respectively, if the SMO gains are determined by solving the LMI optimization problem described in Theorem 2, the transformed error system is defined by Equations (7.1.7) and (7.1.8), and if (γ_i) being the constant gain of output error estimation term is constrained to satisfy (7.1.24) to ensure the stability of observers, i.e.,

$\gamma_i \geq \|T\bar{A}_{21}\|\|e_s\| - \|TE_o\|\alpha' - \|TD_o\|\xi_o + \eta,$

then sliding surface attained in reduced order gives the estimated sensor fault (f^*)/ disturbance (ξ^*) to be:

$$f^* = \beta E_o^{-1} T^{-1} \psi_{eq}.$$

$$\xi^* = f - f^* - E_o^{-1} T^{-1} A_{21} e_s,$$

where β serves as a scaling constant.

Proof: When observers enter the sliding mode, that is, the sliding surface is reached, the condition in terms of the error surface ideally is ($Ce = 0$); however, for the considered perturbed and faulty sensor MG systems, the sliding mode/surface is reached only for the output error term ($e_o = \dot{e}_o = 0$) and not for the state estimation error term(e_s). However, if there is no

disturbance term, then ($e_s \to 0; \dot{e}_s \to 0$) are also approached in finite time.

$$\dot{e}_s = \bar{A}_{11} e_s - L E_o f - L D_o \xi + \Gamma \psi_{eq} \tag{7.1.31}$$

$$0 = \bar{A}_{11} e_s - T E_o f - T D_o \xi + T \psi_{eq} \tag{7.1.32}$$

From above Equation (7.1.32),

$$f = E_o^{-1} T^{-1} \bar{A}_{21} e_s - E_o^{-1} D_o \xi + E_o^{-1} T^{-1} \psi_{eq} \tag{7.1.33}$$

Using the fault estimate equation (7.1.33) in the state error Equation (7.1.31), yields the reduced-order state error equation

$$\dot{e}_s = (\bar{A}_{11} - L T^{-1} \bar{A}_{21}) e_s - L T^{-1} \psi_{eq}. \tag{7.1.34}$$

This DE needs to be solved linearly at every instant of time to be back-substituted in the fault estimation Equation (7.1.33) to obtain a closer fault estimate. As evident from Equation (7.1.34), the solution to DE also requires a run time evaluation of factor (ψ_{eq}), because the aforementioned approach is necessary for disturbance estimation. Considering the terms in the fault estimate Equation (7.1.33), because the state error term e_s in the fault equation cannot be removed or isolated by the transformation (T_L) applied to the system (7.1.1), but its magnitude becomes insignificant for the considered MG application, whereas the disturbance term in the equation is known to be an undesired and diverging term, the reconstructed fault should be approximated equivalently by (ψ) term only, which is based on the output estimation error (e_o) term, design

matrices (E_o, T), and gamma (γ) parameter.

So from Equation (7.1.33) the reconstructed fault is

$$f^* = E_o^{-1} T^{-1} \psi_{eq}. \tag{7.1.35}$$

The equivalent switched control in sliding mode is ψ_{eq} is

$$\psi_{eq} = -\gamma \frac{P_o e_o}{\|P_o e_o\| + \delta}, \tag{7.1.36}$$

where the term ψ_{eq} is meant to maintain the sliding motion in reduced-order motion in the presence of disturbances and faults, and δ is a constant control parameter for this purpose.

Remark 7.1: (γ) is constant gain factor of discontinuous control term (ψ_{eq}) whereas (δ) is its additional constant control parameter. The (ψ_{eq}) term controls the gradually increasing reduced-order state error (ϵ_s) and the value of (γ) being in a closed loop, which, if not controlled properly, causes a rapidly increasing reduced-order state error (ϵ_s) and hence the total divergence of the whole process. It is empirically suggested that, for the considered MG application, the reconstructed fault is

$$f^* = \beta E_o^{-1} T^{-1} \psi_{eq}. \tag{7.1.37}$$

where β is a constant magnitude scaling parameter that is required to adjust the attenuation achieved by stable filtering on the output error term.

Because $E_o = D_o \Rightarrow E_o^{-1} D_o = Identity$, using Equation (7.1.37) in Equation (7.1.33), the

estimated disturbance in the system is given by

$$\xi = f - f^* - E_o^{-1} T^{-1} A_{21} e_s. \tag{7.1.38}$$

The Simulink blocks performing computations of ψ, ψ_{eq} γ and Reduced-order error e_s estimation are shown in Figure 7.1, whereas the Simulink computation of estimated faults and disturbances are shown in Figure 7.2

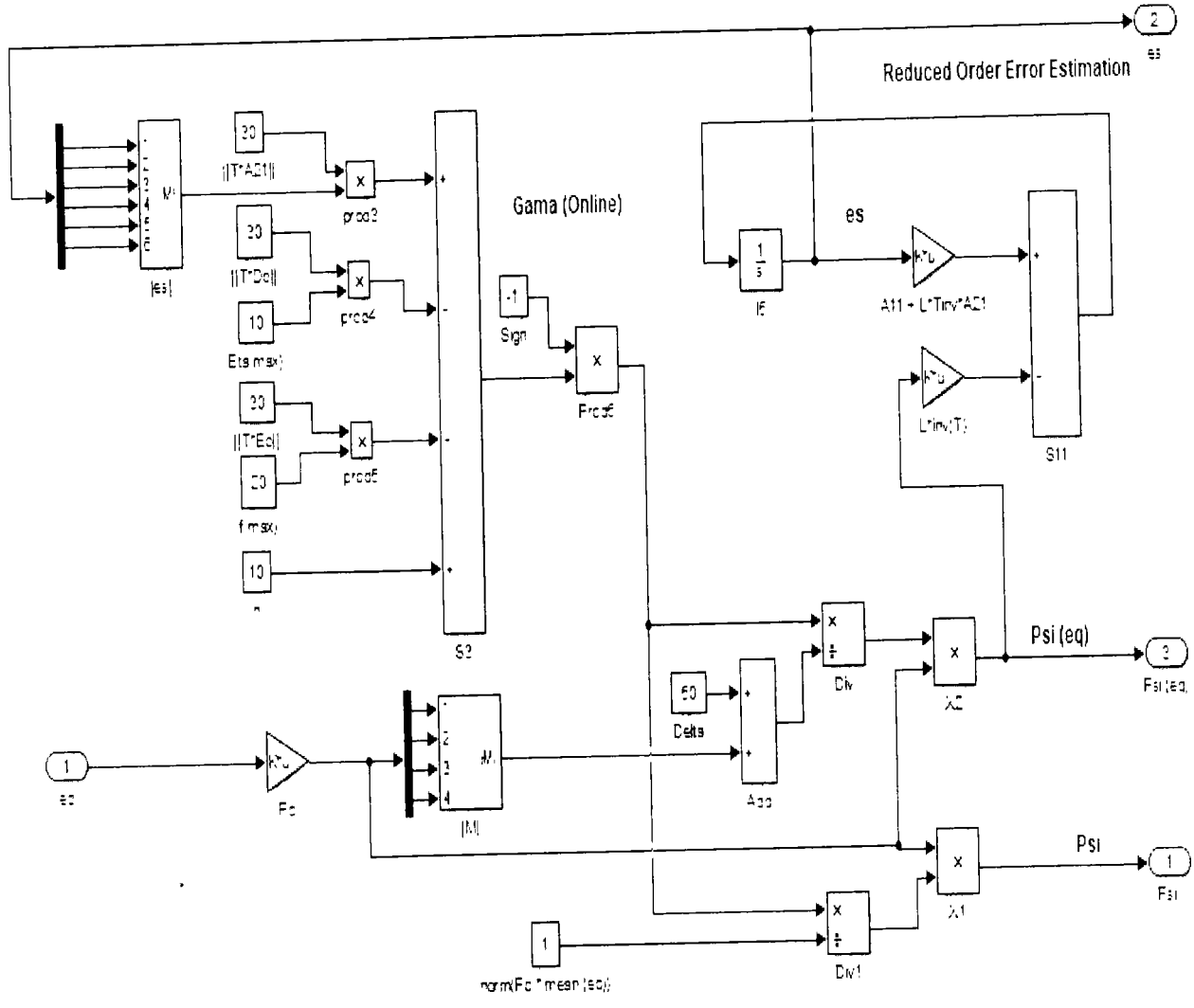

Figure 7.1: Computations of ψ, ψ_{eq} γ and Reduced-order error e_s estimation

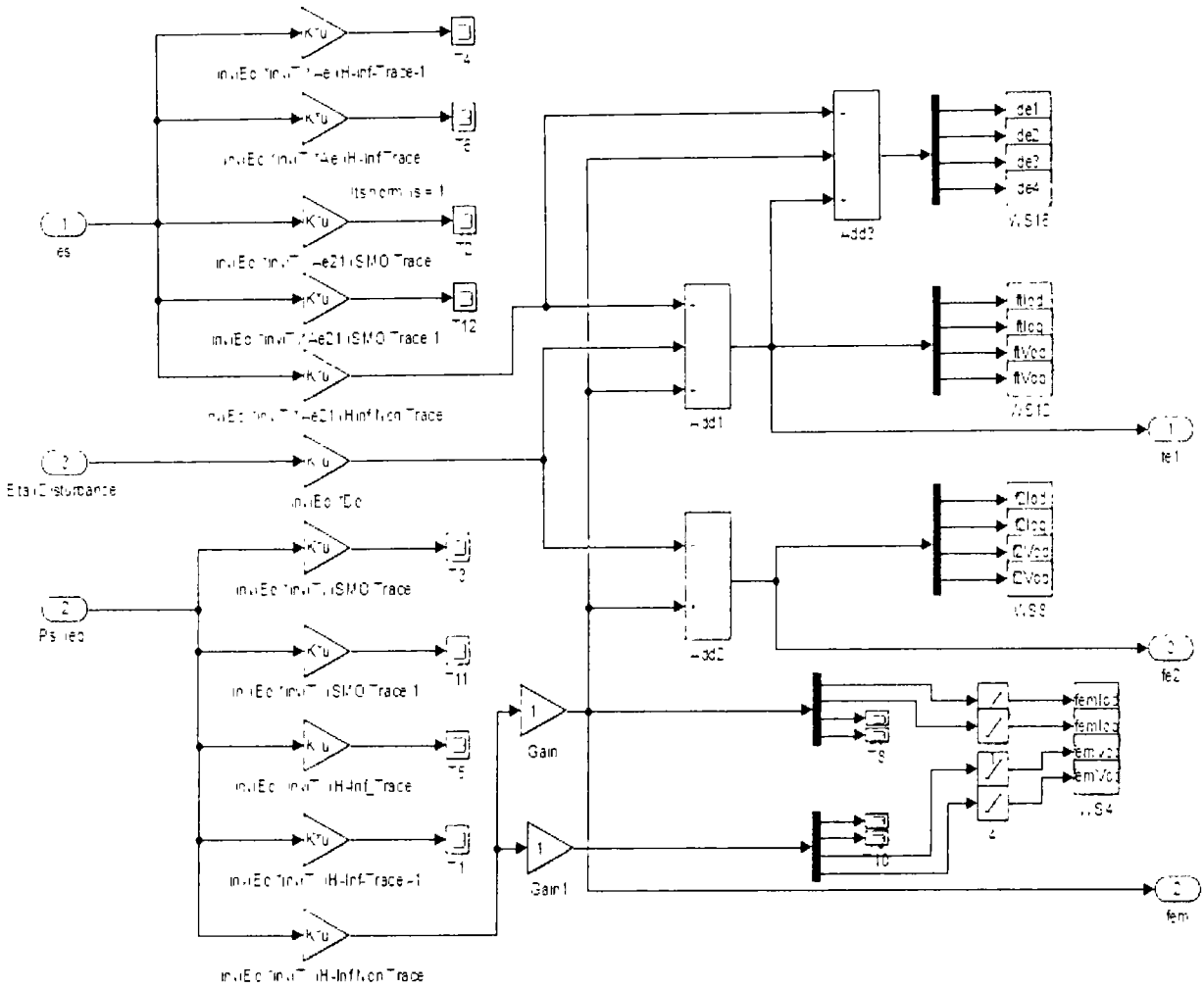

Figure 7.2: Computations for fault and disturbance estimations

Remark 7.2: The values of parameters (δ, β, γ) are considered in this paper intuitively by hit and trial, however setting the parameters sub-optimally can be addressed in future work, which would also provide generic applicability of observer-based fault-tolerant approach for many other applications with different fault/disturbance magnitudes and sensitivity requirements.

Remark 7.3: The presence of disturbances and faults results in the sliding motion is not attained in a strict sense; however the effect of disturbances and faults on fault estimation can be minimized using (H_∞) norm as presented in Theorem 2 which is ratio of L_2 norms of residual

$(r(t) = e_o(t))$ and disturbance (ξ), respectively.

Remark 7.4: The state error term (e_s) in the output error term and fault term in the state error term are undesired in terms of fault estimation. Although the transformation (T_L) cannot ideally achieve the desired elimination of undesired terms, it provides control through the gain matrix (L), which is determined by the LMIs.

Remark 7.5: Moreover the transformation (T_L) reduces the effect of state error part (e_s) in estimated fault to quite negligible order in terms of magnitude for the considered system which is almost zero in the case of micro-grids. The results were verified through simulations

Chapter Summary: The chapter presents asymptotic Lyapunov stability and finite-time reachability of fault-estimation SMO filter. In sliding mode, it attains the reduced order and estimates the faults and disturbances by a modified rather corrected approach.

CHAPTER 8

Part I: Voltage-Frequency Control Enhanced with Fault-Tolerant Control. Part II: Procedural Algorithms

8.1 FTC Approach/Working

[1]. The estimated faults by using SMOs are added/subtracted from the faulty sensor readings and the corrected values are fed to the PI-based control block, which is also working for the common microgrid problems, i.e., balancing the voltage and frequency sags. The accurate fault estimation/reconstruction will provide the correction closest to the actual one, which is added/subtracted from the faulty sensor readings to get the actual one. So, fault tolerance surely depends upon accurate fault estimation and the least fault estimation error in the results and discussion section. The estimated fault is subtracted from the faulty sensors' output vector.

$$\boldsymbol{Y_c} = \boldsymbol{Y_s} - E_s * \boldsymbol{f^*} - D_s * \boldsymbol{\xi^*}, \tag{8.1.1}$$

where $\boldsymbol{f^*}$ is the estimated fault and $\boldsymbol{Y_u}$ is the vector of faulty sensor outputs, and $\boldsymbol{Y_c}$ is the corrected sensor outputs vector. The complete working of the system and the proposed solution is shown in the Simulink-based detailed block diagram in Figure 8.6.

Remark 8.1: The above equation shows that the working and effectiveness of fault tolerance depends on accurate fault estimation. The accuracy of fault estimation can be observed in the fault estimation errors with fault estimation performed with various constrained SMOs. The fault estimation error graphs for voltage/currents are given in figures in the results and discussions section.

Remark 8.2: The innovative contribution of this work is not to consider and solve the voltage and frequency sags/droops occurring in the islanded/grid-connected microgrid, but instead, we have considered the faults of C.T/P.T, which are rectified using the SMOs for fault detection

[1]This chapter is part of the both papers [8], [10]

and estimation. The estimated faults are given as corrections of the faulty sensor readings, and in this way, the software-based sensor serves as a replacement sensor, and the corrected readings are used by the control block to serve as a controller for voltage-frequency sags as well. The corrected sensor voltages/currents are given to the voltage-frequency control block for proper tracking of reference reactive and real powers.

8.2 $P-\omega$ and $Q-V$ Control Scheme

The control block mainly utilizes PI control-based current/voltage controllers and uses droop control and a PLL block to regulate real and complex power in relation to frequency and quadrature voltage, respectively. In other words, it is said that the same $P-f$ and $Q-V$ control mechanisms are enhanced as FTC by using observer-based fault estimates for the correction of sensor outputs. The control block is not discussed in detail except for a brief continuation, as it is taken from the work of [26], from which the model of the MG is considered in Section 3.1.2. All the system parameters and PI constants are considered to be the same as those given in the aforementioned paper and detailed PhD thesis.

8.2.1 Droop Control

The voltage and frequency references for the standalone mode of operation of the microgrids must be internally generated i.e.,

$$\omega^* = \omega_n - mP_r, \tag{8.2.1}$$

$$V^* = V_{ogn} - nQ_r, \tag{8.2.2}$$

where $P_r = 3/2 * (V_{oq}I_{oq} + V_{od}I_{od})$ and $Q_c = 3/2 * (V_{oq}I_{od}^{\sim} - V_{od}I_{oq})$. Because the values are accepted directly from the grid and low-pass filtered output power is processed, the high-frequency current and voltage spikes must be neglected.

$P' = \frac{\omega_c PLL}{S+\omega_c PLL} P_r$, $Q' = \frac{\omega_c PLL}{S+\omega_c PLL} Q_r$, where $\omega_{c.PLL} = 7853.98$ rad/s.

$$m = \frac{\omega_1 - \omega_2}{P_1 - P_2}, n = \frac{V_1 - V_2}{Q_1 - Q_2} \tag{8.2 3}$$

The value of $m = n = 1/1000$ is used for the simulation, which can be varied for different grid ratings and other applications. The simulink based block for computation of P_r,Q_c is shown in Figure 8.1.

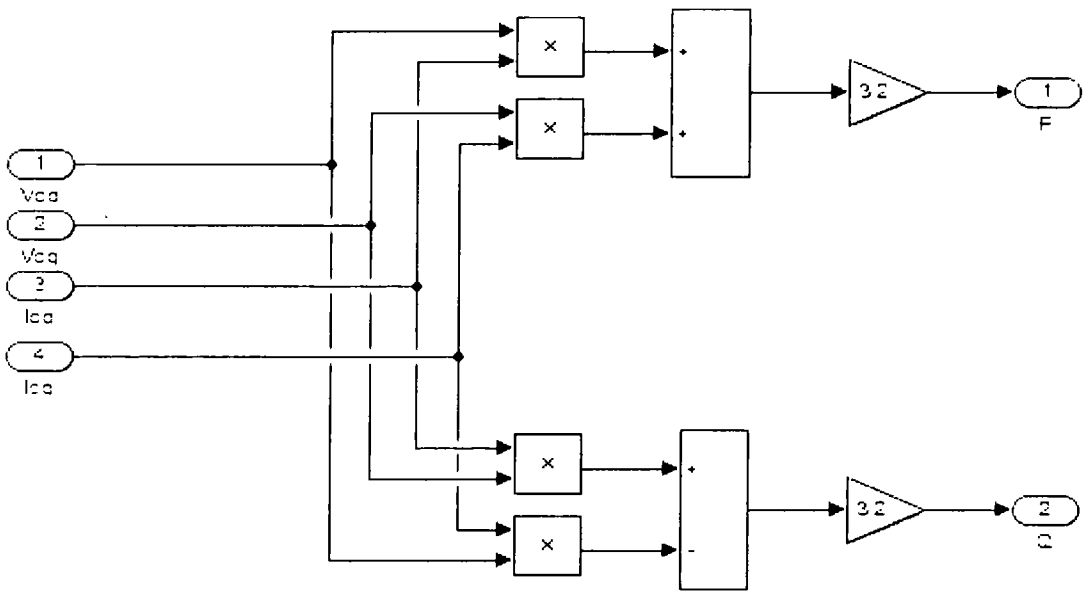

Figure 8.1: Computation of Reference Real and Apparent Powers in Islanded Mode

8.2.2 PLL Block

The block computes the grid angle by using the phase-locked loop (PLL) at the instant that is then used for all dq conversions, SVPWM block, and other required computations.

$$\dot{V_{odf}} = \omega_{c,PLL} V_{od} - \omega_{c,PLL} V_{odf} \tag{8.2.4}$$

$$\theta = \omega_{PLL} \Rightarrow \theta = \int \omega_{PLL} dt \tag{8.2.5}$$

For $f = 60$ Hz $\Rightarrow \omega_{PLL} = 377$ rad/s and $\omega_{c\,PLL} = 7853.98$,

$$w_{PLL} = 377 - k_{p\,PLL} V_{odf} - k_{i\,PLL} \int V_{odf}\, dt. \tag{8.2.6}$$

The values of constants and gains used in simulations are: $k_p = 0.25, k_i = 2$, $w_c = 377$ rad/s. The simulink based PLL block for computation of phase angle required as a reference for all conversions in the system is shown in Figure 8.2.

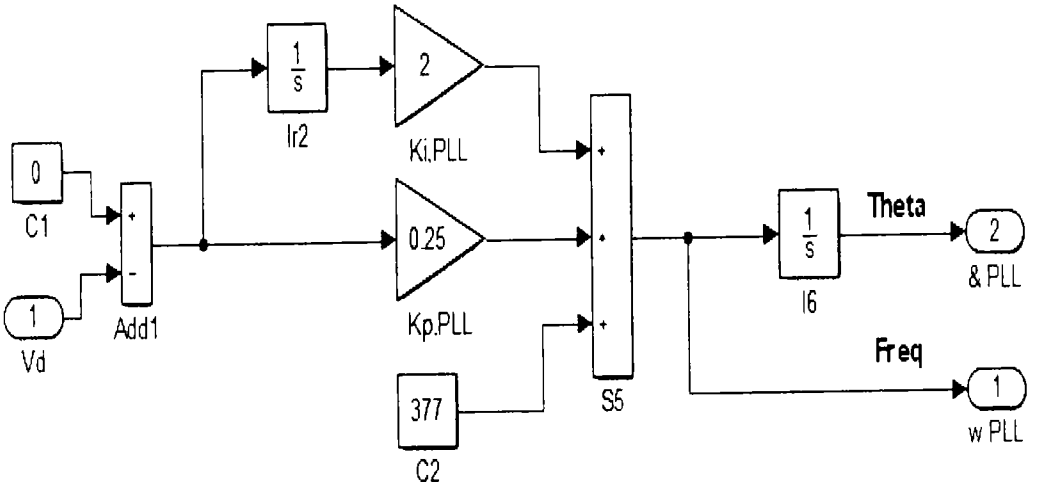

Figure 8.2: Phase Locked Loop for determination of phase

8.2.3 Voltage Controller

The PI-based control equations managing integral-based control serve as a voltage controller and generate the corresponding references of the dq components of the current.

$$i_{id}^{*} = k_{ivd}\int (w_{PLL} - w^{*})dt + k_{pvd}(w_{PLL} \quad w^{*}) \tag{8.2.7}$$

$$i_{iq}^{*} = k_{iiq}\int (V_{oq}^{*} - V_{oq})dt + k_{pvq}((Voq^{*} - V_{oq})) \tag{8.2.8}$$

The values of constants and gains used in simulations are: $k_{ivd} = 0.25. k_{ivq} = 0.25. k_{pvd} = 0.5. k_{pvq} = 0.5$. The simulink block for PI-based voltage controller is shown in Figure 8.3.

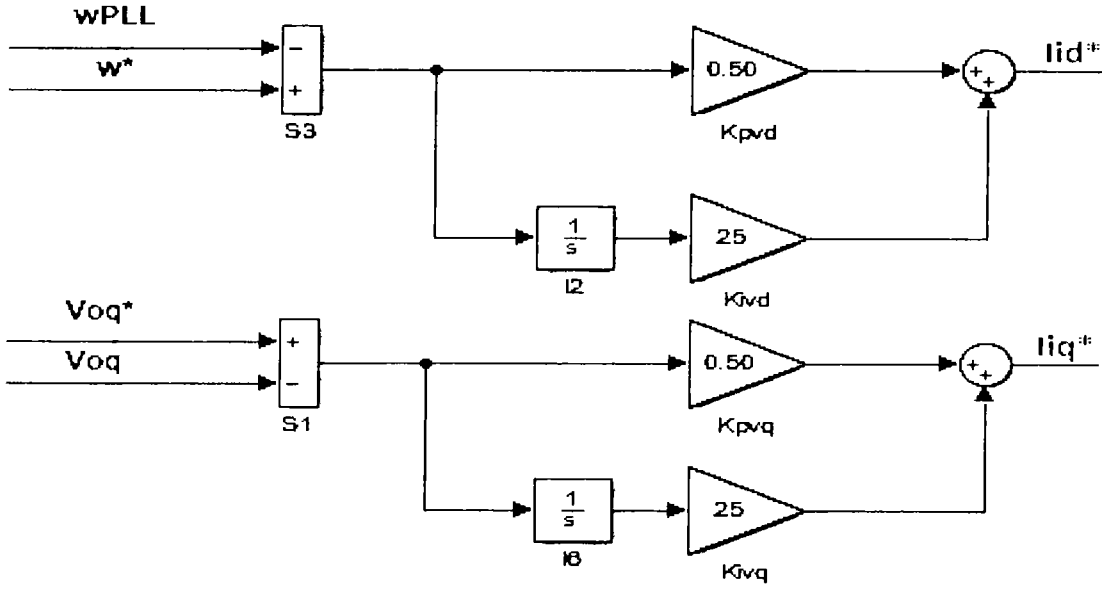

Figure 8.3: PI-based voltage controller to compensate voltage and power sags

8.2.4 Current Controller

The block uses the desired current values generated by the above block and generates the corresponding voltage values.

$$V_{id}^{*} = -w_n L_f i_{iq} + k_{icd} \int (i_{id}^{*} - i_{id})dt + k_{pcd}(i_{id}^{*} - i_{id}) \tag{8.2.9}$$

$$V_{iq}^{*} = -w_n L_f i_{id} + k_{icq} \int (i_{id}^{*} - i_{id})dt + k_{pcq}(i_{iq}^{*} - i_{iq}) \tag{8.2.10}$$

The values of constants and gains used in simulations are $w_n = 377, k_{pcd} = 1, k_{pcq} = 1, k_{icd} = 100, k_{icq} = 100$. The Simulink block for the PI-based current controller is shown in Figure 8.4.

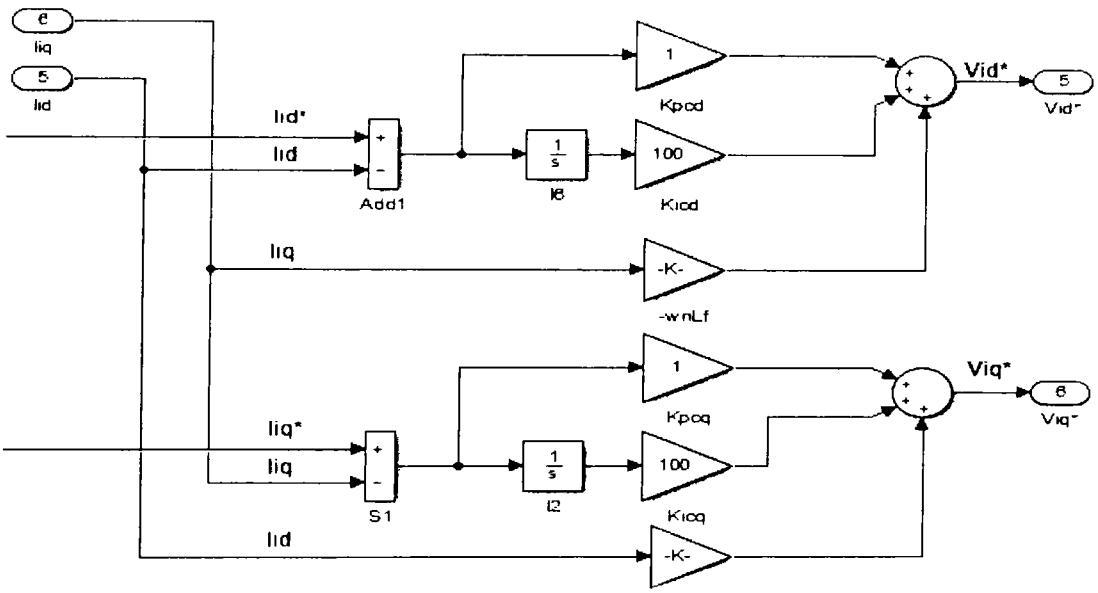

Figure 8.4: PI-based current controller to compensate voltage and power sags

8.2.5 SVPWM Control

The SVPWM control uses a 10,000 Hz frequency for the considered MG operation. The desired voltage values generated by current controllers are transformed back to a three-phase voltage

representation and provided to the SVPWM block, which manages the switching sequences and times of inverter switches to generate the desired values of current and voltage by VSC. These current/voltage values correspondingly manage the real power vs. frequency and complex power vs. voltage sags. The converter model used was a detailed model provided in MATLAB (Simulink) instead of the average model.

The complete PI, droop, and SVPWM-based control for compensating the current/voltage sags for proper tracking of real and reactive powers is shown in Figure 8.5.

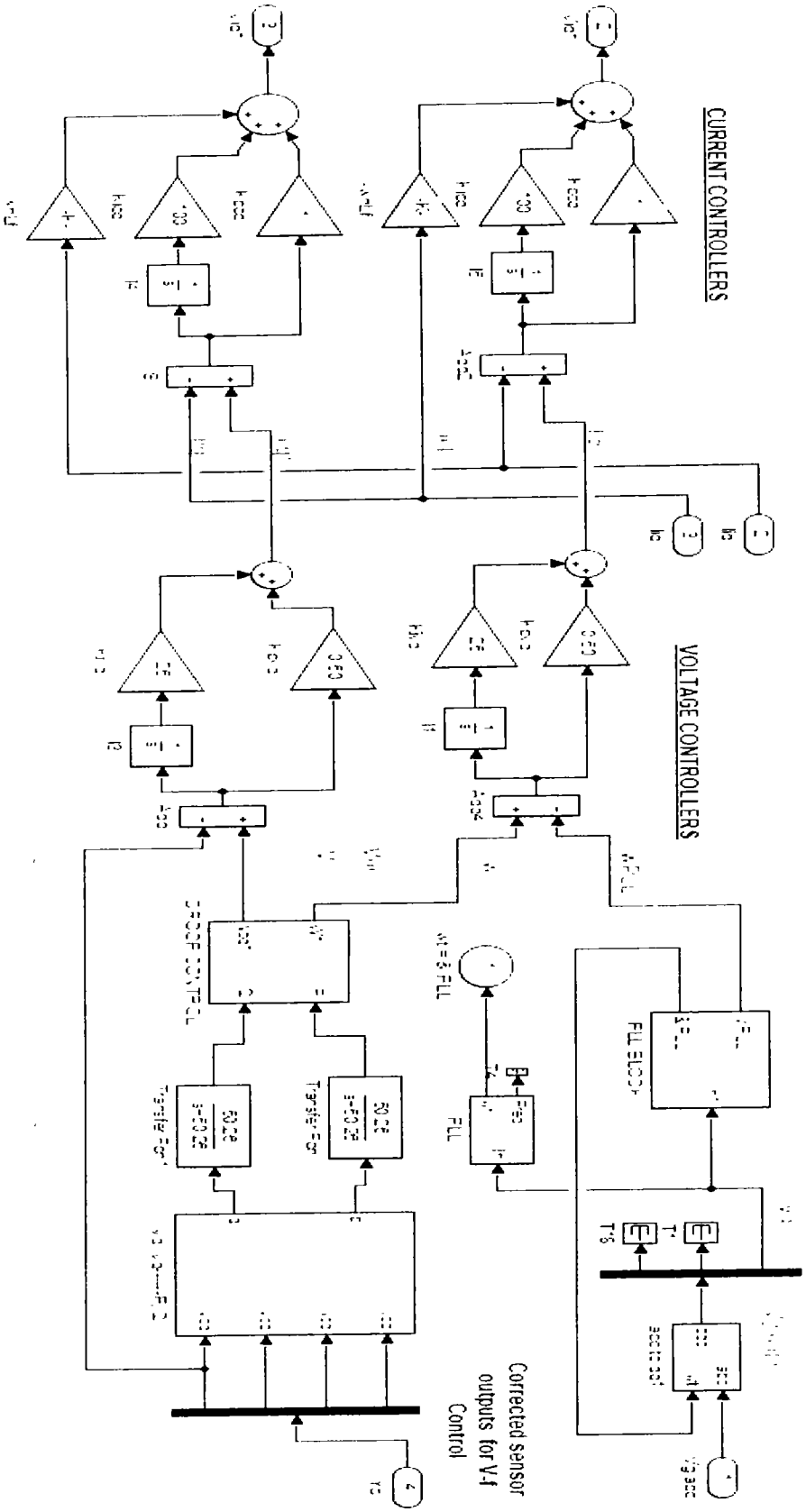

Figure 8.5: PI-based current controller to compensate voltage and power sags (Flow from bottom to top

8.3 Part II: Simulink Based Complete Procedural Block Diagram and Algorithms

A detailed Simulink-based simulation diagram is given in Figure 8.6. From the top right, the block named 'Microgrid System' is the wired microgrid system, as shown in Figure 3.1 in Chapter 3. The inverter and grid input voltages are given to the system by this block. The second block, named the 'Voltage Frequency Control' block, manages the voltage/frequency sags of corrected voltage/current signals. The third block, named 'Fault/Disturbance Injection in sensor Outputs', injects the faults and disturbances according to the fault model in Equation (3.1.1) in a block named 'Simulink Based System Model' (which is mentioned in Equations (3.1.6) and (3.1.7) as well as in a block named 'Augmented System Model and Stable Filtering' (as done in Equations (3.1.10) or (3.1.11). The faulty system outputs are given to the blocks named 'FD Block/State and Output Estimation SMO' (defined by Equation (4.1.1)) and 'Error (State/Output) Estimation SMO' (as defined in (4.1.7)). These outputs are given to the block named 'Reduced Order state Error', which computes the value of γ gain, values of the switched signal in normal and sliding mode (i.e., ψ, ψ_{eq}), and reduced order state estimation error (e_ζ) (which are the parameters required by the equations 7.1.21,7.1.36, while these computed values are also given back to 'FD Block' and 'Error Estimation SMO' particularly required by switch gain term of SMOs. these values are then provided to a block named 'Estimated Faults/Disturbances Computation' to compute the faults/disturbances (unknown inputs). The last block, named 'Data Acquisition', performs data acquisition of all required data to be logged or provided to m-files required for plotting the required results. The gains are not updated on

the run time since that requires GPU based systems. However, the system can easily incorporate the run-time computation of gains. The SMOs and other blocks are using the optimized constant gains computed by Matlab m-files using LMIs' convex optimization toolbox commands.

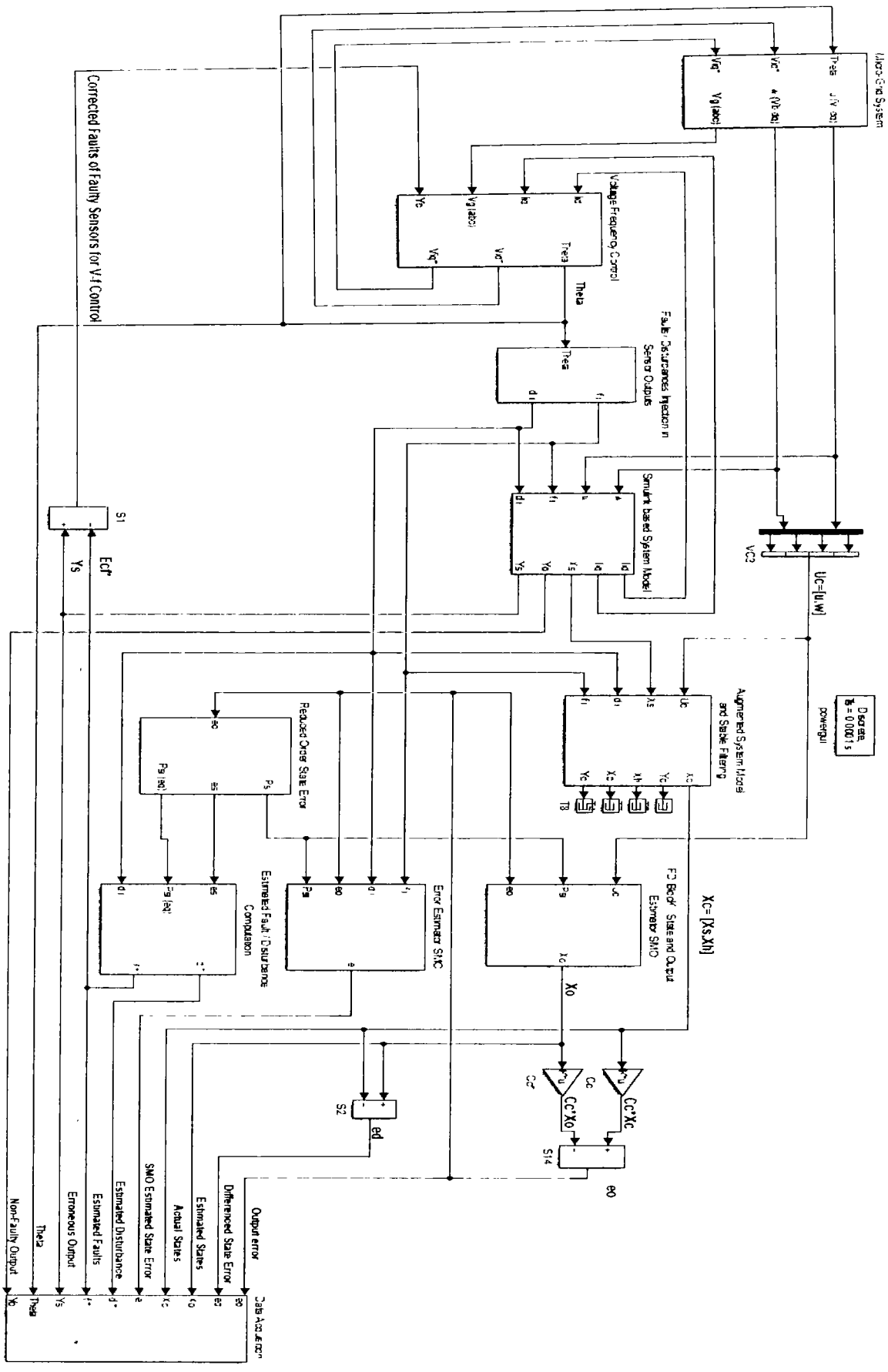

Figure 8.6: Completed Simulink based Model

8.3.1 Algorithm I: Procedure Algorithm Based on Paper [8]

The complete procedure for the proposed observer-based FTC approach in [8] is explained in Algorithm I.

Inputs w, u, ξ, f

Outputs Matrices $P, G_m, G_o, y_s, x_s, x_o, e, \gamma, \Psi_{eq}, \xi^*, f^*, e_s, y_o, e_o$

while (Simulation Time)

START

1: Linearized system model in Equation (3.1.2) is d-q-0 transformed using Equation (3.1.3);

2: Acquisition of grid/converter voltages (u, w) from microgrid in Figure 2 are given to system model ($\dot{x}_s = A_s x_s + B_s u + B_g w$), Equation (3.1.6)

3: Sensor/C.T/P.T faults/disturbances ($f(t) = f_o * sin(\omega_1 t + \phi_1)$), ($\xi_o * sin(\omega_2 t + \phi_2)$) are generated to be added in system output ($y_s = C_s x_s + E_s f + D_s \xi$), Equation (3.1.7)

4: Faulty system output is stable filtered using ($\dot{x}_h = A_h y_s - A_h x_h$) Equation (3.1.8);

5: Augment system states with stable filtered outputs, Equations (3.1.10) and (3.1.11);

6: Determine the SMO gains (G_o, G_m) using convex (feasibility and trace minimization) optimization performed on system parameters according to methods explained in Theorems 5.1 and 5.2:

« i) Perform convex feasibility optimization on the LMI constrained with Lyapunov stability given in Equation (5.1.26) (to be used for trace optimization), ii) Lyapunov stability and H_∞ constrained LMI in Equation (5.1.36) (to be feasibility optimized), and iii) Riccati equation-based modification of H_∞ constrained LMI in Equation (5.1.41) (to be feasibility optimized), to find the respective optimal gains G_o^*, G_m. »

7: Augmented system state is given to state estimator (SMO) ($\dot{x}_o = A_e x_o + B_e u_e + G_o \epsilon_o + G_m \psi$), Equation (4.1.1);

8: Difference between system and observer states/outputs ($\epsilon_d = \epsilon = x_o - x_e$) as defined in Equation (4.1.2) gives Augmented state estimation error;

9: Augmented system state is given to state error estimator SMO ($\dot{\epsilon} = (A_e - G_o C_e)e - E_e f - D_e \xi + G_m \psi$). Equation (4.1.7) or (4.1.8);

10: Stable filtered output estimation error ($\boldsymbol{e}_o = y_o - y_e$) in Equation (4.1.4) is fed to state estimator SMO in step 6 and the state error estimator SMO in step 9 to attain the sliding mode;

11: Determine the gains ($\gamma > \|T\bar{A}_{21}\|\|e_s\| - \|TE_o\|\alpha' - \|TD_o\|\xi_o$) and the suitable value of Delta, Equation (7.1.24);

12: Determine the gain $\boldsymbol{\psi}_{eq} = -\gamma \frac{P_o e_o}{\|P_o e_o\| + \delta}$ as in Equation (7.1.36).

13: Determine the gain reduced order state error $\boldsymbol{e}_s$)) by Simulink based numerical solution of ($\dot{e}_s = (\bar{A}_{11} - LT^{-1}\bar{A}_{21})e_s - LT^{-1}\psi_{eq}$) as in Equation (7.1.34);

14: Compute the estimated fault by ($f^* = \beta E_o^{-1} T^{-1} \psi_{eq}$). Equation (7.1.37) **15:** Compute the estimated disturbance (unknown input) by ($\xi = f - f^* - E_o^{-1} T^{-1} A_{21} e_s$), Equation (7.1.38);

16: The erroneous sensor outputs are corrected using estimated faults/disturbances i.e. ($Y_{sc} = Y_s - E_s * f^* - D_s * \xi^*$), Equation (8.1.1)

17: The corrected sensor output values are fed to PI/ Droop-based voltage/current/complex power/real power control block, Figure 3;

18: Repeat Step 6 and on-wards for the feasibility optimization of H_∞ constrained LMI in Equation (5.1.36) and the Ricatti equation based modification of H_∞ constrained LMI in Equation (5.1.41).

END (while)

8.3.2 Algorithm II: Procedure Algorithm Based on Paper II [10]

The procedure for complete observer based FTC approach proposed in [10] is given in Algorithm II .

Inputs: $\boldsymbol{u}$, $\boldsymbol{w}$, $\boldsymbol{f}$, $\boldsymbol{\xi}$

Outputs: Matrix P, Gains (G_o, G_m), $\boldsymbol{x_s}$, $\boldsymbol{y_s}$, $\boldsymbol{x_o}$, $\boldsymbol{y_o}$, $\boldsymbol{e}$, $\boldsymbol{e_o}$, γ, $\boldsymbol{\Psi_{eq}}$, $\boldsymbol{e_s}$, $\boldsymbol{f^*}$, $\boldsymbol{\xi^*}$

while (For the given Time of simulation/process)

START:

1: d-q-0 transform the linearized system model Equation (3.1.2) by Equation (3.1.3).

2: Take converter/grid voltages $(\boldsymbol{u}, \boldsymbol{w})$ from Simulink hard wired microgrid model in Figure 2;

3: Generate the faults and disturbances to be added (representing) sensor/C.T/P.T faults;

4: Give voltages $(\boldsymbol{u}, \boldsymbol{w})$ as inputs to the Simulink-based mathematical model of a microgrid, in Equation (3.1.6).

5: Add faults/disturbances $(\boldsymbol{f}, \boldsymbol{\xi})$ to the output equation of the system represented by Equation (3.1.7);

6: Pass the faulty system output in Equation (3.1.7) from a stable filter defined in Equations (3.1.8) and (3.1.9) to reduce the magnified effect of faults and disturbances;

7: Augment the system states with stable filtered output, as done in Equations (3.1.10) and (3.1.11).

8: Pass the augmented system state from state/output estimator SMO in Equation (4.1.1);

9: Determine the augmented (state/stable filtered output) estimation error by taking the dif-

ference between system and observer states/outputs as defined in Equation (4.1.2);

10: Use $H-$ constraint mentioned in Equation (6.1.13) (β parameter is worst case/ minimal fault in Equation (6.1.12)) in HJIE in Equation (6.1.15) (to fulfill the saddle point requirement); $<H_\infty$ constraint in parallel is given by Equation (6.1.2), the worst case disturbance upper bound in Equation (6.1.1), and the respective HJIE in Equation (6.1.4)>;

11: Determine the constrained LMIs from the above equation in vector form as defined in (11) for $H-$ and Equation (32) for H_∞;

12: Convex feasibility and optimize the constrained LMI given in Equation (6.1.22) (for $H-$ constraint) and Equation (6.1.11) (for H_∞ constraint) using the function 'feasp' in the appendix in Section A.4 to find the optimal gain G_o^* as defined in the Theorem 6.1 statement, and switch term gain G_m^*, as defined in Lemma 1; <Gains are determined from Lyapunov P or Q matrices , using Lemma (1) and given in detail in [8] >;

13: Use the same SMO gains in state/output estimator SMO in step 8;

14: Determine the state estimation error as determined in Equation (4.1.2),

15: Give stable filtered output estimation error part of the total error vector ($\boldsymbol{e}$), i.e., ($\boldsymbol{e}_o$) in Equations (4.1.4) and (4.1.5) to state/output estimator SMO in step 8 and the state error estimator SMO in Equations (4.1.7) and (4.1.8) to attain the sliding mode;

16: If (the sliding mode is attained in Equations (4.1.7) or (4.1.8)), Feed the state estimation error to the reduced order state estimation error, explained in Lemma 7 (details in [8]);

17: Determine the gains (γ (defined in Lemma 7), $\boldsymbol{\Psi}_{\boldsymbol{eq}}$, reduced order state error $\boldsymbol{e}_s$)) (details in [8]),

18: Compute the estimated fault as done in Equation (7.1.37) and the disturbance as in Equa-

tion (7.1 38);

19: Use the estimated faults and correct the faulty sensor readings by adding/ subtracting from it, as done in Equation (8.1.1).

20: Feed the corrected sensor output values to PI and Droop-based current/voltage/real power/complex power control as shown in the detailed Simulink-based block diagram with details in the FTC section of [8],

21: Repeat Step 10 onward for the H_∞ constraint in (6.1.2) and the compromised H_- / H_∞ constraints

END (of while loop)

Summary: The chapter has 2 parts. The first part discusses the fault-tolerant control approach being used and additionally, the conventional voltage-frequency control for the VSI-based microgrid. The Simulink-based detailed control block diagram illustrates graphically the working. The second part of the chapter gives the simulink-based complete procedural block diagram with the explanation of each block and algorithms mentioning sequential execution of each step performed for the research tasks executed in papers [8], [10]

CHAPTER 9

Results and Discussions

According to the literature [2, 33, 38], the most commonly occurring faults in sensors are impulsive (incipient), occurring at regular intervals (intermittent), linearly increasing, constant measurement error, and random faults. However, for current and potential transformers in saturation, the faults occurring are mainly sinusoidal magnitude, phase, and harmonic faults. The simulations are performed for state/output estimation, stable filtered state/output estimation, state estimation error, stable filtered output estimation error, state estimation filter error, reduced order state estimation error, disturbance estimation, fault reconstruction, and fault tolerant control (FTC) performance. All these are performed for six fault cases: constant, ramp, sawtooth, square sinusoidal, and random types of additive faults along with additive sinusoidal disturbances of the first, second, and third harmonics. The same types of faults are considered for both voltage and current sensors simultaneously with sinusoidal additive disturbances of different and same frequencies; however, the proposed FD and FTC mechanisms are quite robust against the cross options as well. To avoid unnecessary details and length of paper, the reduced

order errors and stable filtered states/outputs are not given for any case, whereas the FTC performance is given for worst-case sinusoidal faults (among the considered ones). The behavior of the system and the results for all simulations were consistent, and no statistical analysis was required for a deterministic system and simulation platform.

After detailed testing of the system, the results are quite good in terms of accuracy, except for the fault and disturbance signals in the near frequency range of 60^{o}, which produced scaled current fault estimation in some cases and delayed current fault estimation results in some cases; however, the voltage faults are accurately estimated in all cases. Moreover, there is an occurrence of time delay problem, which needs discrete time compensation for the phase. Some fault estimation errors and less accurate FTC performance of current is due to the very reason. However the problem is not corrected here, instead will be considered for future works.

A Simulink-based detailed three-phased inverter model was considered in the simulation. The grid/ DC source voltage both operate at 600 V, the phase of the grid voltage is used for PLL block and all abc-dq transformations; SVPWM operates at a frequency of 10,000 Hz with sampling time of 0.0001s. The discontinuities are caused by greater sampling times, which can be reduced to improve accuracy at the cost of lesser ability of online working due to the increased response time. Because the continuous time simulations move at very low speeds, which are not viable for real-time online performance; therefore, fixed-step solvers are used for simulation in Simulink (MATLAB) with single task handling to avoid complexities with very minor compromises on accuracy.

The microgrid system model parameters are listed in Table 9.1, and the controller parameters are listed in Table 9.2.

Table 9.1: Microgrid system parameters.

Parameter	Value	Parameter	Value
V_{dc}	600 V	V_g	600 V
L_{f1}	4.20 mH	L_{f2}	4.20 mH
L_{c1}	0.50 mH	L_{c2}	0.50 mH
C_{f1}	15 F	C_{f2}	15 F
R_{d1}	2.025 Ω	R_{d2}	2.025 Ω
r_{f1}	0.50 Ω	r_{f2}	0.50 Ω
r_{f1}	0.09 Ω	r_{f2}	0.09 Ω
ω_c	50.26 rad/s	ω_n	377 rad/s
V_{oqn}	85 V	m, n	1/1000
θ_{grid}	60°	L_{f3}	4.20 mH
L_{c3}	0.50 mH	C_{f3}	15 F
R_{d3}	2.025 Ω	r_{f3}	0.50 Ω
r_{f3}	0.09 Ω	ω_{PLL}	377 rad/s
$\omega_{c\,PLL}$	7853.98 rad/s		

Table 9.2: Controller gains/parameters.

PI Gains	Parameter	Value
Voltage	k_{pvd}, k_{pvq}	0.5
Controllers	k_{ivd}, k_{ivq}	25
Current	k_{pcd}, k_{pcq}	1
Controllers	k_{icd}, k_{icq}	100
PLL	kp_{PLL}	0.25
Controller	ki_{PLL}	2

9.1 Results for Proposed Work in Chapter 5 [8]

For the proposed work in Chapter 5, regarding some other simulation constants, since the residual magnitude if considered peak to peak is 0.2 for the (dq) currents/voltages for the considered time of simulation; whereas the $\|(max(\xi)\| = 6.32$: so the H_∞ norm μ in this case has the numerical value 0.01. The value of η is a small positive constant considered $\eta = 10$ to ensure the constraint in inequality (90), whereas the upper bounds for the current and voltage are $\alpha' = 1A/10V$, respectively. However, for the worst cases and increased magnitudes, it is considered up to 10 A/100 V for I/V, whereas the upper bounds of ξ are normally considered as 0.2 A/2 V for I/V, and for the worst case with increased magnitudes in simulations 3 A/10 V for I/V.

9.1.1 Case I–Sinusoidal Faults and Disturbances/Worst Case Scenario (Among the Considered Ones)

For the proposed work in Chapter 5, the simulations were performed for randomly considered different frequencies and phases for both faults and disturbances and quite high fault/disturbance magnitudes, and they provided quite good performance. The voltage and current fault magnitudes are 100 V and 10 A, the frequencies are 120 Hz and 180 Hz, and the phases are 75° and 240°, respectively, whereas the disturbance magnitudes are 10 V and 3 A, the frequencies are 75 Hz and 300 Hz, and the phases are 45° and 310°, respectively.

The results are shown for the state/output estimation in Figures 9.1, 9.2, 9.3, the state/output estimation errors in Figures 9.4, which are performed with modified H_∞ constrained SMO gains only. The results in Figure 9.5 present voltage fault reconstruction, whereas the current fault reconstruction is presented in Figure 9.6, voltage fault estimation error in Figure 9.7, current fault estimation error in Figure 9.8, current disturbance estimation in Figure 9.9, FTC performance for q-component of output current in Figure 9.10, FTC performance for d-component of output voltage in Figure 9.11 and current and voltage faults reconstruction for ramp/linearly increasing faults in Figure 9.12.

The above-mentioned results are compared for SMO gains which optimized for Trace minimization algorithm proposed by Edwards in [57], feasibility optimization of H-infinity enhanced SMO, and Riccatti equation based modification of H-infinity enhanced feasibility optimized gains. Voltage fault reconstruction has a deformation of the lesser grade; however, the current fault reconstruction and fault estimation error increases due to time delay issue, which can be dealt with separately in future works.

An important Remark on Results: The trace minimization of Ricatti-equation-based modification of H_∞-enhanced LMI may not be feasible for some forms of LMIs: however the feasibility optimization of the LMI works well nearly in all cases. The minimization of the trace is a linear objective for convex optimization, which can work well on some forms of LMIs or some systems depending upon its parameters. However, the trace minimization of Ricatti equation-based modification of LMIs not enhanced with H_∞ criterion presented by Edwards in [57] also works well nearly in all cases, but it does not give the accuracy of results in the considered microgrid system, which is included in comparisons. This particular aspect still requires much rigorous testing to comment in a more deterministic way The feasibility optimized H_∞-enhanced-LMIs also have a phase lag effect, particularly in the current signal, which needs to be compensated, but compensation of phase is not considered in this study.

Figures 9.1, 9.2, 9.3 are showing the state/output estimation using SMO gains determined by the proposed Riccati equation-based modification of H_∞ enhanced gains. Instead of all states, the state estimation performance results are given for the estimation of input current (d-component), output current (d-component), Iod, and output voltage)q-component). The results are apparently quite close in terms of estimation except for some scaling which can be adjusted further as well.

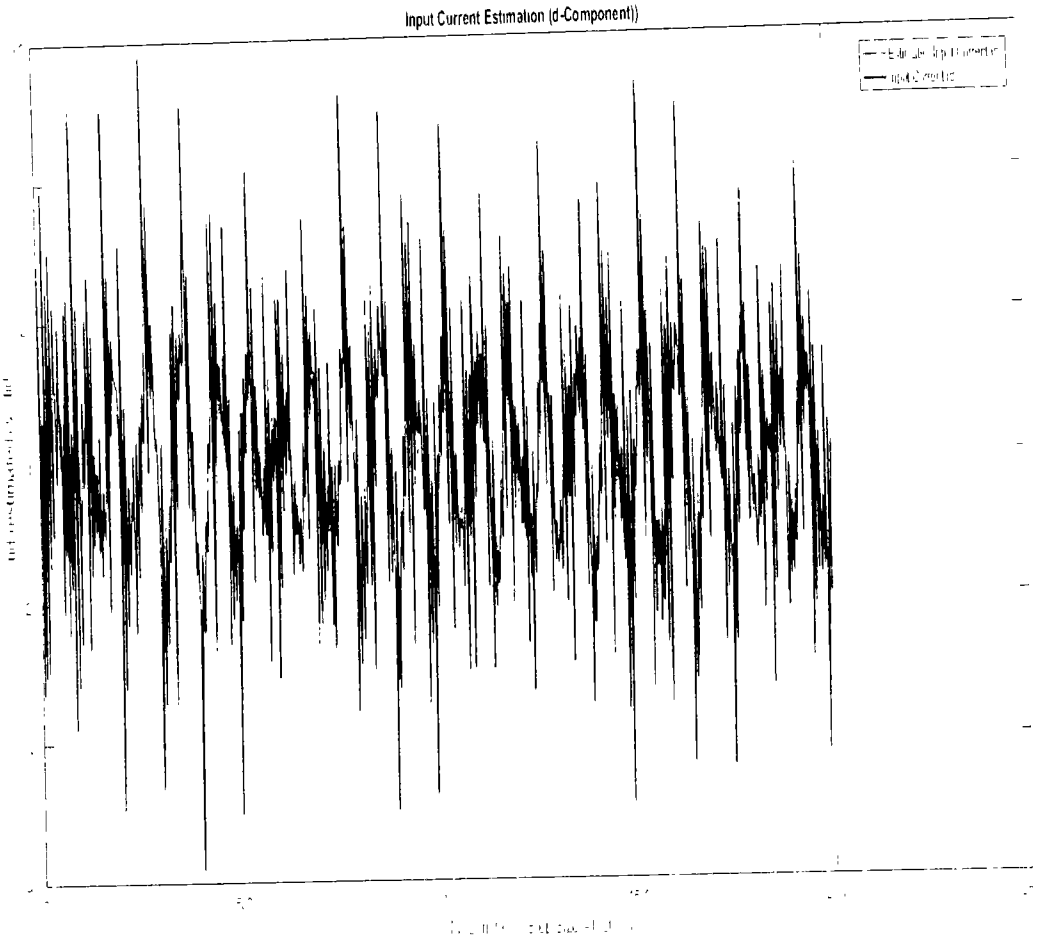

Figure 9.1: Fault diagnostic observer based input current estimation (d-component)

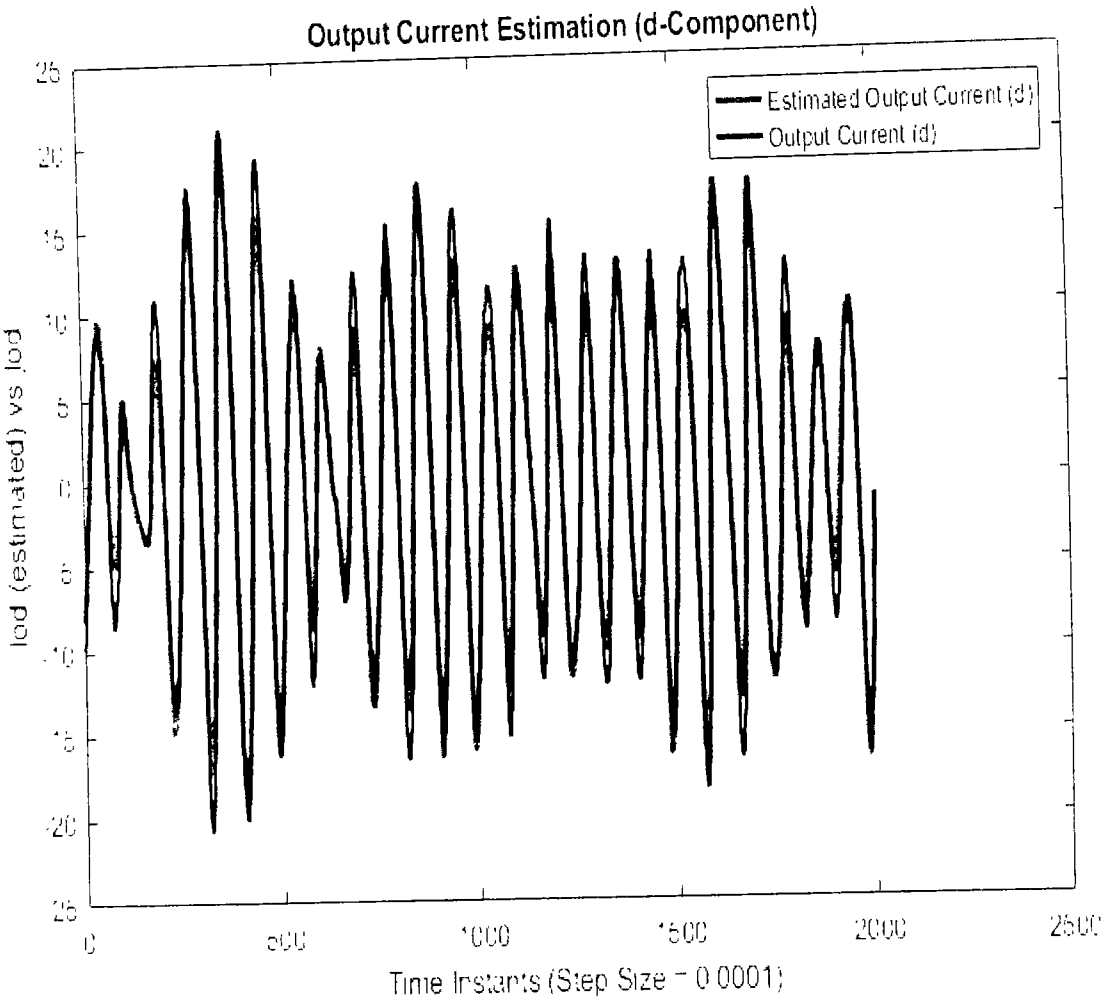

Figure 9.2: Fault diagnostic observer-based output current estimation (d-component).

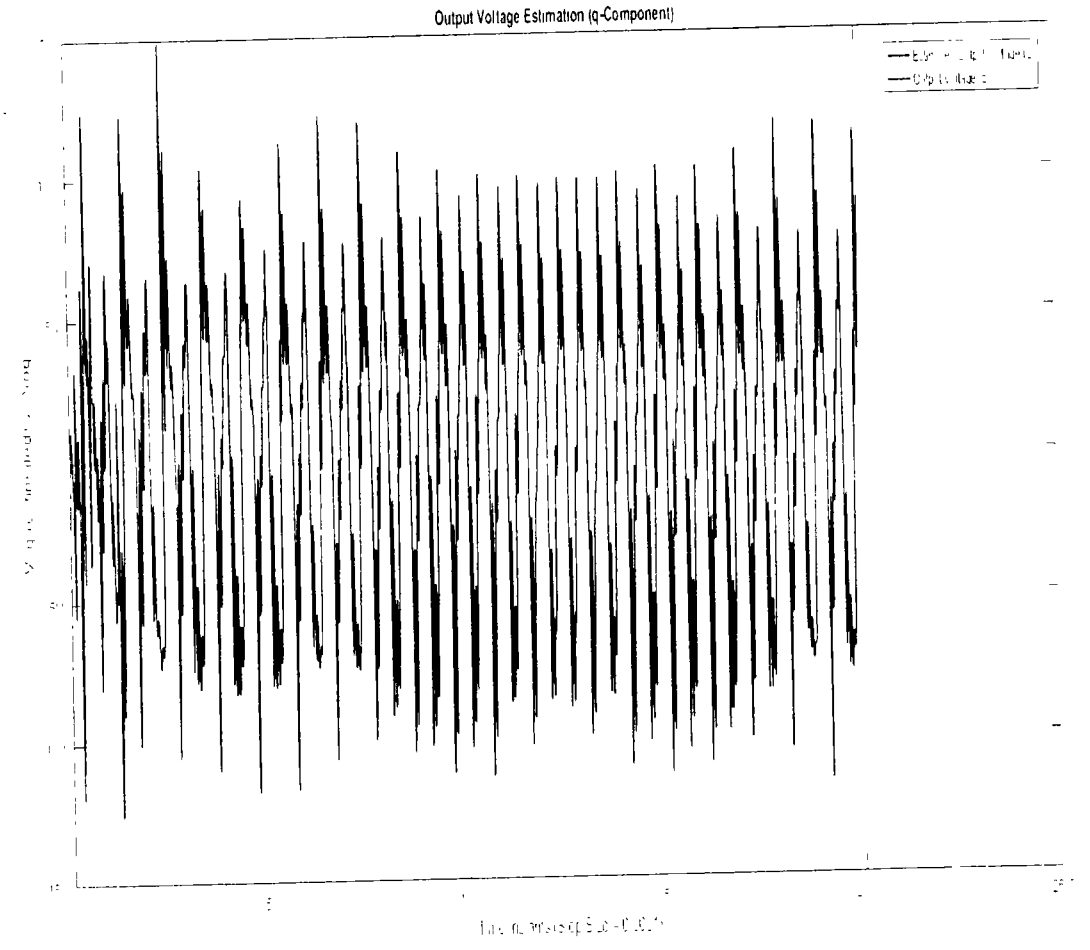

Figure 9.3: Fault diagnosticobserver-basedd state output voltage estimation (q-component).

Figure 9.4 is showing the state/output estimation error using the modified method of determination of SMO gains. The state estimation error can be considered as a performance index for the working of state/output estimator SMO, which also acts as a fault detection filter. In the fault magnitude of 10 A/100 V, the index stays within a controlled range effectively 1 V/0.5 A, with a negligibly small mean value.

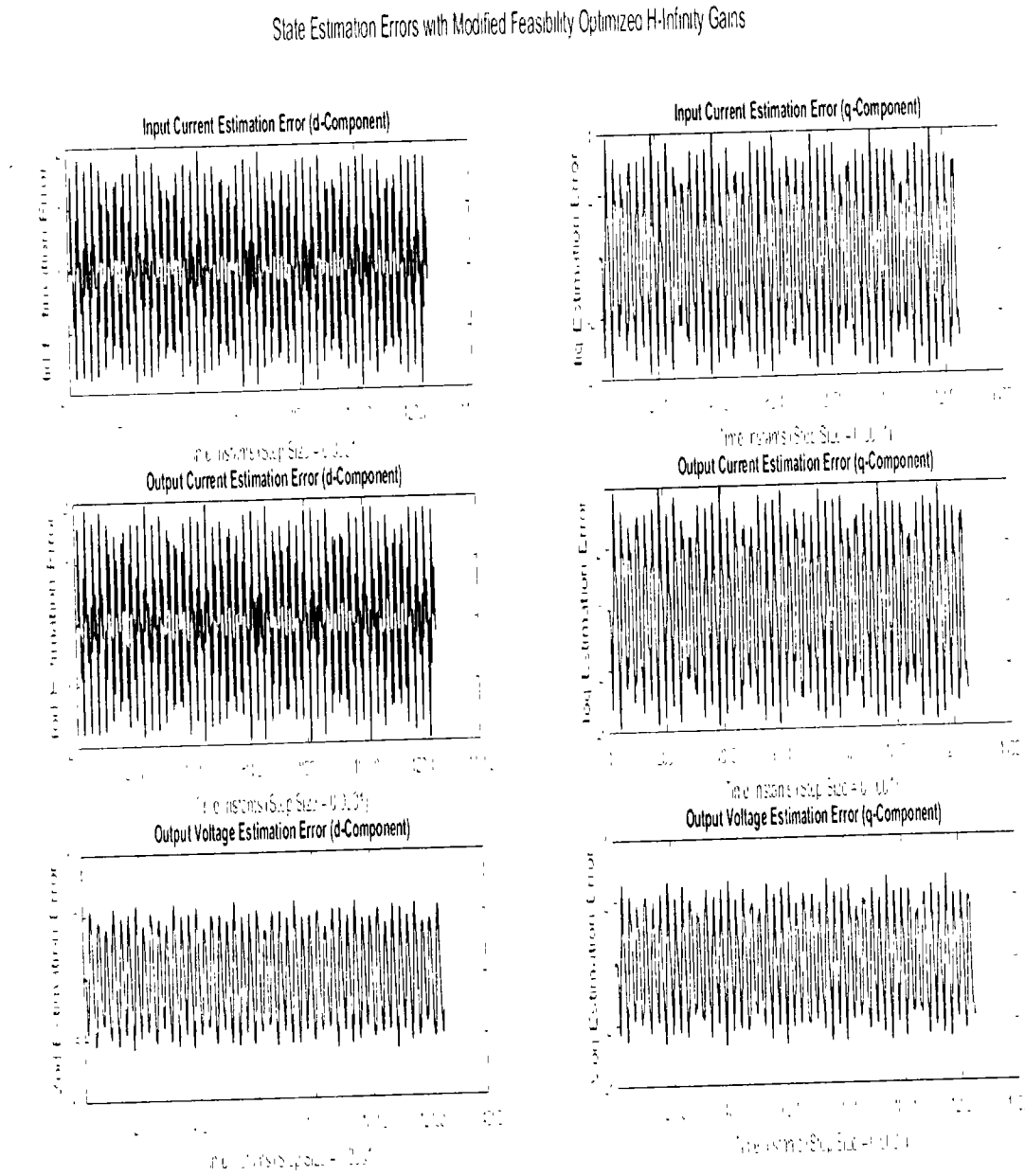

Figure 9.4: Fault diagnostic observer-based state estimation error (dq-components).

Figures 9.5 and 9.6 show the voltage and current faults estimation/reconstruction using SMOs using the gains optimized with Trace optimization, feasibility optimization of H_∞ constrained LMIs, and trace/feasibility optimization of Ricatti equation based modification of H_∞ constrained LMIs. The results of the latter two as given in the proposed technique in Theorem 2

are quite better in terms of accuracy of reconstruction.

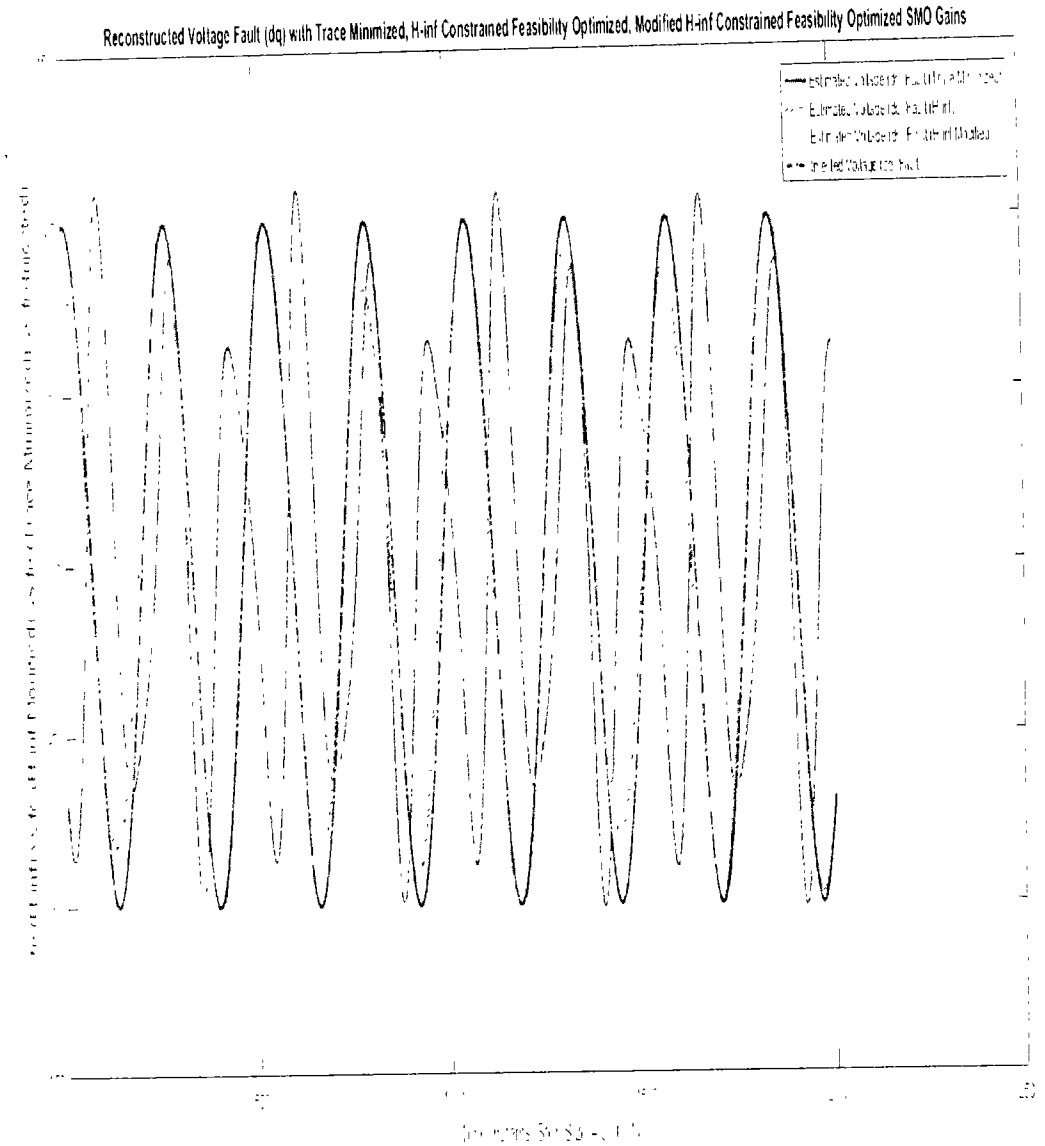

Figure 9.5: Voltage (dq) fault reconstruction.

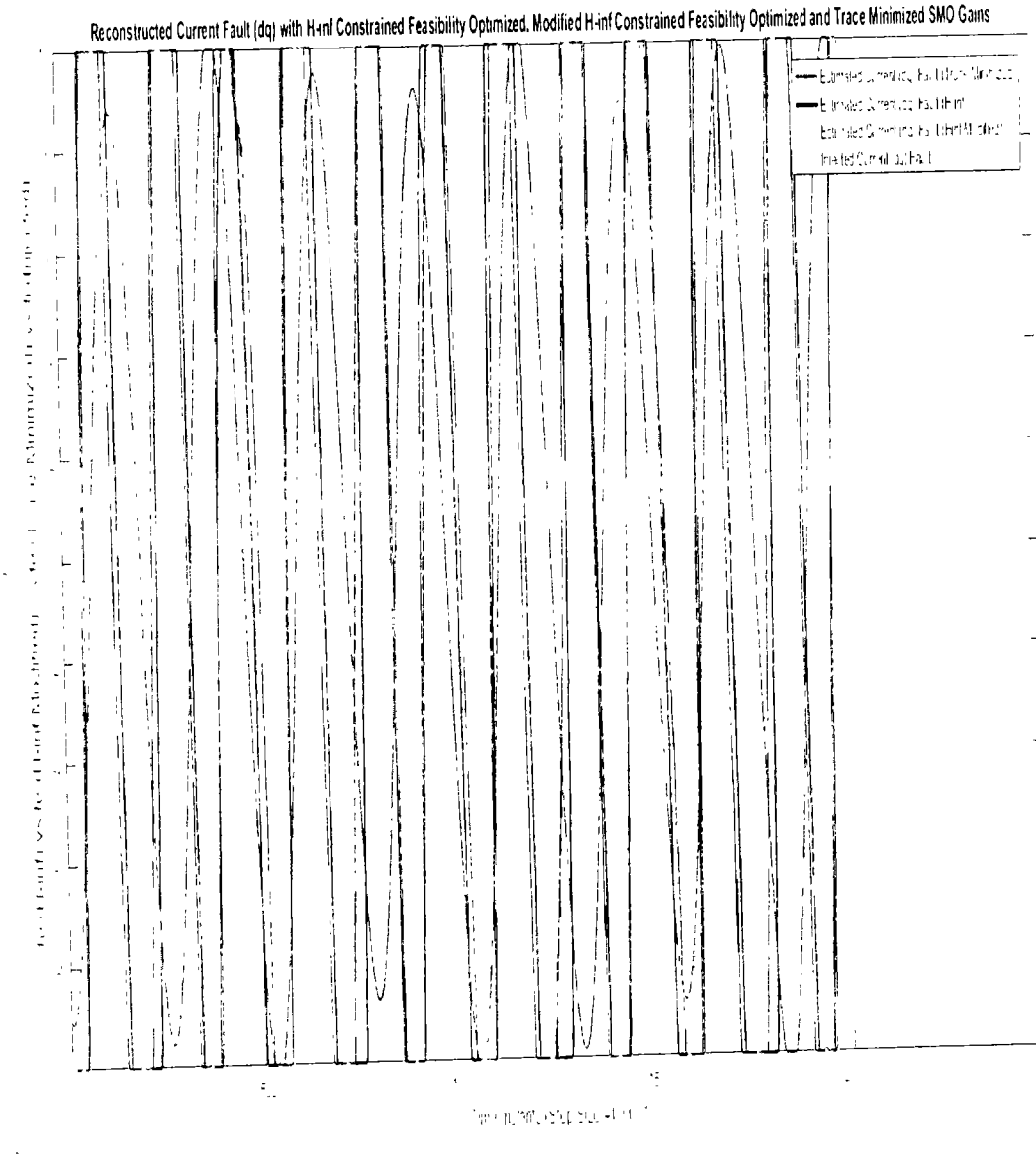

Figure 9.6: Current (dq) fault reconstruction.

Figures 9.7 and 9.8 show voltage and current fault estimation errors, which can be considered as the performance index of working of fault estimations and ultimately the FTC, whose accuracy depends. The results are compared for voltage/current fault estimations performed with SMOs using the gains optimized with Trace optimization, feasibility optimization of H_∞ constrained LMIs, and trace/feasibility optimization of Ricatti equation-based modification of H_∞

constrained LMIs. The results of the latter two are nearly comparable.

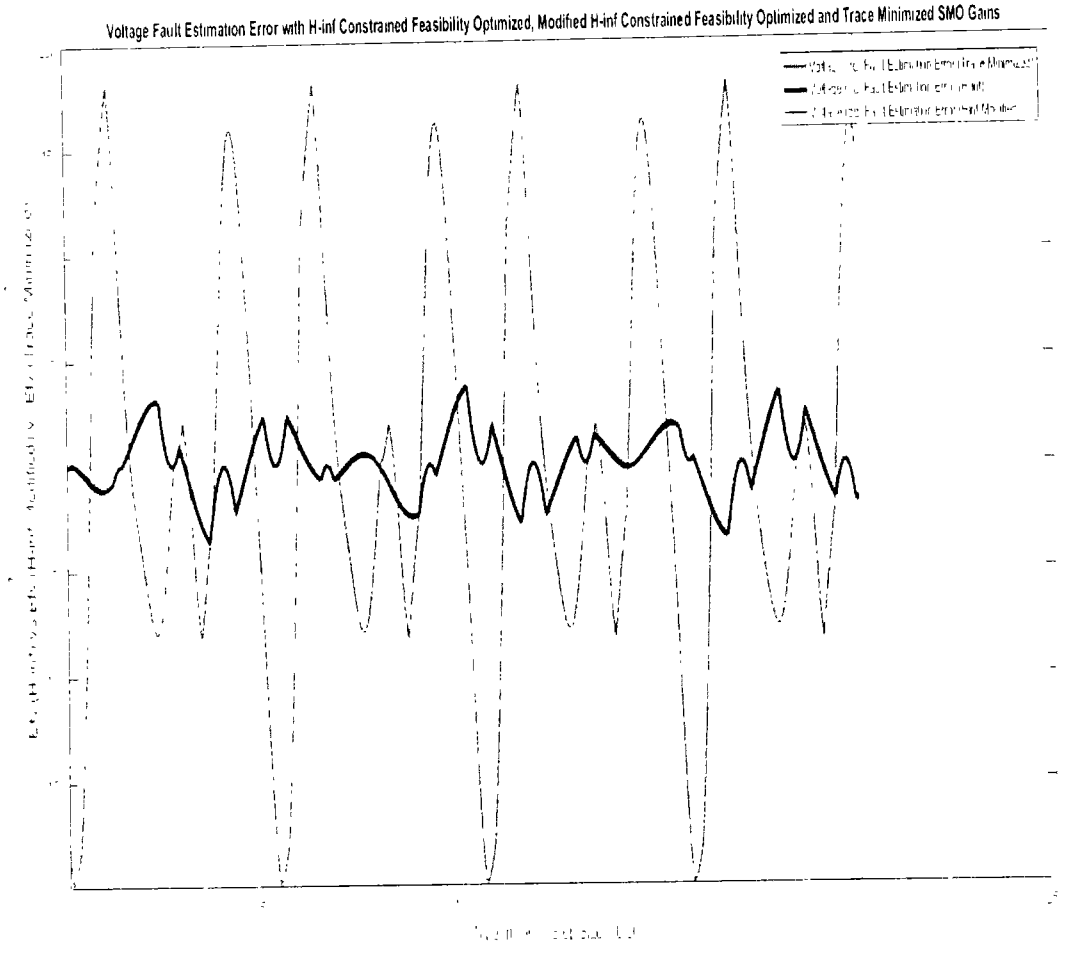

Figure 9.7: Voltage (dq) fault estimation error.

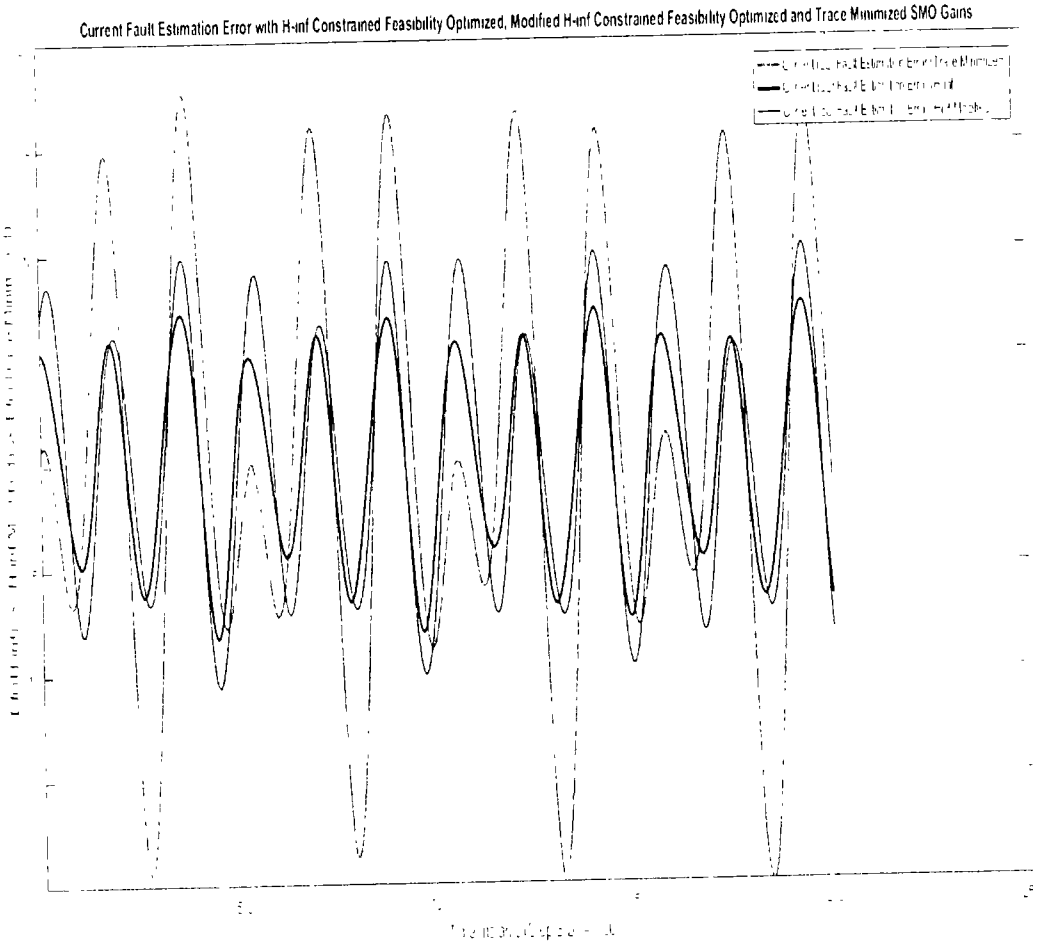

Figure 9.8: Current (dq) fault estimation error.

Figure 9.9 is showing the current disturbances estimation/reconstruction using SMO using gains with the above three methods to lead towards a comparison analysis with the proposed work. The results for all three methods are in compromise and no one method can apparently be said to be better than the others. This accuracy is achieved due to the modified and corrected disturbance estimation procedure mentioned in Corollary 1

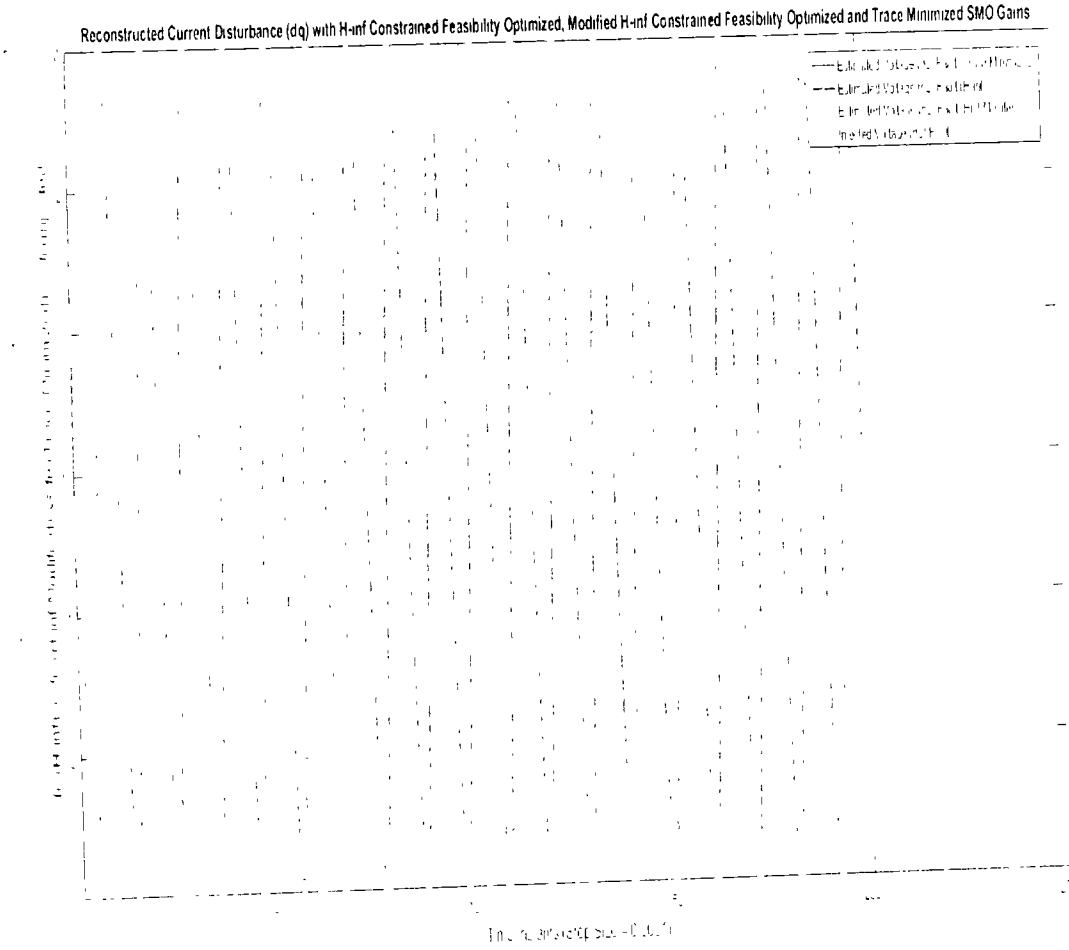

Figure 9.9: Current (dq) disturbance estimation.

Figures 9.10 and 9.11 give the FTC analysis shown for q-components of output voltage. The faulty q-components are corrected by SM observer-based fault estimation. The fault estimate and correction using the above-mentioned techniques of SMO is taken as a comparison because the accuracy of fault/disturbance estimation ensures reliable FTC working. The FTC achieved through the proposed SMO observer is better as shown by the graphical result.

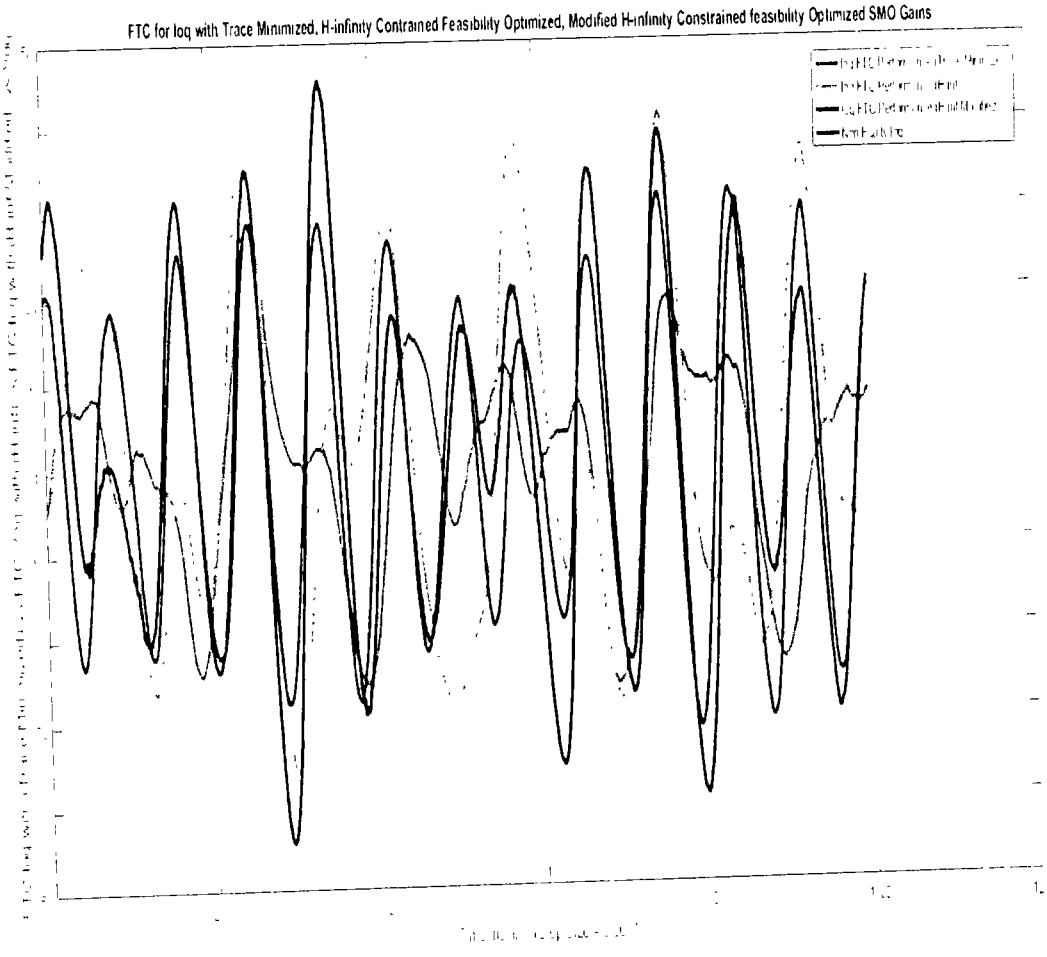

Figure 9.10: FTC performance for q-component of output current

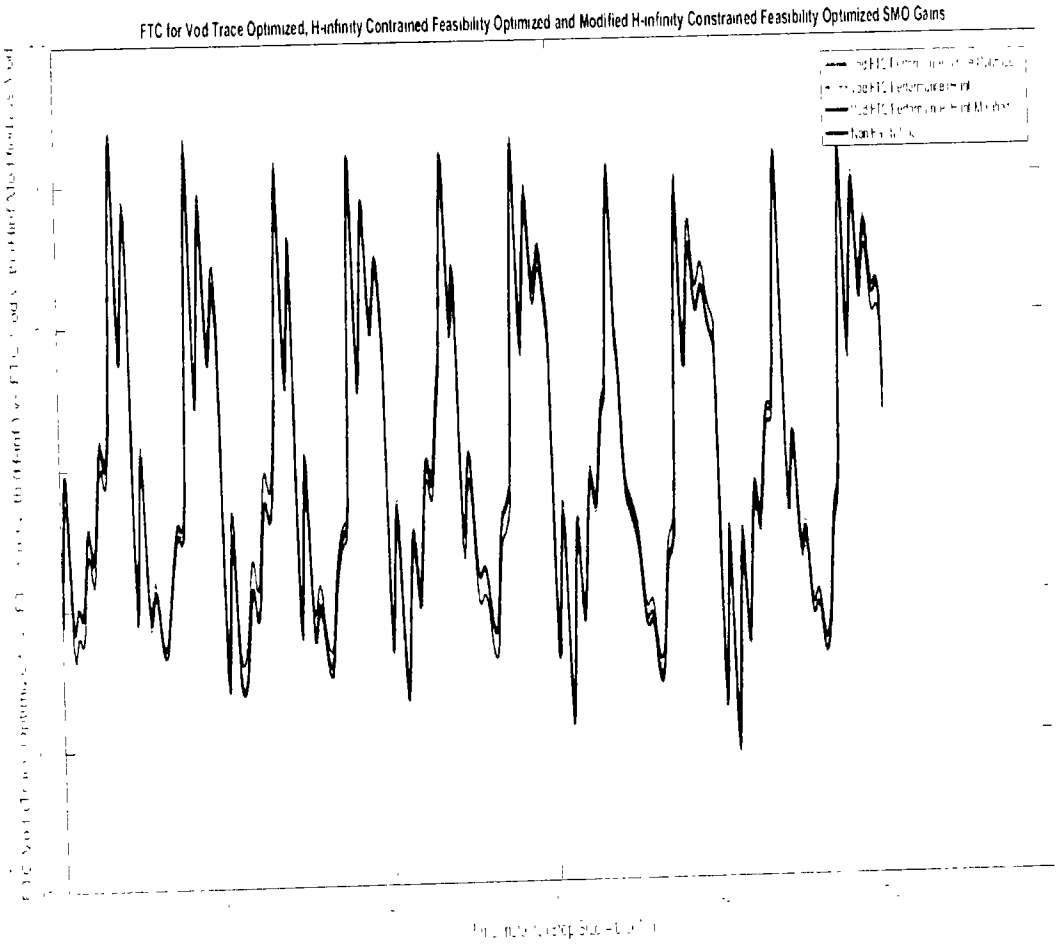

Figure 9.11: FTC performance for d-component of output voltage.

9.1.2 Case II-Ramp Faults and Sinusoidal Disturbances

Simulations are performed in this case for current/voltage injected linearly increasing faults with gradients 4 and 1, respectively, and third-harmonic sinusoidal disturbance, that is, 180 Hz for both V/I. The results for current/voltage fault reconstruction in Figure 9.12 are given.

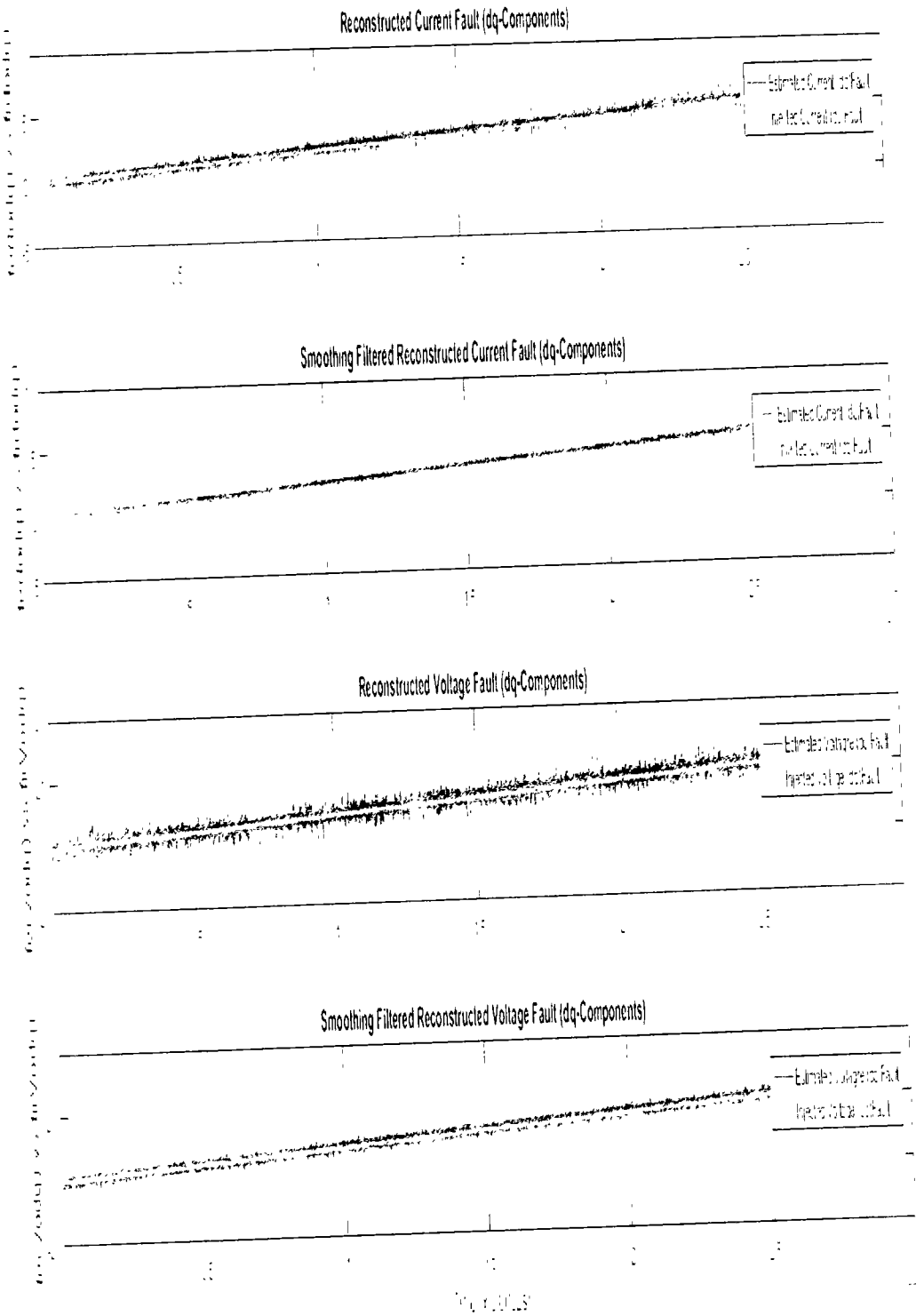

Figure 9.12: Current (dq) and voltage (dq) fault reconstruction (ramp fault/Case-II).

The simulations are also performed for detection and estimation of square/rectangular pulse (intermittent faults) in Figure 9.13, constant faults in Figure 9.14, saw-tooth faults Figure 9.15 and random pattern-based faults Figure 9.16 using the H_∞ enhanced trace optimized fault detection/estimation SMO observers. These graphical results of estimated/reconstructed faults are given below.

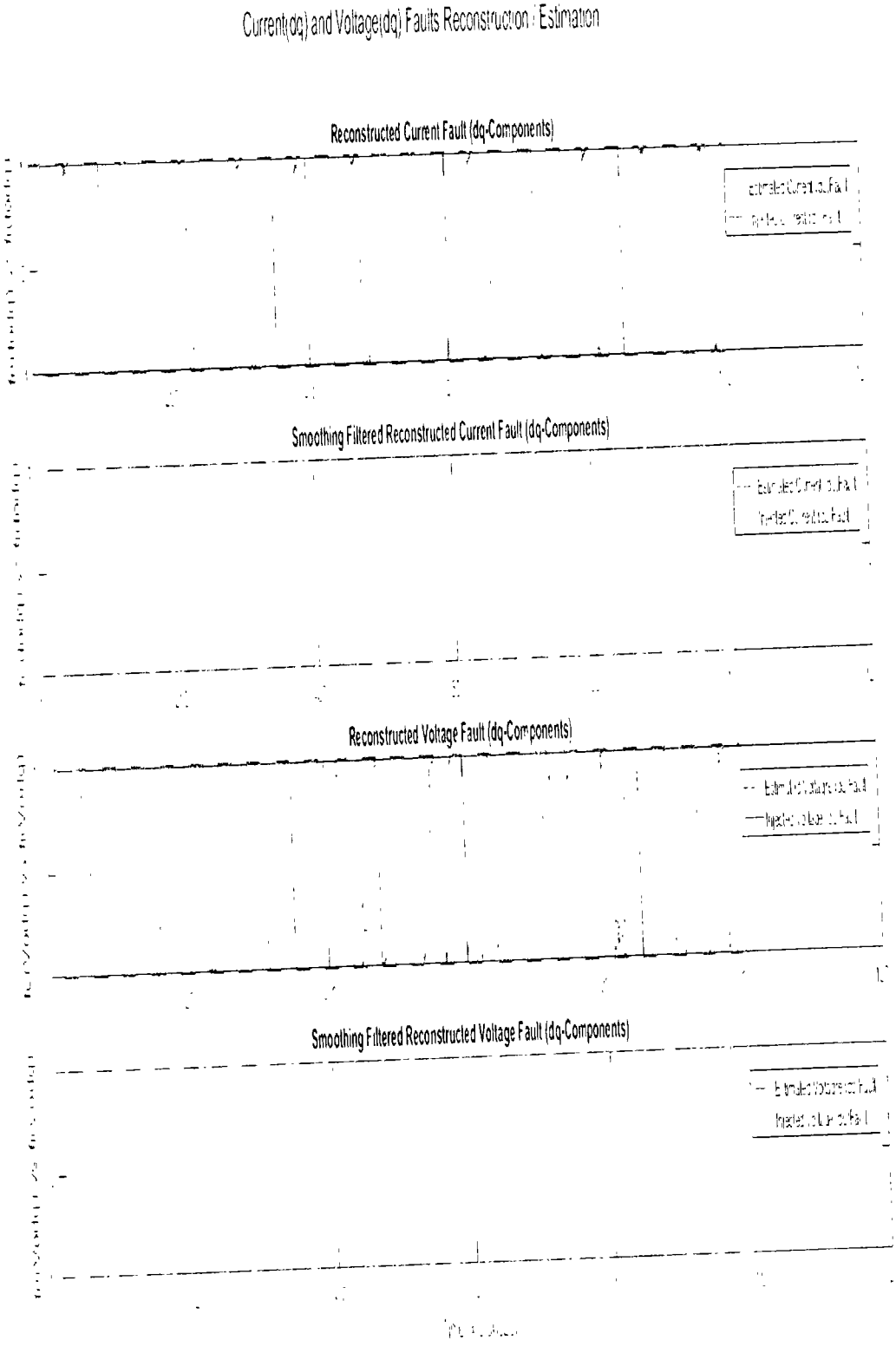

Figure 9.13: Current (dq) and voltage (dq) fault reconstruction (Intermittent (square pulse) fault/Case-III).

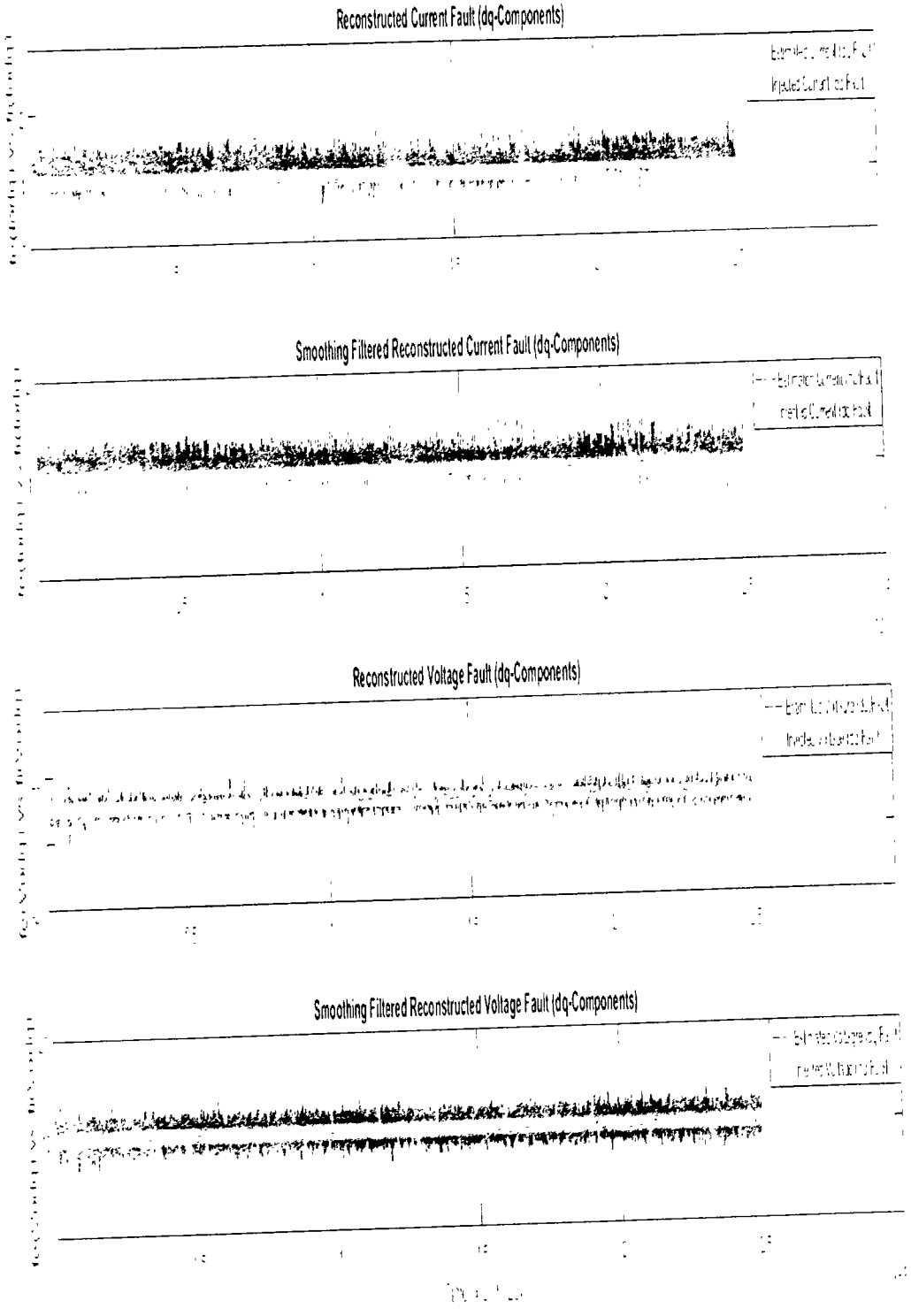

Figure 9.14: Current (dq) and voltage (dq) fault reconstruction (Constant fault/Case-IV)

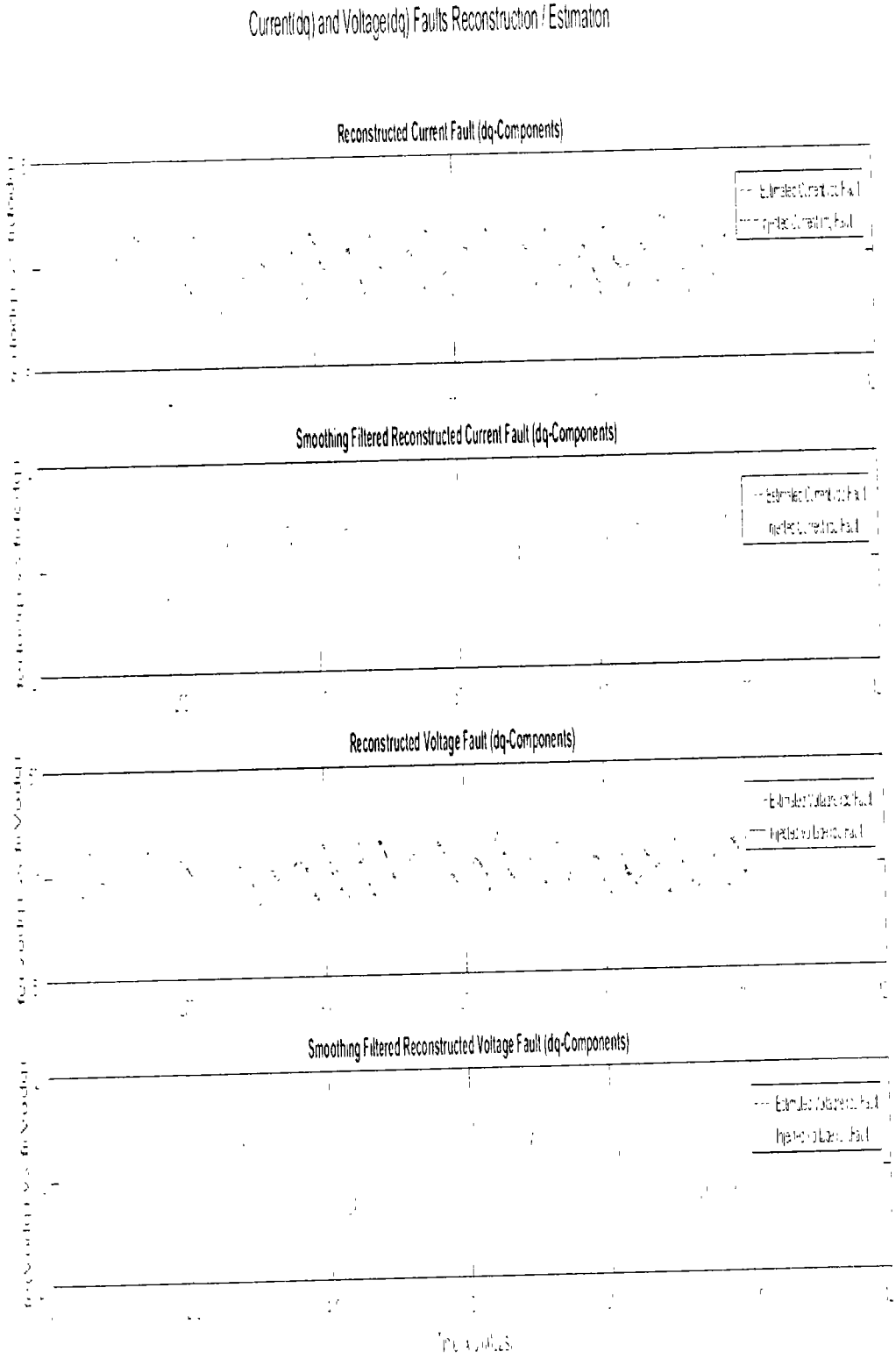

Figure 9.15: Current (dq) and voltage (dq) fault reconstruction (saw-tooth fault/Case-V)

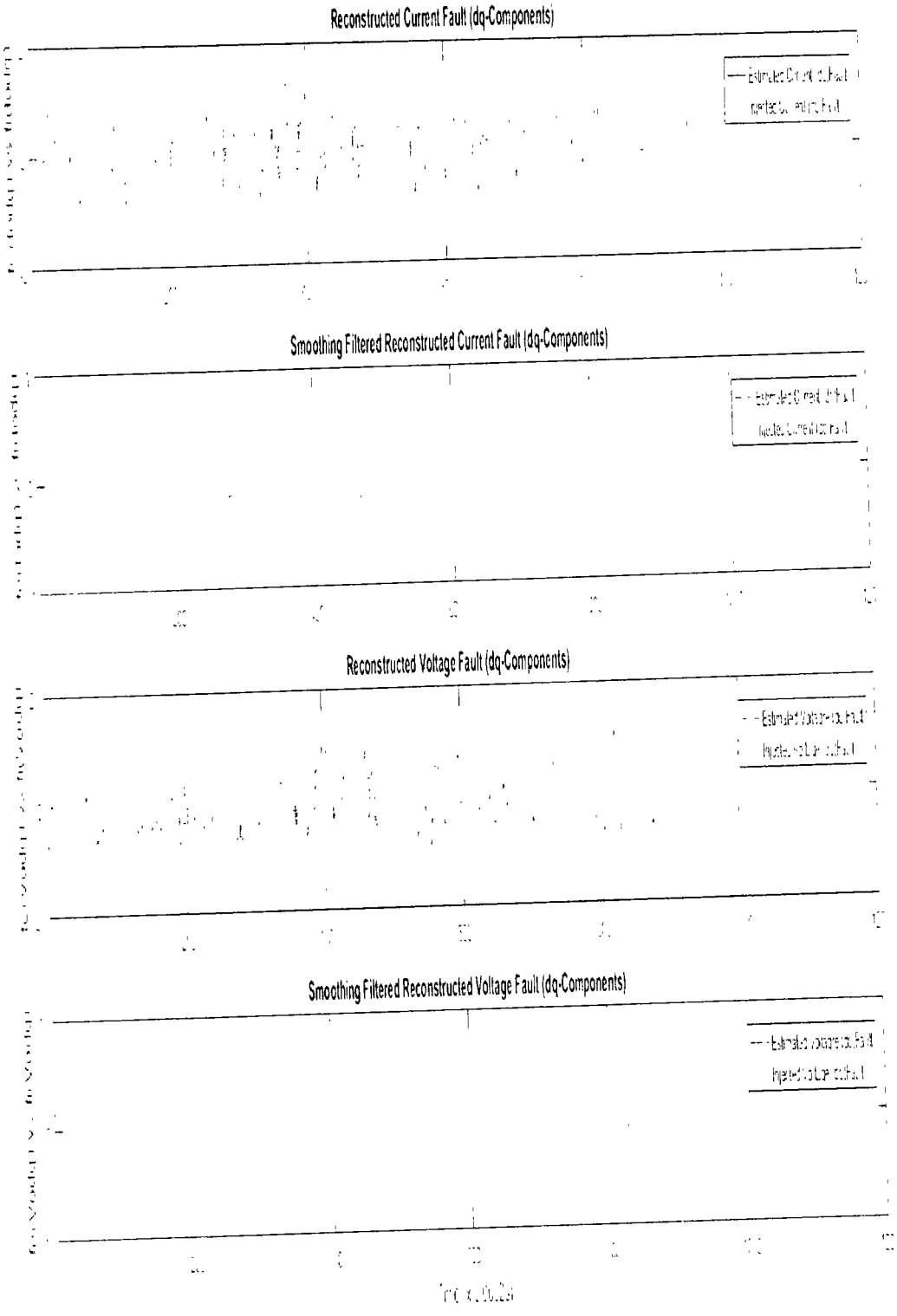

Figure 9.16: Current (dq) and voltage (dq) fault reconstruction (Random fault/Case-VI)

The FTC performance results are shown for magnified sinusoidal faults/disturbances of frequency 60 Hz in Figure 9.17, for magnified sinusoidal faults and disturbances of frequency 180 Hz in Figure 9.18, for magnified sinusoidal faults and disturbances of frequencies 120 Hz and 180 Hz respectively in Figure 9.19 using H_∞ enhanced trace optimized fault detection/estimation SMOs. The FTC results comprise simulations, which give a comparison of (i) non-faulty sensor outputs, (ii) uncorrected sensor output values in feedback (UC-FB), that is, the sensor outputs without being corrected by observer-based estimated faults given to the FTC block, (iii) FTC applied on corrected output values in feedback (C-FB), that is, the sensor outputs corrected by observer-based estimated faults and then given to the FTC block, and (iv) the observer-based fault-corrected sensor output values being given to the FTC block, separately for the d and q components of currents and voltages.

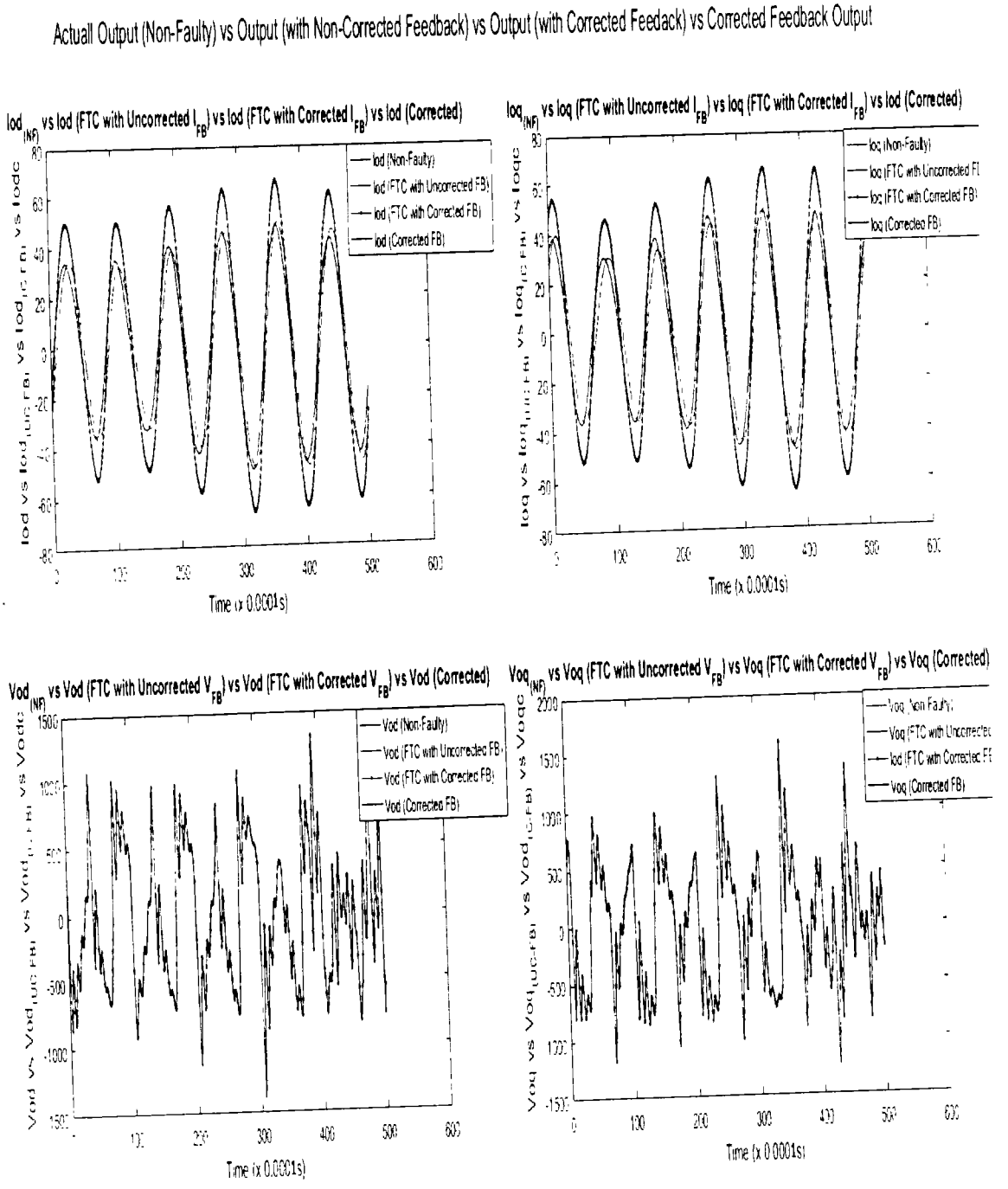

Figure 9.17: FTC Performance for magnified sinusoidal faults/disturbances of 60 Hz/60 Hz respectively

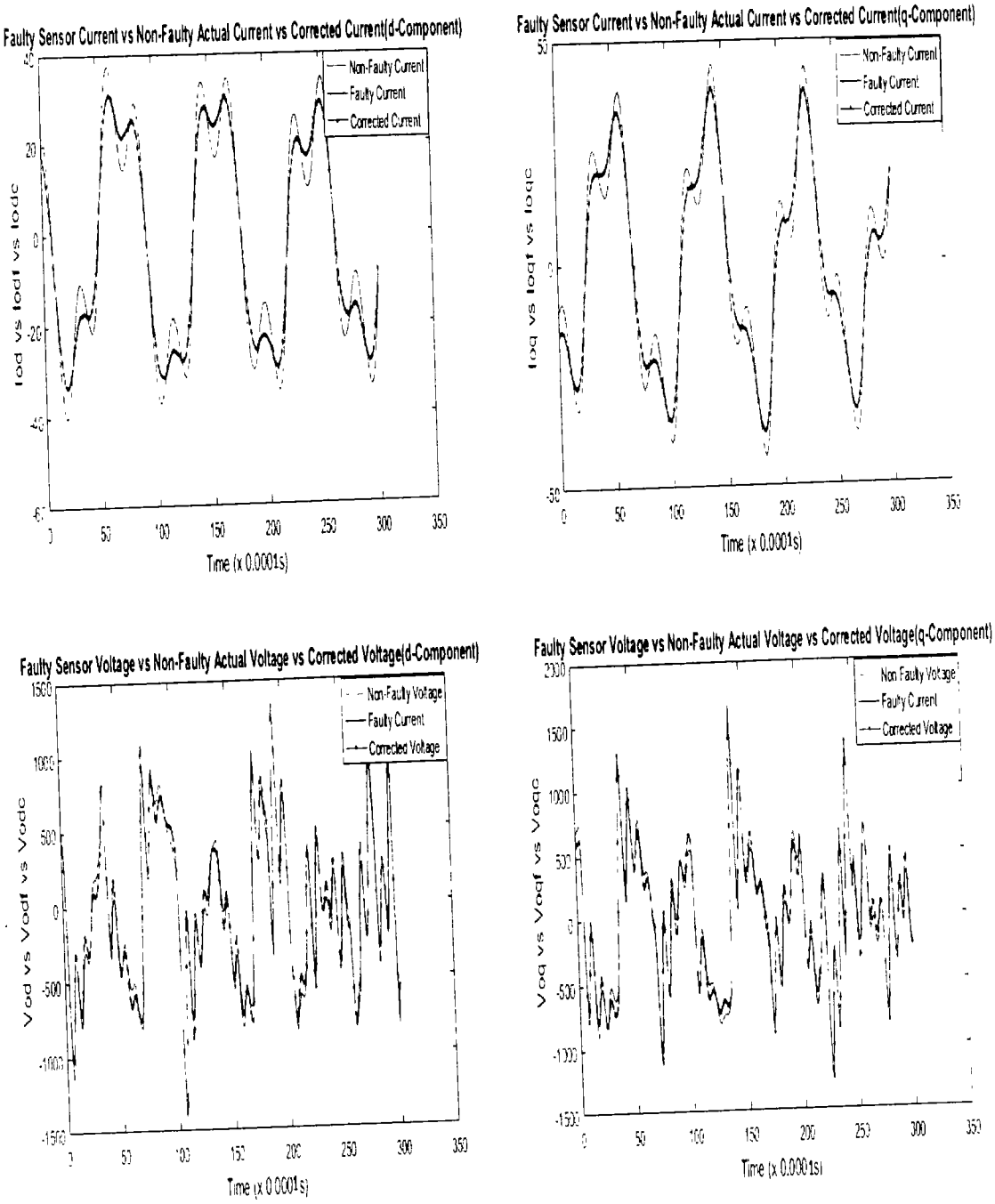

Figure 9.18: FTC Performance for magnified sinusoidal faults/ disturbances of 180Hz/180 Hz respectively

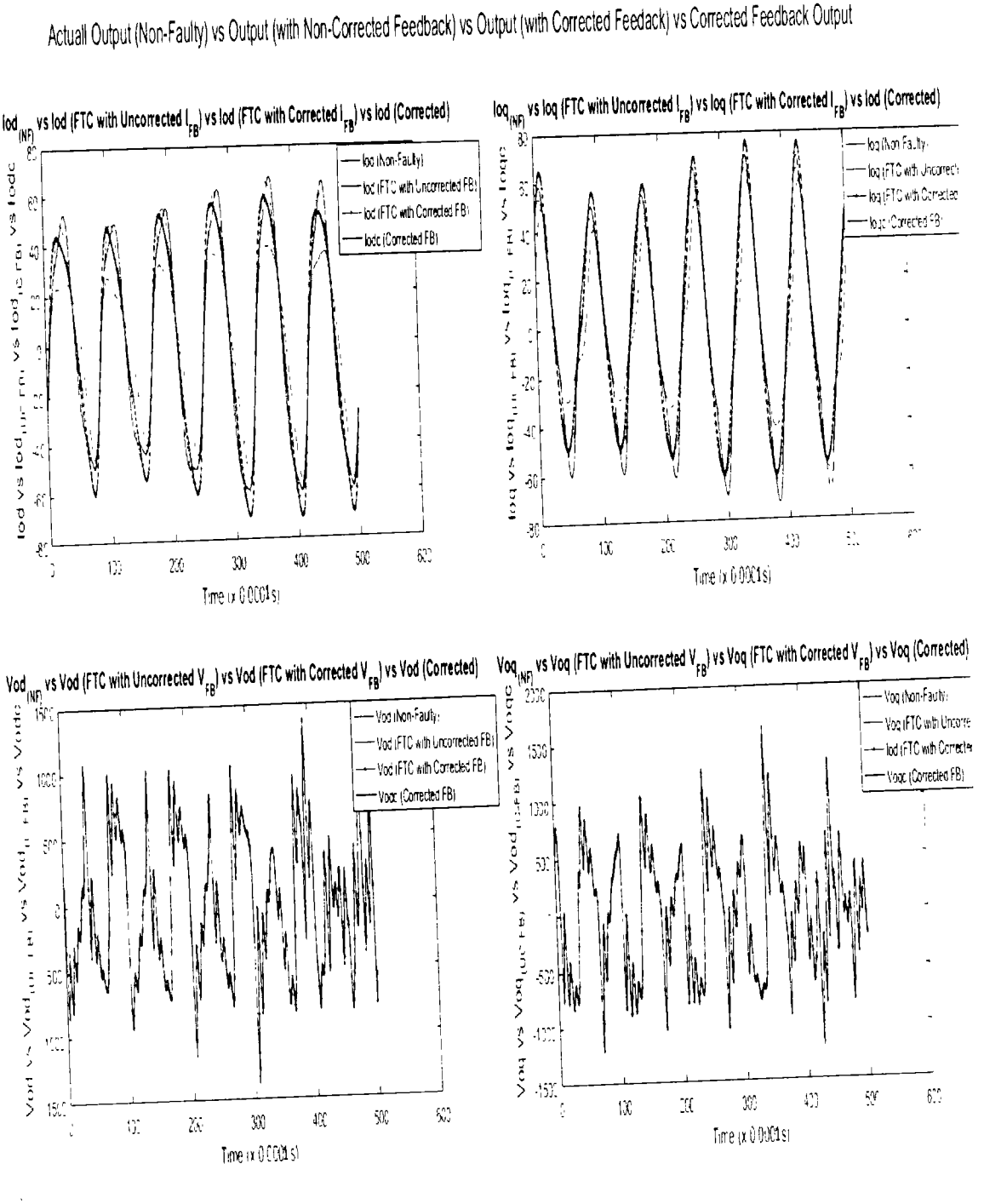

Figure 9.19: FTC Performance for magnified sinusoidal faults/disturbances of 120Hz/180 Hz respectively

9.2 Results for Proposed Work in Chapter 6 [10]

Now considering the proposed work From the Second Paper, Regarding some other simulation constants, for the considered time of simulation, as an estimate using the minimum/maximum values of faults, disturbances, and stable filtered output error, the H_∞ constant $\alpha = 3.76 \times 10^{-9}$ and $H-$ constant $\beta = 4.44 \times 10^{-19}$.

The value of η is a small positive constant considered $\eta = 10$ to ensure the constraint in inequality (7.1.24), whereas the upper bounds for current and voltage is considered up to $f_o = 10A/100V$ for I/V, respectively; whereas the upper bounds of ξ_o are $3A/10V$ for I/V.

Figure 9.20 shows the reconstruction of voltage fault compared using SMO with gains optimized with fault sensitivity parameter ($H-$), robustness to disturbance parameter (H_∞), and a mixed ($H-/H_\infty$). The voltage fault reconstruction using ($H-$) and ($H-/H_\infty$) are similar and nearly accurate, whereas that with (H_∞) is thought to be accurate but lagged with a phase of π radian. The constant multiple S_f used in Equation (47) for voltage fault reconstruction for (H_∞), ($H-$) and ($H-/H_\infty$) are 4×10^3, 0.5×10^{11} and 7×10^{11}, respectively. The multiples are required to compensate for the stable filtering scaling effect in output error term ϵ_o and are in direct relation with multiple of Luenberger gain G_o used in SMO.

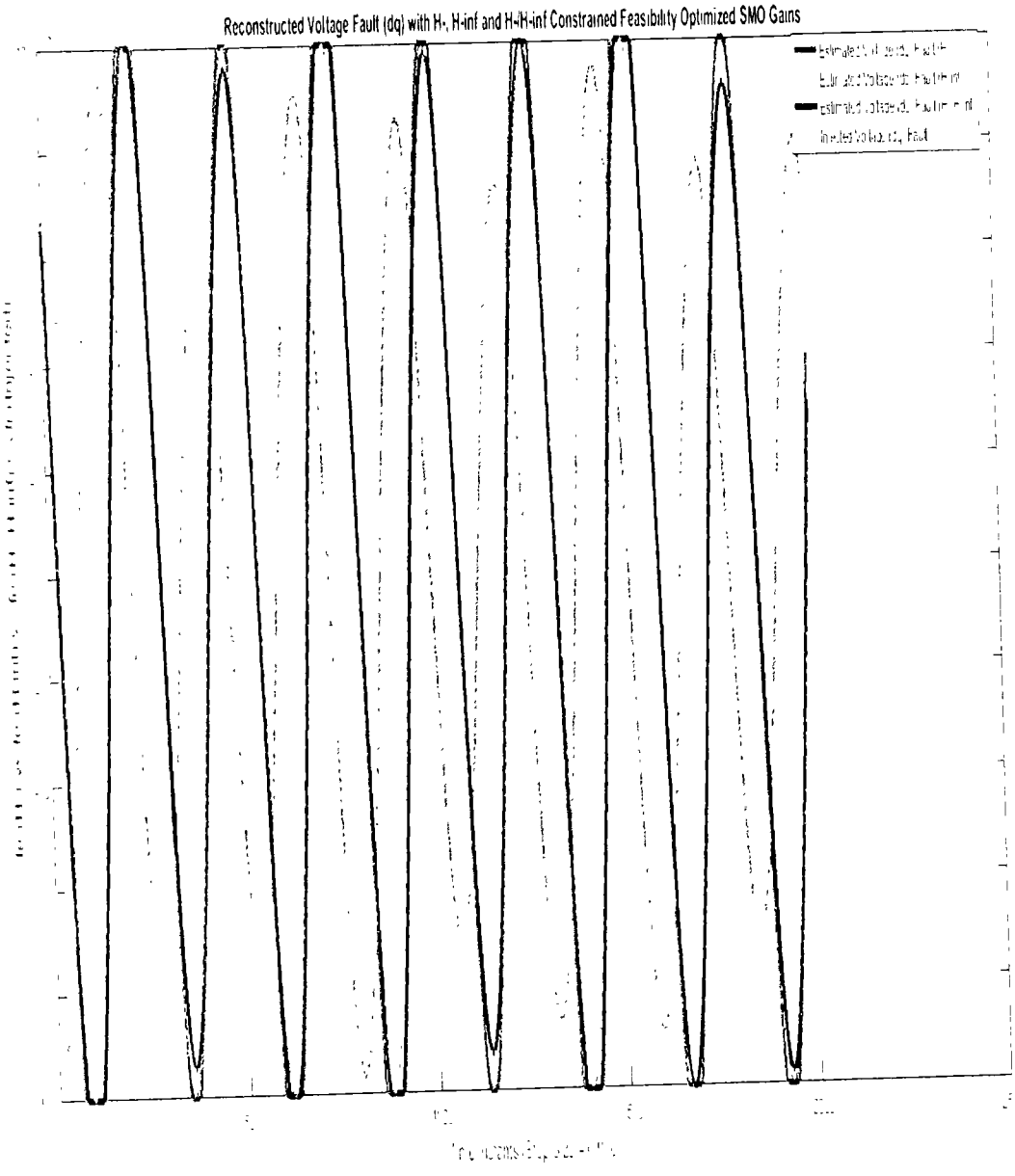

Figure 9.20: Reconstructed voltage fault (dq) with feasibility optimized ($H-$) and $H-/H_\infty$ SMO gains.

Figure 9.21 shows the reconstruction of the current fault compared using SMO with gains optimized with fault sensitivity parameter ($H-$), robustness to disturbance parameter (H_∞), and a mixed ($H-/H_\infty$). The current fault reconstruction using ($H-$) is nearly accurate while using

($H - /H_\infty$ is relatively accurate in one-half cycle and inaccurate in another half cycle, whereas the result with (H_∞) is thought to be accurate but lagged with a phase of π radian, which can be corrected using the phase compensation of π radian. The constant multiple S_f used in Equation (51) for current fault reconstruction for (H_∞), ($H-$) and ($H - /H_\infty$) are 2.5×10^3, $1 + 0.43 \times 10^{14}$ and $1 + 3 \times 10^{11}$, respectively.

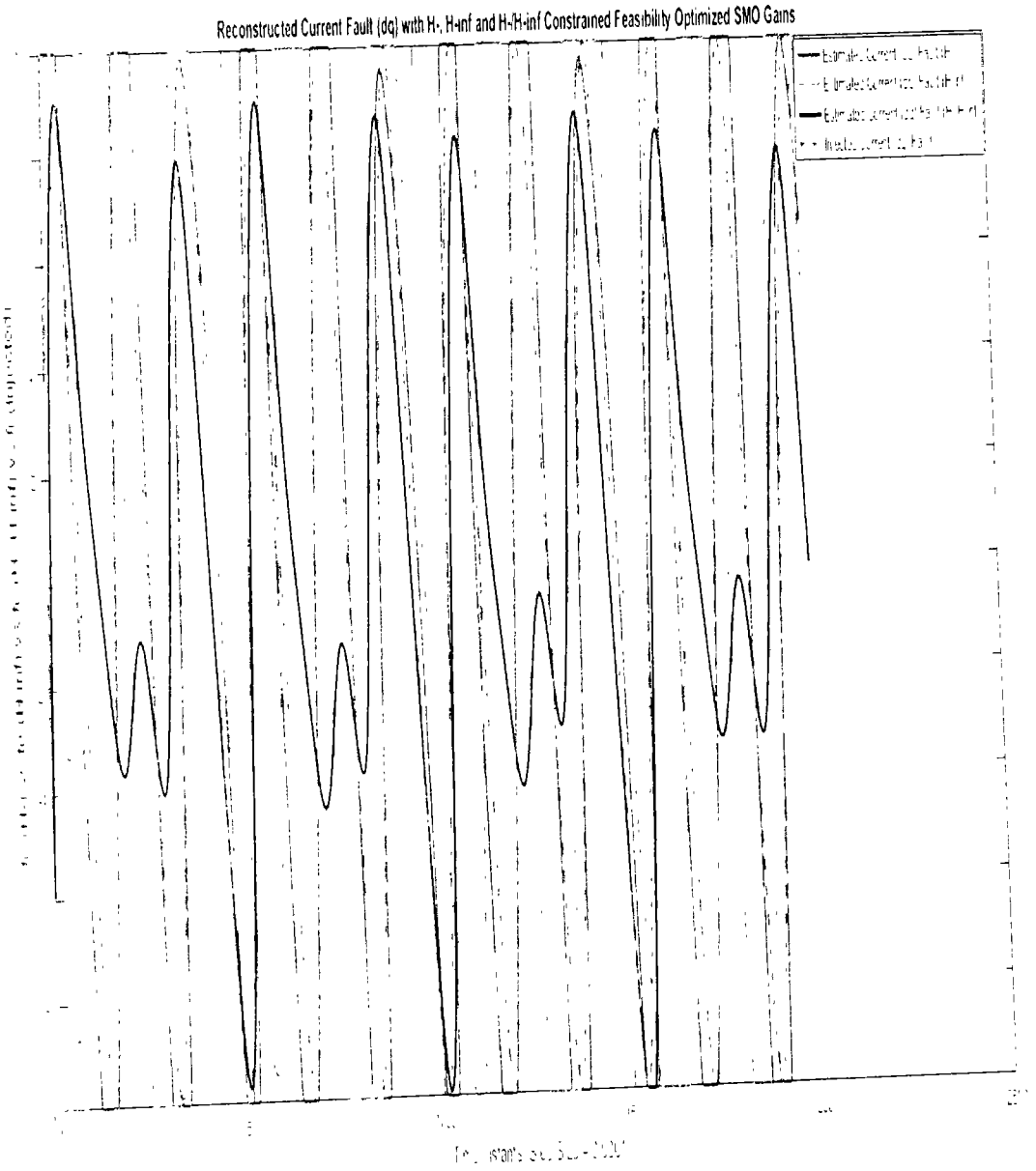

Figure 9.21: Reconstructed current fault (dq) with feasibility optimized $H-$ and $H-/H_\infty$ SMO gains.

Figure 9.22 shows voltage fault estimation errors compared using SMO with gains optimized with fault sensitivity parameter ($H-$), robustness to disturbance parameter (H_∞), and a mixed ($H-/H_\infty$). The error is harmonic sinusoidal variation, which approaches the peak value of

nearly 20 V for a very small instance of time using ($H-$) and ($H - /H_\infty$, being quite similar, whereas that with (H_∞) is nearly a pure sinusoidal variation of 60 Hz that approaches the peak value of 175 V due to phase lag of the π radian.

Figure 9.23 shows current fault estimation errors compared using SMO with gains optimized with fault sensitivity parameter ($H-$) and robustness to disturbance parameter (H_∞). However, for $/H_\infty$ and mixed ($H-/H_\infty$) parameters, the peaks approach 20 A and 11 A, respectively, which is relatively higher and impractical. The error could be reduced to minimal if phase compensation of π radian is used in the estimated faults.

Figure 9.24 shows state estimation errors compared using SMO with gains optimized with robustness to disturbance parameter (H_∞). The state estimation error is a sinusoidal variation with line frequency with the peak magnitudes of $V_{o,q}$ and $I_{o,q}$ being $0.006V$ and $0.00015A$, respectively.

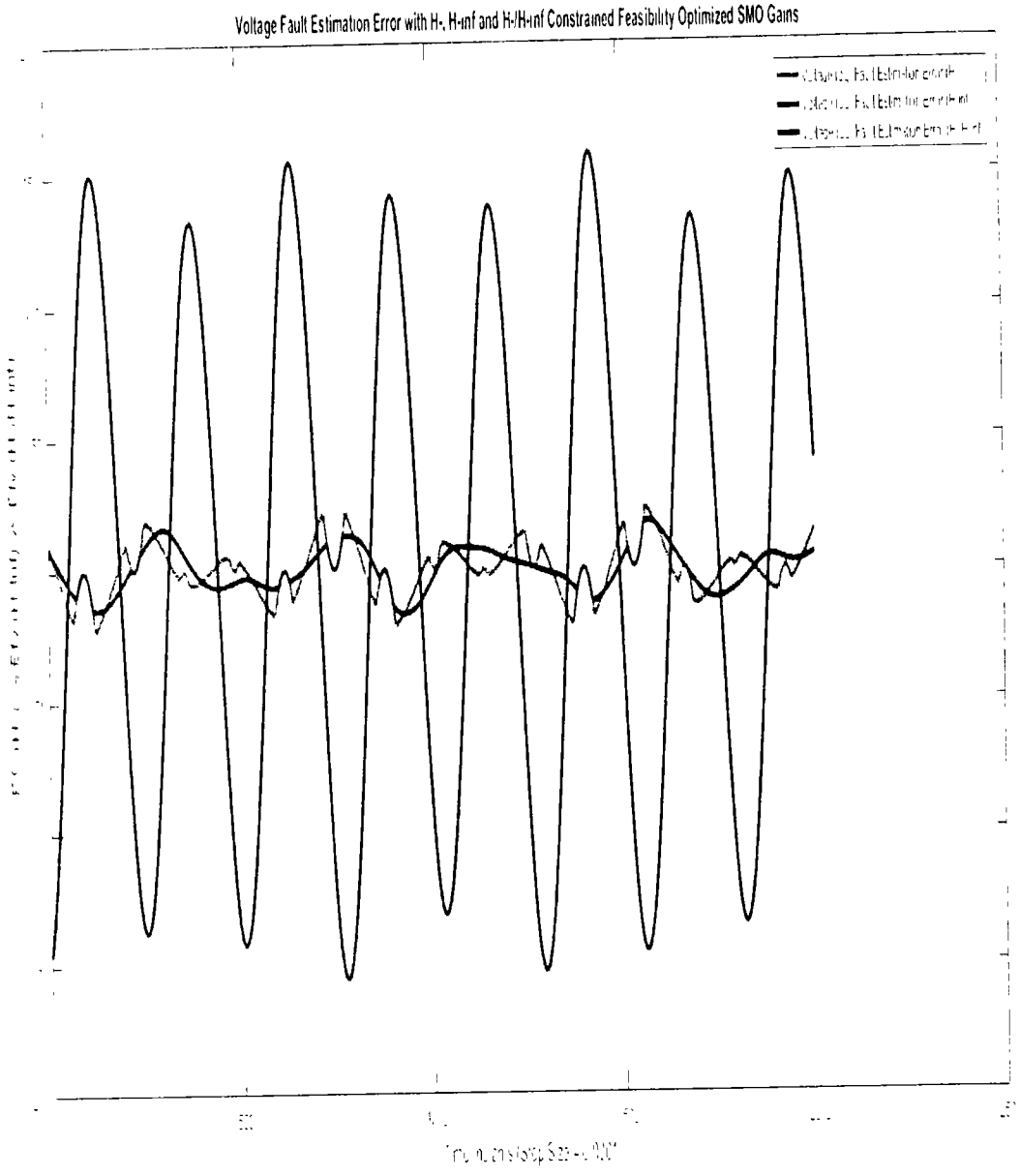

Figure 9.22: Voltage fault estimation error with feasibility optimized $H-$ and $H-/H_\infty$ SMO gains.

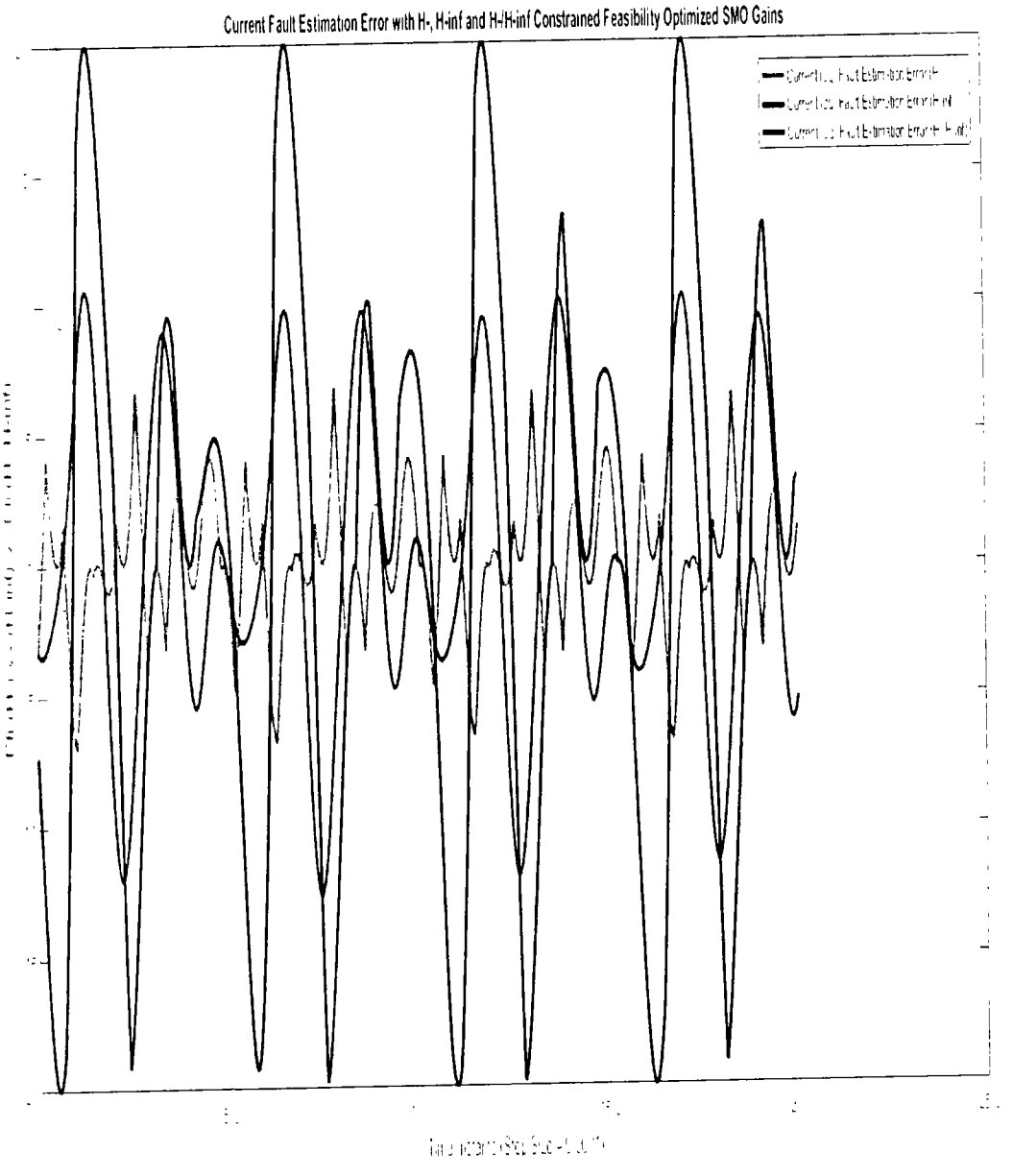

Figure 9.23: Current fault estimation error with feasibility optimized $H-$ and $H-/H_\infty$ SMO gains

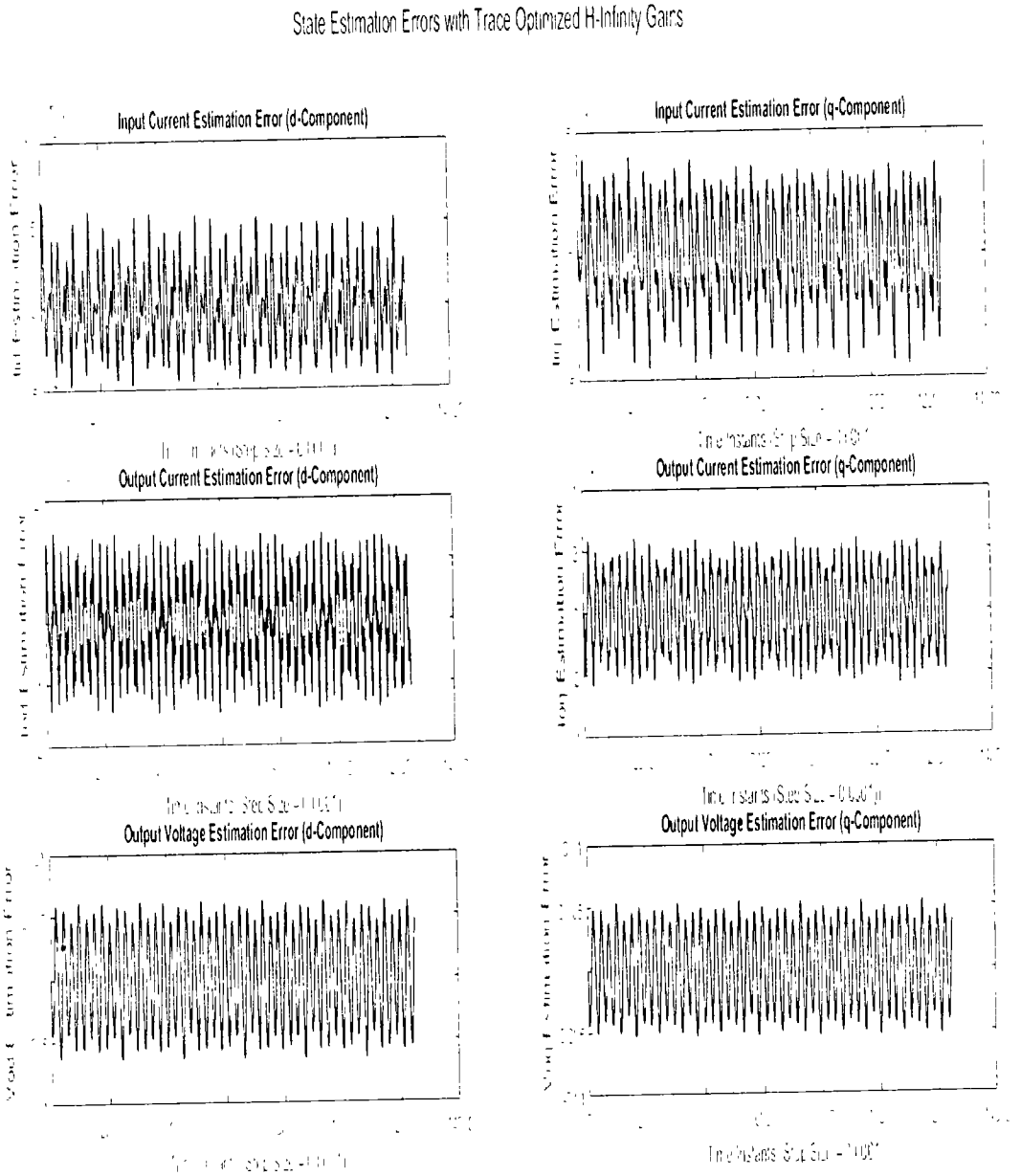

Figure 9.24: State estimation errors with trace optimized H_∞ SMO gains.

Figure 9.25 shows state estimation errors compared using SMO with gains optimized with robustness to disturbance parameter (H_∞). The state estimation error is the sinusoidal variation with line frequency with the peak magnitudes of V_{oaq} and I_{oaq} being $8V$ and $0.14A$, respectively.

Figure 9.26 shows state estimation errors compared using SMO with gains optimized with robustness to disturbance parameter (H_- / H_∞). The state estimation error is a sinusoidal variation with line frequency with the peak magnitudes of $V_{o,dq}$ and $I_{o,dq}$ being $0.1 - 0.1V$ and $0.025A$, respectively.

Figure 9.27 shows the FTC performance for the d-component of sensor output current (I_d) compared using SMO with gains optimized with fault sensitivity parameter (H_-), robustness to disturbance parameter (H_∞) and a mixed (H_- / H_∞) with non-faulty actual I_q. The results with (H_-) are best among the other two, the mixed problem (H_- / H_∞) also stays relatively closer, whereas the results with (H_∞) are more faulty.

Figure 9.28 shows FTC performance for q-component of sensor output current (I_q) compared using SMO with gains optimized with fault sensitivity parameter (H_-), robustness to disturbance parameter (H_∞), and a mixed (H_- / H_∞) with non-faulty actual I_d. The results with (H_-) are best among the other two, the mixed problem (H_- / H_∞) also stays relatively closer, whereas the results with (H_∞) are more faulty.

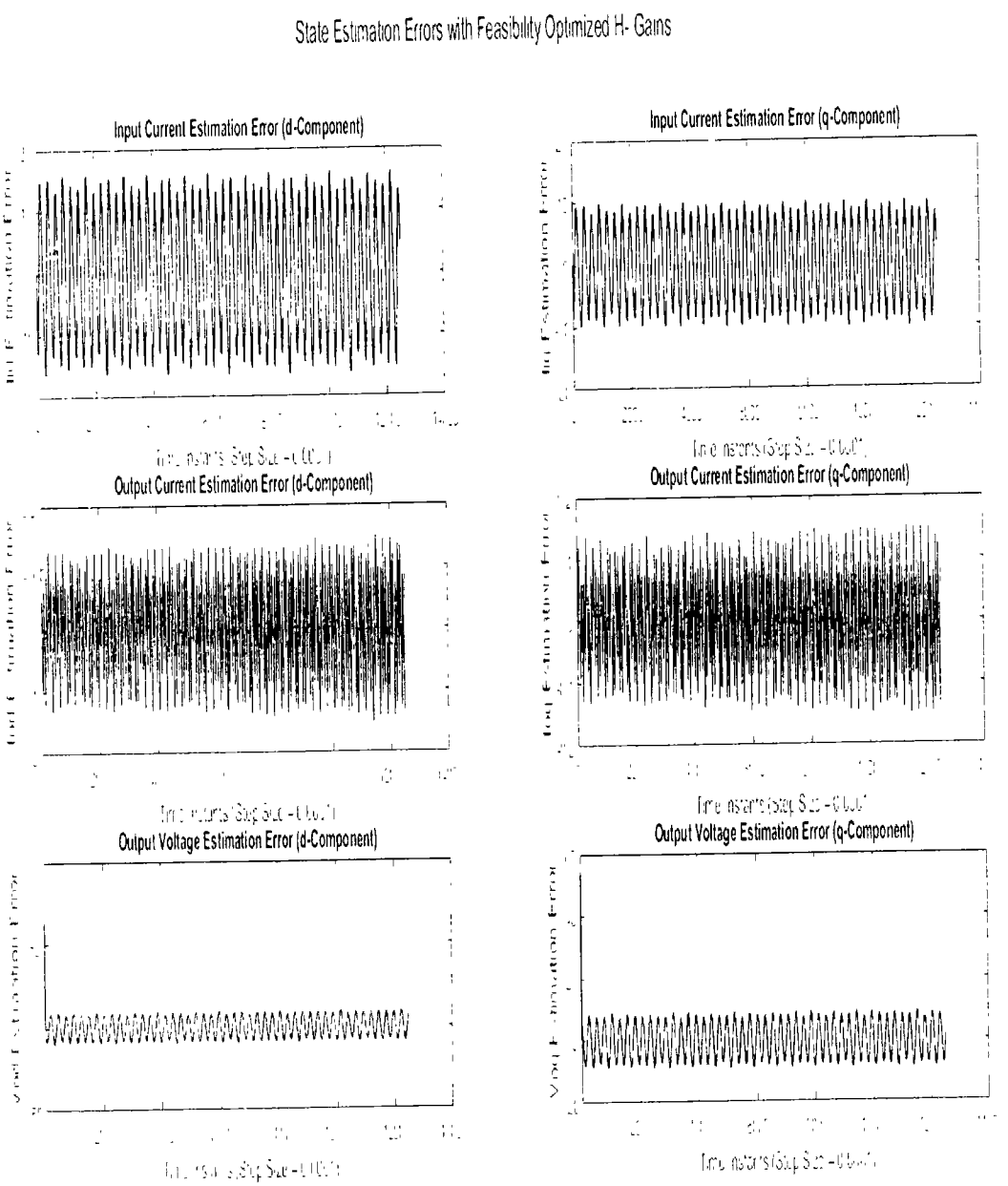

Figure 9.25: State estimation errors with feasibility optimized $H-$ SMO gains.

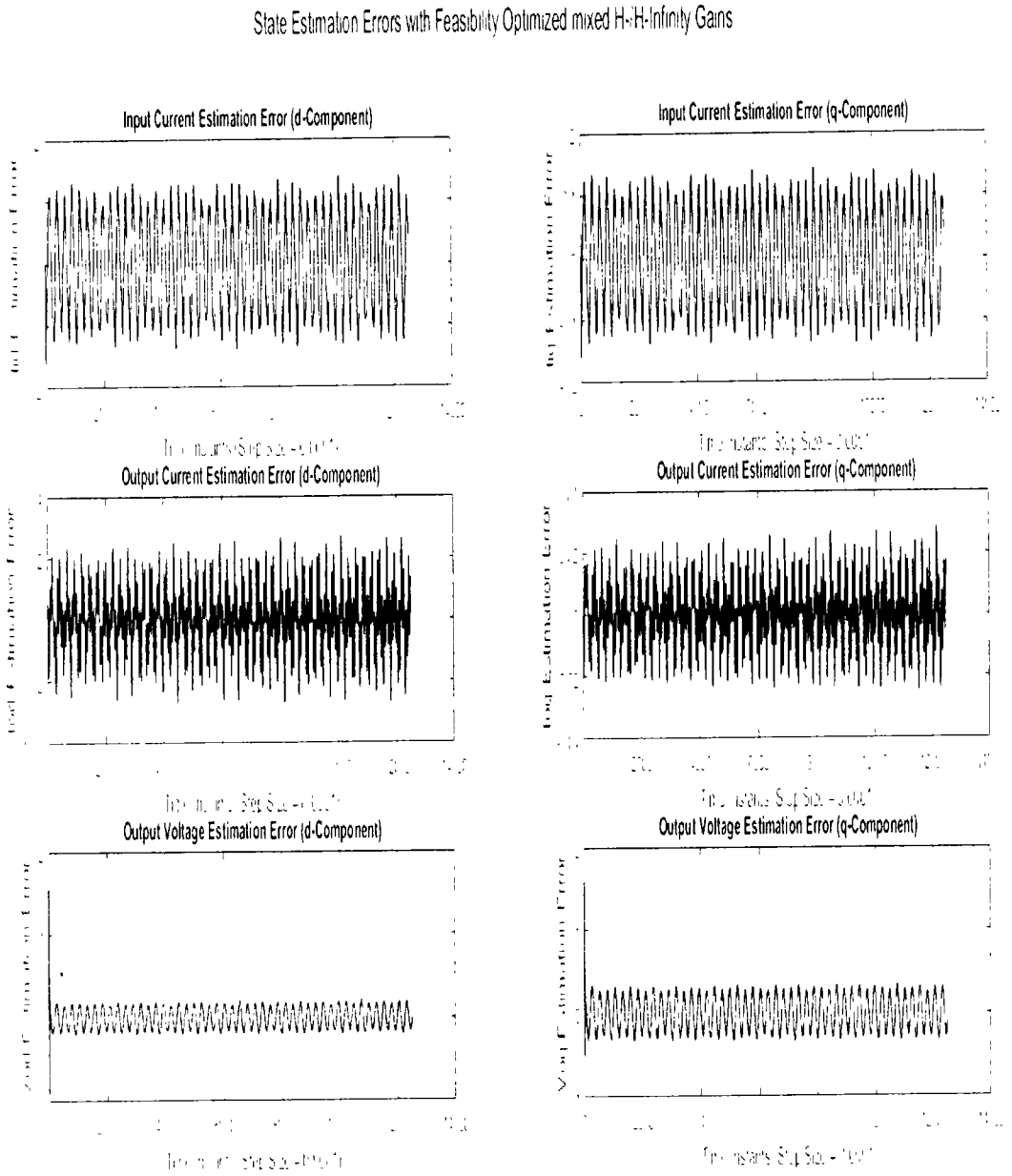

Figure 9.26: State estimation errors with feasibility optimized H_2/H_∞ gains.

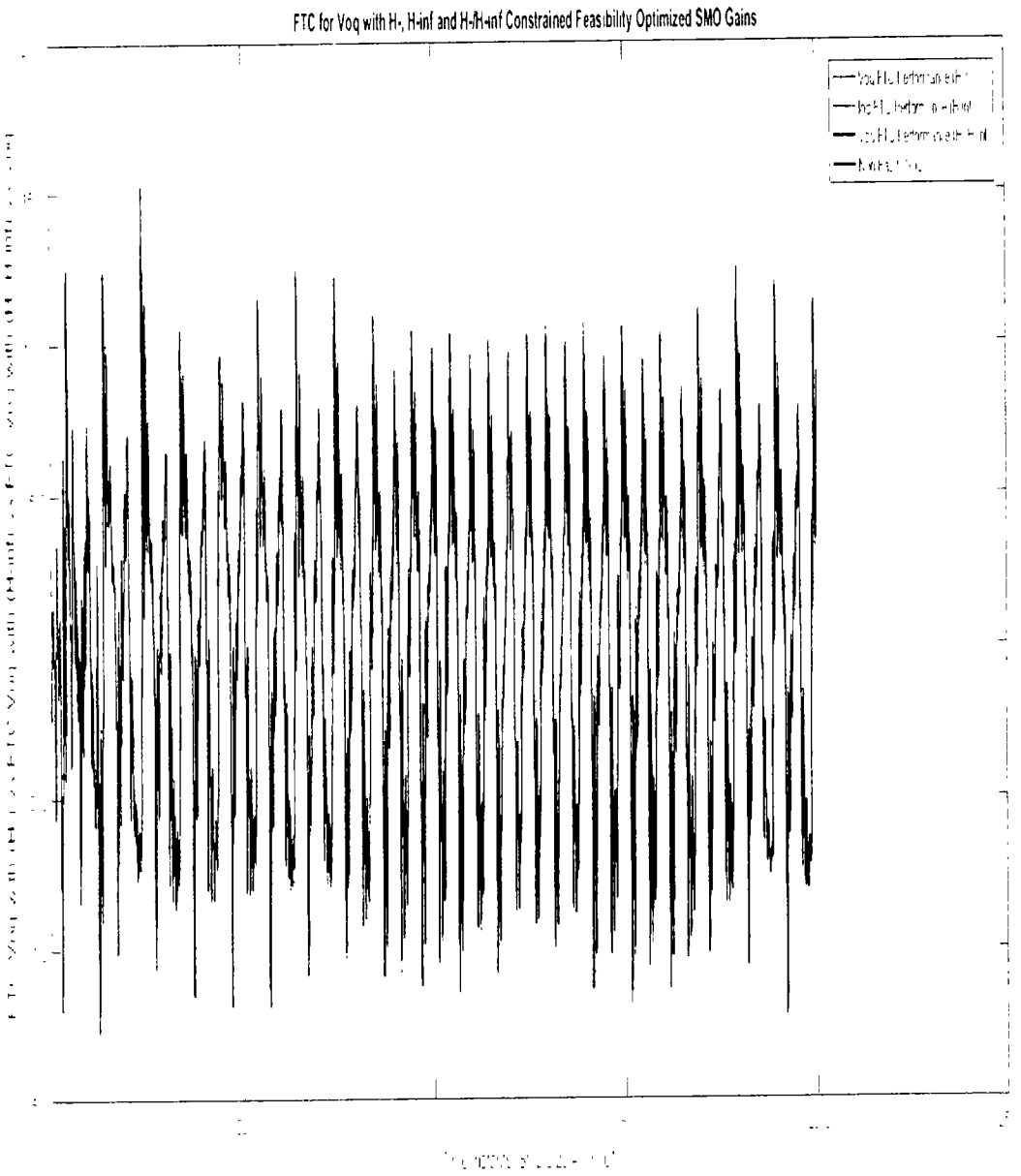

Figure 9.27: FTC for Ioq compared with feasibility optimized $H-$ and $H-/H_\infty$ SMO gains.

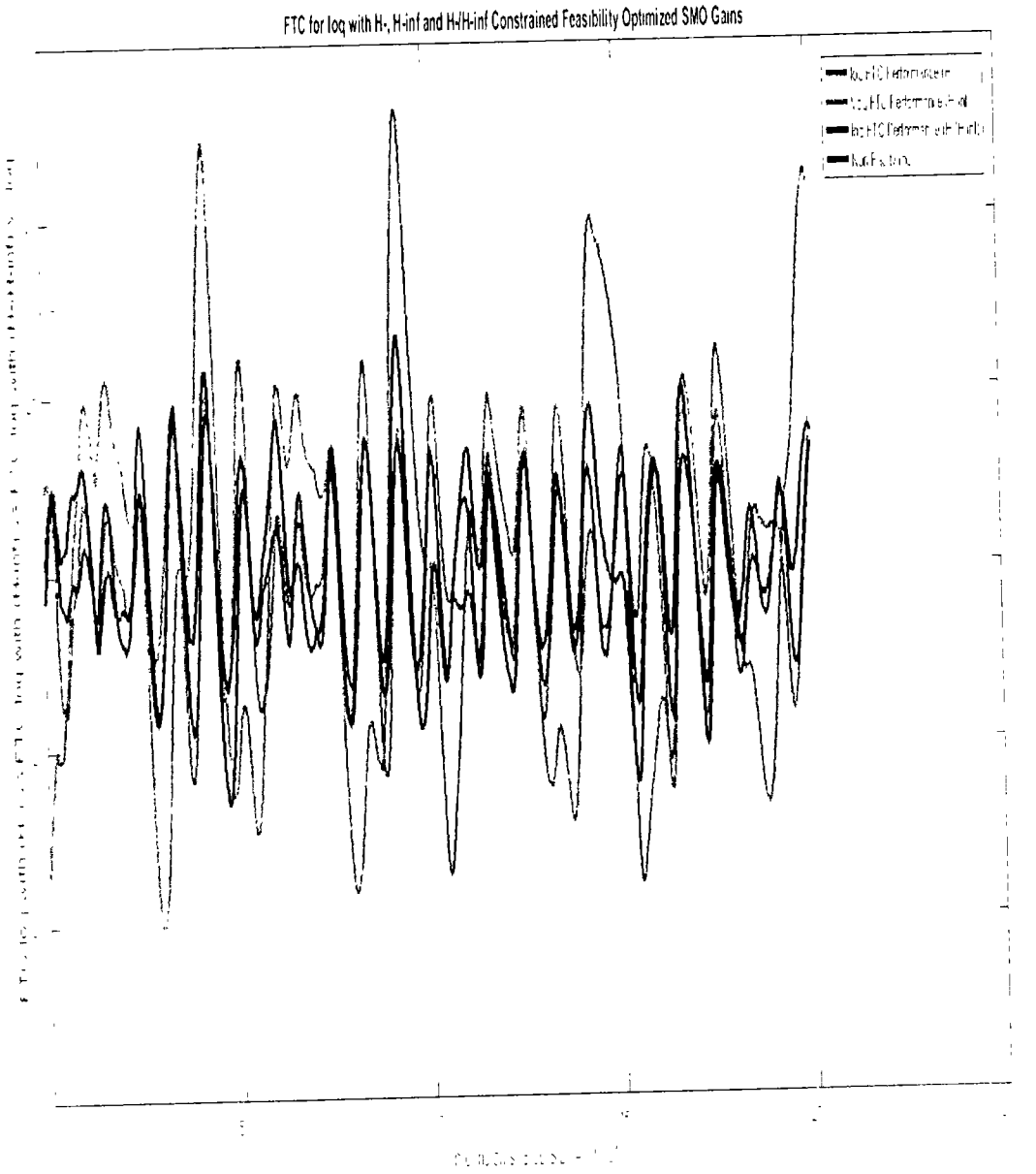

Figure 9.28: FTC for Ioq compared with feasibility optimized $H-$ and $H-/H_\infty$ SMO gains.

Figure 9.29 shows the FTC performance for the d-component of sensor output voltage (V_d) compared using SMO with gains optimized with fault sensitivity parameter ($H-$), robustness to disturbance parameter (H_∞) and a mixed ($H-/H_\infty$) with non-faulty actual V_q. The results with all three are comparable and not much differing w.r.t each other.

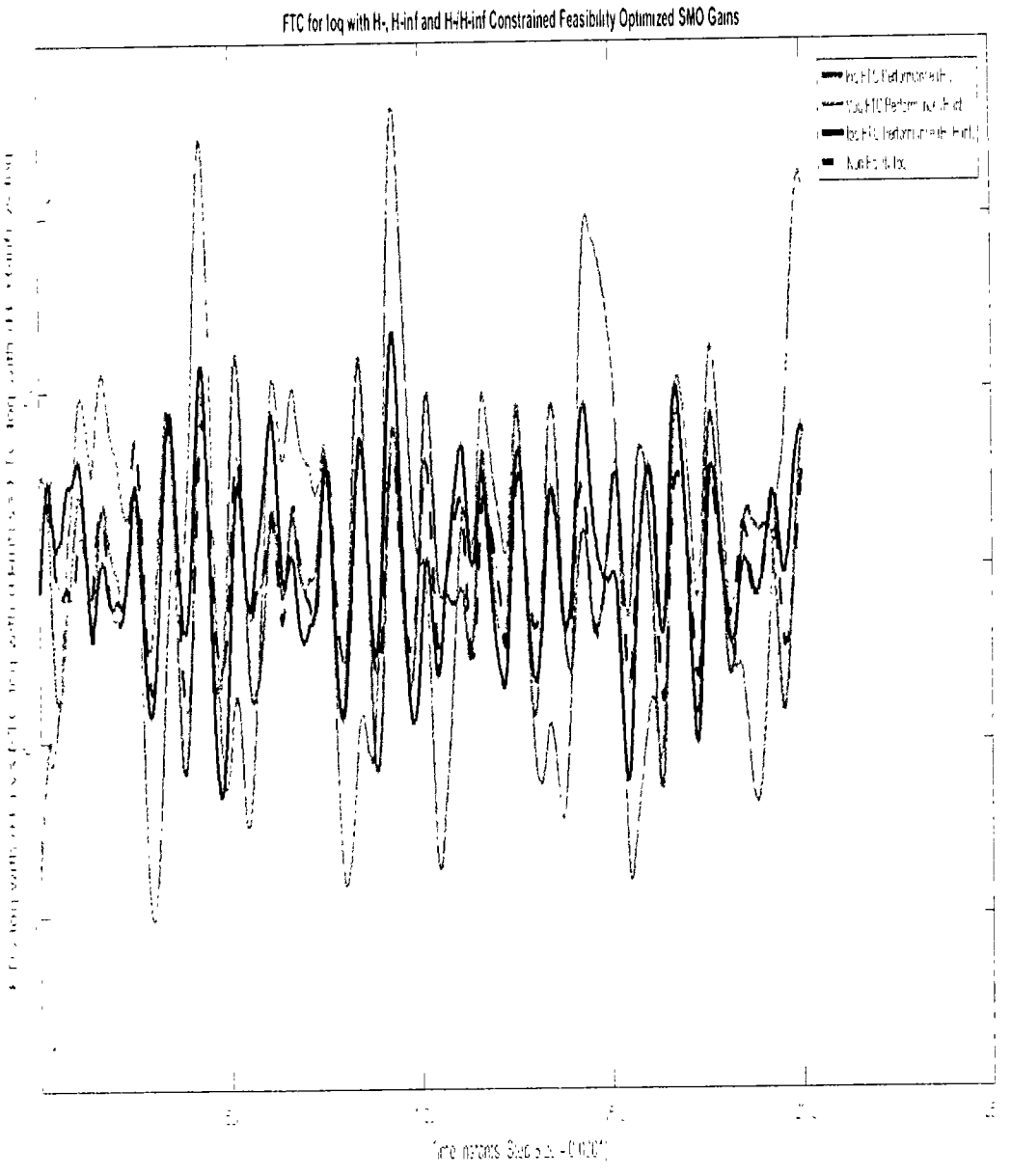

Figure 9.29: FTC for Vod compared with feasibility optimized $H-$ and $H-/H_\infty$ SMO gains

Figure 9.30 shows the FTC performance for the q-component of sensor output voltage (V_q) compared using SMO with gains optimized with fault sensitivity parameter ($H-$), robustness to disturbance parameter (H_∞), and a mixed ($H-/H_\infty$) with non-faulty actual V_q. The results with all three are comparable and not very differentiating from each other.

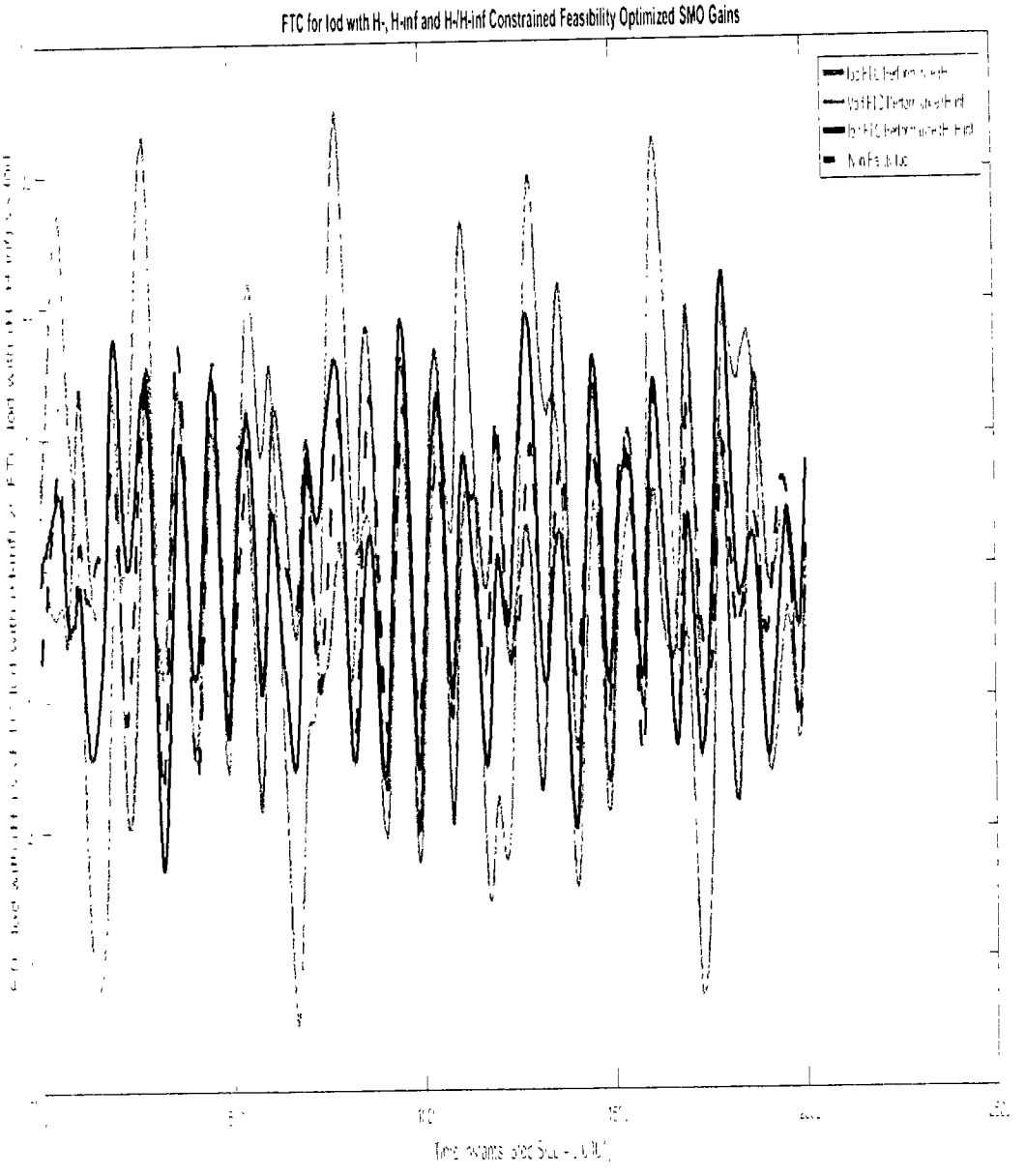

Figure 9.30: FTC for Voq compared with feasibility optimized $H-$ and $H-/H_\infty$ SMO gains

Summary: The chapter gives a detailed explanation of the physical state of the system, its parameters, and operating conditions along with the results and discussions on the results of both the published papers in separate sections. The distinct parameters and operating conditions are given in the respective sections. The results are included for state/output, faults, and

disturbances estimations for various scenarios, meanwhile also including the FTC performance of the proposed schemes.

CHAPTER 10

Conclusions and Future Directions

10.1 Conclusions

1. The study uses SMO theory for detection, isolation, estimation, and correction of faults as a scheme of fault-tolerant control, for faults occurring in sensors (current/potential transformers) mounted on microgrid, by using aVSI-based microgrid model.

2. The work is generally applicable for a wide range of sensor/actuator faults and systems. The estimation and correction of faults using SMOs is like providing software based sensors (transformers) replacing the real ones at the time of occurrence of faults.

3 The saturation faults of current/potential transformers (which are mounted on LCL filters are specifically considered, along with the general applicability mentioned above.

4 The SMO-based estimated faults are used to correct the faulty readings of the dq-currents/voltages,

to be supplied to PI-based conventional voltage-frequency control block, to determine the actual instantaneous values of reactive and real powers, and hence providing the correct SVPWM pulses provided to VSI. The gains of SMOs are determined using convex optimization of Lyapunov stability ensured LMIs.

5. The comparison of ordinary voltage-frequency control without the proposed SMO-observer-based corrective mechanism is also shown. The state and fault estimation errors are considered as indices to show the effectiveness of the proposed method.

6. The comparisons for results produced with SMO gains determined by proposed technique to those determined by earlier/base works [3], [4], Tan [5] used in this study, are also presented, which shows the improvements.

7. The finite-time reachability of detection/estimation SMOs are also presented to show the real-time applicability of the study in VSI-based microgrids.

8. The work sums up various previous works along with modifications in fault estimation and LMI optimization algorithm for determination of SMO gains. The method is transformable to provide fault detection/estimation/tolerance in various types of systems by selecting the suitable parameters.

9. Further, the VSI-based microgrid model is also used as an application to apply the enhanced (in robustness or sensitivity to fault) sliding-mode observer for fault diagnosis and fault-tolerant control.

10. H_∞ and $H-$ parameters of robust control similar in nature to the game theoretic saddle points are used to derive the inequality version of HJIE, which is in terms of the Lyapunov function, faults, or disturbances, and the output error estimation vector as variables. The

HJIE in inequality form not only proves the stability of observers but also gives the LMIs, which are convex optimized, to find the (H_∞ and $H-$) constrained SMO gains providing the optimal/sub-optimal values of SMO gains (G_o^*, G_m^*, f^*, ξ^*), as mentioned in the pair of saddle points, i.e., (Go^*,f^*) and (G^*, ξ^*). The sliding-mode observer using the above gains in terms of the error vector is used to estimate the faults and disturbances;

11 The main results computed are estimations of current/voltage faults of sensors (C.T/P.T), current/voltage fault estimation errors, and fault tolerance performance by the control block, which is provided by the corrections performed according to the faults estimated by SMOs, which are (i) robust to disturbance, (ii) sensitive to faults, and (iii) both the criteria used together. Moreover, all of the above-mentioned results are given and compared for SMOs with the above three constraints. The gain optimization is accordingly done in Theorems 6.1—6.3, which is the main contribution of this research along with the applicability to composite faults (phase, magnitude, harmonics) occurring in sensors (C.T/P.T) mounted on LCL filters on the inverter outputs.

10.2 Proposed Works for Future Directions

1. The design issue of an active fault tolerant controller for an islanded-AC MG inverter system can be studied with a view to the sensor drift fault. The controller should be capable of effectively suppressing external disturbances using finite energy. For a standalone AC MG inverter system with an external finite energy disturbance, a closed-loop system state space model can be created. The estimated value of the sensor fault and the system state variable can be acquired simultaneously through the suggested extended observer by using

the knowledge about the sensor fault occurring in the system as an auxiliary state vector. The concept of fault compensation can be used to create a fault-tolerant controller. Finally, MATLAB simulation programming can be used to confirm the accuracy and efficacy of this strategy.

2 One of the key challenges the energy sector is currently facing is meeting the increased demand for electricity in a safe, secure, and ecologically friendly manner. For a very long time, utility companies used fossil fuels including coal, oil, and natural gas as their main sources of energy generation. The disadvantages of these conventional energy sources include harmful environmental repercussions, a lack of resources, and frequent outages. To diversify their energy supplies and promote environmental awareness, governments from all over the world are currently investing in renewable energy technology, particularly wind turbines and solar photovoltaic arrays. Small-scale power plants that can only produce a few megawatts of electricity typically use renewable energy sources. It is simpler to incorporate these resources into the existing power system, thanks to the MG idea. An MG is a group of interconnected loads and distributed energy resources that may operate in either islanded mode or grid-connected mode and serve as a single, controllable entity. Two of the key enabling technologies for guaranteeing the trustworthy and efficient operation of such a complex MG system may be fault-tolerant control and advanced health monitoring and diagnosis. Research is particularly advised to be conducted on novel fault detection and diagnosis, fault-tolerant control methods, and applications to MGs that use renewable energy sources. The schemes and methods can be tested through a series of simulations on a sophisticated and well-designed MG benchmark in the MATLAB/Simulink environment.

3. For the energy management of renewable MGs, a fault-tolerant control and mitigation technique is conceivable. The system may consist of a Model Predictive Control (MPC) algorithm based on a Linear Parameter Varying (LPV) model for the MG energy dispatch While employing fault diagnosis information to precisely plan the MG model, the MPC may modify the process limitations to the level and position of faults. A closed-loop stability can be ensured by using easy quadratic terminal ingredients and solutions that can solve linear matrix inequality Nonlinear simulation data for a genuine MG benchmark may be given to demonstrate the method's effectiveness.

4. Future studies can concentrate on fault-tolerant control and large power systems (LPS) prone to sensor failure (FTC). The fact that the faults are hidden from the controller allows it to operate in the defective system loop. The controller can assume faults that contradict a subsystem's observability, therefore it cannot rely on specific subsystems that are broken when estimating states. He can use a cutting-edge method for the control of these faults that lead to the unobservability of subsystems. The approach recommends swapping out troublesome subsystems for other subsystems until a new subsystem is achieved that can be seen. The best subsystems among the candidates can then be selected, and a thorough method for FTC of LPS can be provided using GRAMMIAN definition and structural analysis tools The proposed methodology can be applied to the IEEE 14-bus test case, and nonlinear interactions can be considered. Simulation results can show that the given technique operates as predicted.

5. An innovative FTC technique for an AC/DC pulse-width modulation (PWM) converter operating in an MG framework may be described in the next work. A distributed renewable

energy source, such as a wind farm, solar photovoltaic (PV) farm, or battery energy storage, can be viewed of as an MG, which is a collection of interconnected loads. It is possible to design the AC/DC PWM converter's control system to withstand the fault effects that problems with the solar system's power loss can cause. A passive fault tolerant control technique based on model predictive control can be utilized to demonstrate how effective it is using an advanced MG benchmark model built in the MATLAB/Simulink environment.

6. Future research may concentrate on developing an FTC system using the nonlinear state-dependent RICCATI equation (SDRE) method. The proposed mechanism can be composed of a master controller, an observer-based fault detection and isolation system, and three emergency controllers, all developed using SDRE methodology. In typical operating conditions, the master controller can be designed to return the DC MG back to the desired equilibrium point as a suboptimal nonlinear regulator. On the other hand, an SDRE observer can be used to create a uniform architecture for fault isolation and detection in the DC MG. In the event of an unanticipated malfunction, the suggested method can actually isolate the problematic DG, at which time the emergency controllers can be turned on right away to stabilize the MG. The simulation's outcomes might demonstrate that the offered technique is successful in meeting the control goals and MG internet security.

7. Wind turbines frequently function as distinct systems and make control decisions in dispersed applications. They often manage internal problems with little concern for the rest of the power system while operating at their peak power output. Despite the fact that fault detection and tolerance techniques are extensively researched and used, controls to

mitigate such flaws are rare in research and industry. In small or isolated grid settings, the sudden loss of a single wind turbine may cause grid instability and serious system stress, while the sudden shutdown of a wind turbine in a sizable transmission-connected wind facility will have little impact on a major power system. The fault impact reduction control (FIRC) module of a wind turbine may use bigger warning levels near fault thresholds, according to future studies. The controller can broadcast its anticipated action to the grid controller when the wind turbine hits a warning threshold, assisting the grid operator to recognize a potential wind turbine problem and then take the required action to address the defect. In both MG- and grid-connected contexts, several scenarios can demonstrate the grid benefit of an FIRC, and multiple test cases can demonstrate the controller's behavior under various fault conditions. The FIRC can increase wind turbine generation and streamline generation switching for a variety of fault scenarios. All that is required for the FIRC module to be integrated with the majority of current controllers are de-rating capabilities. It is also easy to add any necessary warnings and thresholds to the FIRC module. MATLAB and Simulink-based research wind turbine models can be largely employed for this examination.

8. This work may present a novel fault detection and classification approach for both DC and AC failures on a DC MG network. The instantaneous amplitude and frequency of the decomposed modes of the signal can be found using the HILBERT-HAUNG transform approach after using variational mode decomposition (VMD) to separate the derivative of DC current signal into a number of intrinsic modes. A weighted KURTOSIS index can be utilized to generate the most sensitive technique, which may be used to compute a

sudden shift in discrete TEAGER energy (DTE), indicating the presence of the defect A stacked auto-encoder-based neural network can be used to classify faults as a pole to ground (PG), pole-to-pole (PP), line-to-ground (LG), line-to-line (LL), and three-phase line-to-ground (LLLG). The efficiency of the recommended security method can be verified in MATLAB/SIMULINK by taking into account a number of test scenarios. The recommended approach can provide a DC MG system with a very prompt, reliable, and precise protection mechanism.

9. In a forthcoming study, it will be possible to propose a distributed fault-tolerant finite-time control approach that takes input saturation and faults into consideration for the secondary voltage and frequency restoration of islanded inverter-based AC MGs. The majority of distributed techniques currently in use typically build the secondary control layer based on perfect conditions for the control input channels of the MG that are free of errors and disturbances. Affected actuators can significantly affect control and put MGs in dangerous situations. MGs are also prone to these problems. Another frequent practical limitation in MGs and other multi-agent systems is saturation. The second novel idea is a consensus-based method that synchronizes the voltage and frequency of the islanded MG to its nominal levels for all DGs in a limited amount of time, despite saturation and multiple faults, including partial loss of efficacy and stuck faults concurrently. Finally, to evaluate the performance of the proposed control systems, an offline digital time-domain simulation on a test MG system employing a few scenarios in the MATLAB/Simulink environment can be used. To assess the effectiveness and accuracy of the suggested control methods for islanded AC MGs, one can contrast them with past studies.

10. The study activity may take into consideration the fault detection (FD) problem for discrete-time stochastic systems with constrained communication. To create the residual model for defect detection, one could propose a filter structure. Due to the limited network resources, a novel event-triggered technique can be utilized to limit the amount of data that can be transmitted from the sensor to the filter. The residual system can be ensured to be stochastically stable while taking into consideration the stochastic model and the constrained network resources. It can also be ensured to achieve the stated fault sensitivity level and disturbance attenuation level. When compared to the traditional FD method, the suggested design strategy can preserve the scarce network resources while also providing the needed fault detection performance. The effectiveness of a design concept can be demonstrated through a variety of simulated situations.

11. The integration of fault isolation and detection activities may be improved by a study's provision of a fault diagnostic strategy based on interval observers and a timed discrete-event methodology. The interface between fault detection and fault isolation may take into account the activation level and the instant of the occurrence time of the diagnostic signals by combining a number of theoretical fault signature matrices, which store the knowledge of the relationship between diagnostic signals and faults. The fault isolation module can be developed using a timed discrete event technique that detects the commencement of a defect by identifying a specific sequence of observable events (fault signals). The states and transitions that characterize such a system can be readily inferred from the link between fault signals and faults. The proposed fault diagnosis approach can be used to identify and isolate problems in the Barcelona urban sewer system (level meter sensors). The

results of such a case study might show the benefits of using the recommended strategy in comparison to the traditional fault detection and isolation strategy.

12. Future work aims to improve the work for several microgrids operating in parallel by employing applicable fault-tolerant control methods in the distributed control paradigm and maintaining the best power flow control between them. Future research in this area might potentially focus on machine learning methods.

[1] I would like to express my sincere gratitude to the reviewers for their suggestions for strengthening the dissertation. The future directions are, with the exception of the last point,

References

[1] K. Sayed and H. A. Gabbar, "Scada and smart energy grid control automation," in *Smart energy grid engineering*. Elsevier, 2017, pp. 481–514.

[2] M. Abid, "Fault detection in nonlinear systems: An observer-based approach," *Universitat Duisburg-Essen*, 2010

[3] C. Edwards and C. P. Tan, "Sensor fault tolerant control using sliding mode observers," *Control Engineering Practice*, vol. 14, no. 8, pp. 897–908, 2006.

[4] S. Dhahri, A. Sellami *et al.*, "Robust sliding mode observer design for a class of uncertain linear systems with fault reconstruction synthesis," *International Journal of Physical Sciences*, vol. 7, no. 8, pp. 1259-1269, 2012.

[5] C. P. Tan and C. Edwards, "An lmi approach for designing sliding mode observers," *International Journal of Control*, vol. 74, no. 16, pp. 1559–1568, 2001.

[6] S. Gholami, S. Saha, and M. Aldeen, "Sensor fault tolerant control of microgrid," in *2016 IEEE Power and Energy Society General Meeting (PESGM)*. IEEE, 2016, pp. 1–5.

[7] E. Kontos, R. T. Pinto, S. Rodrigues, and P. Bauer, "Impact of hvdc transmission sys-

tem topology on multiterminal dc network faults," *IEEE Transactions on Power Delivery*, vol. 30, no. 2, pp. 844–852, 2014.

[8] E. Shahzad, A. U. Khan, M. Iqbal, A. Saeed, G. Hafeez, A. Waseem, F. R. Albogamy, and Z. Ullah, "Sensor fault-tolerant control of microgrid using robust sliding-mode observer," *Sensors*, vol. 22, no. 7, p. 2524, 2022.

[9] J. C. Vasquez, J. M. Guerrero, J. Miret, M. Castilla, and L. G. De Vicuna, "Hierarchical control of intelligent microgrids," *Ieee Ind. Electron. Mag.*, vol. 4, no. 4, pp. 23–29, 2010.

[10] E. Shahzad, A. U. Khan, M. Iqbal, F. Albalawi, M. A. Khan, A. Saeed, and S. S. Ghoneim, "Fault diagnostics and tolerance analysis of a microgrid system using hamilton-jacobi–isaacs equation and game theoretic estimations in sliding mode observers," *Sensors*, vol. 22, no. 4, p. 1597, 2022.

[11] R. Li, L. Xu, D. Holliday, F. Page, S. J. Finney, and B. W. Williams, "Continuous operation of radial multiterminal hvdc systems under dc fault," *IEEE Transactions on Power Delivery*, vol. 31, no. 1, pp. 351–361, 2015.

[12] R. Safaeian, S. Ebrahimi, and M. Parniani, "Performance improvement of steady-state and transient operation of offshore wind farm hvdc power transmission," in *2015 IEEE 16th Workshop on Control and Modeling for Power Electronics (COMPEL)*. IEEE, 2015, pp. 1–7.

[13] A. Hossam-Eldin, A. Lotfy, M. Elgamal, and M. Ebeed, "Protection oriented observability in multi-terminal hvdc systems," in *2016 7th International Conference on Information and Communication Systems (ICICS)*. IEEE, 2016, pp. 102–108.

[14] M. Claus, D Retzmann, D. Sorangr, and K. Uecker, "Solutions for smart and super grids with hvdc and facts, technical article published by siemens ag," 2008.

[15] Z. Xueqing, L. Jun, D. Xiaoming, and R. Jingguo, "Study for regulation and controlling strategy of power grids based on gradual learning," in *IEEE PES Innovative Smart Grid Technologies*. IEEE, 2012, pp. 1–4.

[16] L. Tang, "Future transmission grids, hvdc and facts-systems aspects," in *ARPA-E GENI Workshop*, 2010

[17] D E Olivares, A Mehrizi-Sani, A. H. Etemadi, C. A. Cañizares, R. Iravani, M Kazerani, A. H. Hajimiragha, O. Gomis-Bellmunt, M. Saeedifard, R. Palma-Behnke *et al.*, "Trends in microgrid control," *IEEE Trans. Smart Grid*, vol. 5, no. 4, pp. 1905–1919, 2014.

[18] J. Rocabert, A. Luna, F. Blaabjerg, and P. Rodriguez, "Control of power converters in ac microgrids," *IEEE Trans. Power Electron.*, vol 27, no. 11, pp. 4734–4749, 2012.

[19] L Priyadarshanee, "Modeling and control of hybrid ac/dc microgrid," Ph.D. dissertation, 2012

[20] R. Zeng, L. Xu, and L. Yao, "Dc/dc converters based on hybrid mmc for hvdc grid interconnection," 2015.

[21] O. Alarfaj, "Modeling and control of low-voltage dc microgrid with photovoltaic energy resources," Master's thesis, University of Waterloo, 2014.

[22] A. M. Amani and M. Jalili, "Power grids as complex networks: Resilience and reliability analysis," *IEEE Access*, 2021

[23] A. T. Alexandridis and P. C. Papageorgiou, "A complex network deployment suitable for modern power distribution analysis at the primary control level," *IFAC-PapersOnLine*, vol. 50, no. 1, pp. 9186–9191, 2017.

[24] J. Poon, I. C. Konstantakopoulos, C. Spanos, and S. R. Sanders, "Real-time model-based fault diagnosis for switching power converters," in *2015 IEEE Applied Power Electronics Conference and Exposition (APEC)*. IEEE, 2015, pp. 358–364.

[25] P. F. Odgaard, C. Aubrun, and Y. Majanne, "Fault tolerant control of power grids," *Int. J. Robust Nonlinear Control*, vol. 24, no. 8-9, pp. 1281–1282, 2014.

[26] M. Rasheduzzaman, J. A. Mueller, and J. W. Kimball, "An accurate small-signal model of inverter-dominated islanded microgrids using *dq* reference frame," *IEEE J. Emerg. Sel. Top. Power Electron.*, vol. 2, no. 4, pp. 1070–1080, 2014.

[27] M. Hassan and M. Abido, "Optimal design of microgrids in autonomous and grid-connected modes using particle swarm optimization," *IEEE Trans. Power Electron.*, vol. 26, no. 3, pp. 755–769, 2010.

[28] J. Li, X. Zhang, and W. Li, "An efficient wind-photovoltaic hybrid generation system for dc micro-grid," 2009.

[29] N. Kroutikova, C. A. Hernandez-Aramburo, and T. C. Green, "State-space model of grid-connected inverters under current control mode," *Iet Electr. Power Appl.*, vol. 1, no. 3, pp. 329–338, 2007.

[30] F. Andrade, L. Romeral, K. Kampouropoulos, and J. Cusido, "New mathematical model of

an inverter-based generator for stability studies of microgrid systems," in *4th International Conference on Power Engineering, Energy and Electrical Drives* IEEE, 2013, pp. 944–949.

[31] K. Hu and C. Liaw, "On the flywheel/battery hybrid energy storage system for dc microgrid," in *2013 1st International Future Energy Electronics Conference (IFEEC)*. IEEE, 2013, pp. 119–125.

[32] B. Johnson and R. Lasseter, "An industrial power distribution system featuring ups properties," in *Proceedings of IEEE Power Electronics Specialist Conference-PESC'93*. IEEE, 1993, pp. 759–765.

[33] A. Qayyum Khan, "Observer-based fault detection in nonlinear systems," Ph.D. dissertation, Ph. D. thesis, Institute of Automatic Control and Complex Systems (AKS ..., 2010.

[34] M. Prochazka, "Modeling of current transformers under saturation conditions." *Advances in Electrical and Electronic Engineering*, vol. 5, no. 1, pp. 94–97, 2011.

[35] R. Matussek, C. Dzienis, J. Blumschein, and H. Schulte, "Current transformer model with hysteresis for improving the protection response in electrical transmission systems," in *Journal of Physics: Conference Series*, vol. 570, no. 6. IOP Publishing, 2014, p. 062001.

[36] D. Muthumuni, L. Ruchkall, R. Jayasinghe *et al.*, "Modeling current transformer (ct) saturation for detailed protection studies," *Pulse, Manitoba HVDC Res. Centre J*, pp. 1-5, 2011.

[37] M. T. Raza, "Fault diagnosis and fault tolerant control of switched dynamical systems," Ph D. dissertation, Pakistan Institute of Engineering and Applied Sciences, Nilore, Islamabad . , 2016

[38] W. Chen, *Fault detection and isolation in nonlinear systems: observer and energy-balance based approaches.* Südwestdeutscher Verlag für Hochschulschriften, 2012.

[39] H. Hammouri, M. Kinnaert, and E. El Yaagoubi, "Observer-based approach to fault detection and isolation for nonlinear systems," *IEEE transactions on automatic control*, vol. 44, no. 10, pp. 1879–1884, 1999.

[40] X. Zhang, M. M. Polycarpou, and T. Parisini, "A robust detection and isolation scheme for abrupt and incipient faults in nonlinear systems," *IEEE transactions on automatic control*, vol. 47, no. 1, pp. 576–593, 2002.

[41] J. M. Maciejowski and C. N. Jones, "Mpc fault-tolerant flight control case study: Flight 1862," *IFAC Proceedings Volumes*, vol. 36, no. 5, pp. 119–124, 2003

[42] Y.-T. Shi, Q. Kou, D.-H. Sun, Z.-X. Li, S.-J. Qiao, and Y.-J. Hou, "H fault tolerant control of wecs based on the pwa model," *Energies*, vol. 7, no. 3, pp. 1750–1769, 2014.

[43] A. M. Pertew, H. J. Marquez, and Q. Zhao, "Lmi-based sensor fault diagnosis for nonlinear lipschitz systems," *Automatica*, vol. 43, no. 8, pp. 1464–1469, 2007.

[44] S. X. Ding, A. Q. Khan, Y. Wang, and M. Abid, "A note on unknown input fault detection filter design," *IFAC Proceedings Volumes*, vol. 41, no. 2, pp. 5523–5528, 2008.

[45] P. Zhang and S. X. Ding, "An integrated trade-off design of observer based fault detection systems," *Automatica*, vol. 44, no. 7, pp. 1886–1894, 2008.

[46] H. Alwi, C. Edwards, and A. Marcos, "Fault reconstruction using a lpv sliding mode observer for a class of lpv systems," *J. Frankl. Inst.*, vol. 349, no. 2, pp. 510–530, 2012.

[47] K. Kalsi, S. Hui, and S. H. Żak, "Unknown input and sensor fault estimation using sliding-mode observers," in *Proceedings of the 2011 American Control Conference*. IEEE, 2011, pp. 1361-1369.

[48] B. Walcott and S. Zak, "State observation of nonlinear uncertain dynamical systems," *IEEE Trans. Autom. Control*, vol. 32, no. 2, pp. 166–170, 1987.

[49] E. A. Garcia and P. M. Frank, "Deterministic nonlinear observer-based approaches to fault diagnosis: A survey," *Control Eng. Pract.*, vol. 5, no. 5, pp. 663–670, 1997.

[50] J. Chen, R. J. Patton, and Z. Chen, "Active fault-tolerant flight control systems design using the linear matrix inequality method," *Trans. Inst. Meas. Control*, vol. 21, no. 2-3, pp. 77–84, 1999.

[51] M. Arsan, P. Mouyon, and J.-F. Magni, "Fault diagnosis in the presence of parametric variations," *Ifac Proc. Vol.*, vol. 27, no. 5, pp. 83–88, 1994.

[52] Y. Zhang and J. Jiang, "Active fault-tolerant control system against partial actuator failures," *IEE Proc. -Control Theory Appl.*, vol. 149, no. 1, pp. 95–104, 2002.

[53] R. Sreedhar, B. Fernandez, and G. Masada, "Robust fault detection in nonlinear systems using sliding mode observers," in *Proceedings of IEEE International Conference on Control and Applications*. IEEE, 1993, pp. 715–721.

[54] F. Hermans and M. Zarrop, "Sliding mode observers for robust sensor monitoring," *Ifac Proc. Vol.*, vol. 29, no. 1, pp. 6530–6535, 1996.

[55] V. I. Utkin, "Sliding modes in optimization and control problems," 1992.

[56] C. Edwards and S. K. Spurgeon, "On the development of discontinuous observers," *International Journal of control*, vol. 59, no. 5, pp. 1211–1229, 1994.

[57] C. Edwards, S. K. Spurgeon, and R. J. Patton, "Sliding mode observers for fault detection and isolation," *Automatica*, vol. 36, no. 4, pp. 541–553, 2000.

[58] C. P. Tan and C. Edwards, "Sliding mode observers for detection and reconstruction of sensor faults," *Automatica*, vol. 38, no. 10, pp. 1815–1821, 2002.

[59] , "Sliding mode observers for robust detection and reconstruction of actuator and sensor faults," *Int. J. Robust Nonlinear Control: IFAC-Affil. J.*, vol. 13, no. 5, pp. 443–463, 2003.

[60] D. Shin, G. Moon, and Y. Kim, "Design of reconfigurable flight control system using adaptive sliding mode control: Actuator fault," *Proc. Inst. Mech. Eng. Part G: J. Aerosp. Eng.*, vol. 219, no. 4, pp. 321–328, 2005.

[61] X.-G. Yan and C. Edwards, "Robust sliding mode observer-based actuator fault detection and isolation for a class of nonlinear systems," in *Proceedings of the 44th IEEE Conference on Decision and Control*. IEEE, 2005, pp. 987–992.

[62] , "Nonlinear robust fault reconstruction and estimation using a sliding mode observer," *Automatica*, vol. 43, no. 9, pp. 1605–1614, 2007.

[63] M. Aldeen and R. Sharma, "Estimation of states, faults and unknown disturbances in nonlinear systems," *Int. J. Control*, vol. 81, no. 8, pp. 1195–1201, 2008.

[64] H. Alwi, C. Edwards, and C. P. Tan, "Sliding mode estimation schemes for incipient sensor faults," *Automatica*, vol. 45, no. 7, pp. 1679–1685, 2009.

[65] Z. Ning, J. Yu, and T. Wang, "H _/h fault detection filter design for discrete-time stochastic systems with limited communication," *Transactions of the Institute of Measurement and Control*, vol. 41, no. 13, pp. 3808–3817, 2019.

[66] C. Cecati, F. Genduso, R. Miceli, and G. R. Galluzzo, "A suitable control technique for fault-tolerant converters in distributed generation," in *2011 IEEE International Symposium on Industrial Electronics*. IEEE, 2011, pp. 107–112.

[67] L. I. Minchala-Avila, A. Vargas-Martinez, L. E. Garza-Castanón, R. Morales-Menendez, Y. Zhang, and E. R. Calle-Ortiz, "Fault-tolerant control of a master generation unit in an islanded microgrid," *Ifac Proc. Vol.*, vol. 47, no. 3, pp. 5327–5332, 2014.

[68] A. Vargas-Martínez, L. I. M. Avila, Y. Zhang, L. E Garza-Castañón, and E. R. C. Ortiz, "Model-based fault-tolerant control to guarantee the performance of a hybrid wind-diesel power system in a microgrid configuration." in *ANT/SEIT*, 2013, pp. 712–719.

[69] A. Vargas-Martínez, L. I Minchala-Avila, Y. Zhang, L. E. Garza-Castañón, and P. Acosta-Santana, "Fault-tolerant controller design for a master generation unit in an isolated hybrid wind-diesel power system," *Int. J. Robust Nonlinear Control*, vol. 25, no. 5, pp. 761–772, 2015.

[70] M J. Morshed and A. Fekih, "A fault-tolerant control paradigm for microgrid-connected wind energy systems." *Ieee Syst. J.*, vol. 12, no. 1, pp. 360–372, 2016.

[71] A. Abdullah and M. Zribi, "Sensor-fault-tolerant control for a class of linear parameter varying systems with practical examples," *IEEE Trans. Ind. Electron.*, vol. 60, no. 11, pp. 5239–5251, 2012.

[72] Z. Wang, L. Liu, and H. Zhang, "Neural network-based model-free adaptive fault-tolerant control for discrete-time nonlinear systems with sensor fault," *IEEE Trans. Syst. Man Cybern. : Syst.*, vol. 47, no. 8, pp. 2351–2362, 2017.

[73] M. Van, "An enhanced robust fault tolerant control based on an adaptive fuzzy pid-nonsingular fast terminal sliding mode control for uncertain nonlinear systems," *IEEE/ASME Trans. Mechatron.*, vol. 23, no. 3, pp. 1362–1371, 2018.

[74] A. Azizi, H. Noorisola, and S. Shoja-Majidabad, "Fault tolerant control of wind turbines with an adaptive output feedback sliding mode controller," *Renewable energy*, vol. 135, pp. 55–65, 2019.

[75] J. Zhang, S. Li, and Z. Xiang, "Adaptive fuzzy finite-time fault-tolerant control for switched nonlinear large-scale systems with actuator and sensor faults," *J. Frankl. Inst.*, vol. 357, no. 16, pp. 11 629–11 644, 2020.

[76] J. M. Guerrero, M. Chandorkar, T.-L. Lee, and P. C. Loh, "Advanced control architectures for intelligent microgrids–part i: Decentralized and hierarchical control," *IEEE Transactions on Industrial Electronics*, vol. 60, no. 4, pp. 1254–1262, 2012.

[77] A. Bidram and A. Davoudi, "Hierarchical structure of microgrids control system," *IEEE Transactions on Smart Grid*, vol. 3, no. 4, pp. 1963–1976, 2012.

[78] T. L. Vandoorn, J. C. Vasquez, J. De Kooning, J. M. Guerrero, and L. Vandevelde, "Microgrids: Hierarchical control and an overview of the control and reserve management strategies," *IEEE industrial electronics magazine*, vol. 7, no. 4, pp. 42–55, 2013

[79] D. Rotondo and M. Buciakowski, "Guaranteed cost estimation and control for a class of

nonlinear systems subject to actuator saturation," *Eur. J. Control*, vol. 61, pp. 119–132, 2021.

[80] M. Hou and R. J. Patton, "An lmi approach to h-/h fault detection observers," 1996.

[81] A. Edelmayer and J. Bokor, "Optimal h scaling for sensitivity optimization of detection filters." *International Journal of Robust and Nonlinear Control: IFAC-Affiliated Journal*, vol. 12, no. 8, pp. 749–760, 2002.

[82] J. Liu, J. L. Wang, and G.-H. Yang, "An lmi approach to worst case analysis for fault detection observers," in *Proceedings of the 2003 American Control Conference, 2003.*, vol. 4. IEEE, 2003, pp. 2985–2990.

[83] ——, "An lmi approach to minimum sensitivity analysis with application to fault detection," *Automatica*, vol. 41, no. 11, pp. 1995–2004, 2005.

[84] H. Wang, J. Wang, and J. Lam, "Robust fault detection observer design: iterative lmi approaches." 2007.

[85] J. L. Wang, G.-H. Yang, and J. Liu, "An lmi approach to h-index and mixed h-/h fault detection observer design," *Automatica*, vol. 43, no. 9, pp. 1656–1665, 2007.

[86] H. Wang, J. Wang, and J. Lam, "Worst-case fault detection observer design: Optimization approach," *Journal of Optimization Theory and Applications*, vol. 132, no. 3, pp. 175–191, 2007.

[87] A. Q. Khan and S. X. Ding, "Threshold computation for robust fault detection in a class of continuous-time nonlinear systems," in *2009 European Control Conference (ECC)*. IEEE, 2009, pp. 3088–3093.

[88] M. Aliyu and E. Boukas, "Discrete-time mixed 2/ nonlinear filtering," *International Journal of Robust and Nonlinear Control*, vol. 21, no. 11, pp. 1257–1282, 2011.

[89] W. Li, Z. Zhu, G Zhou, and G. Chen, "Optimal h i/h fault-detection filter design for uncertain linear time-invariant systems: an iterative linear matrix inequality approach," *IET Control Theory & Applications*, vol. 7, no. 8, pp. 1160–1167, 2013.

[90] M. T. Raza, A. Q. Khan, G. Mustafa, and M Abid, "Design of fault detection and isolation filter for switched control systems under asynchronous switching," *IEEE Transactions on Control Systems Technology*, vol. 24, no. 1, pp. 13–23, 2015.

[91] S Ahmad, N. Ali, M. Ayaz, and E. Ahmad, "Design of robust fault detection filter using algorithm for a class of lti systems." in *2017 13th International Conference on Emerging Technologies (ICET)*. IEEE, 2017, pp. 1–5.

[92] K Lu, W. Zhou, G. Zeng, and Y. Zheng, "Constrained population extremal optimization-based robust load frequency control of multi-area interconnected power system," *Int. J. Electr. Power & Energy Syst.*, vol. 105, pp. 249–271, 2019.

[93] K.-D. Lu, G.-Q. Zeng, X. Luo, J. Weng, Y. Zhang, and M. Li, "An adaptive resilient load frequency controller for smart grids with dos attacks," *IEEE Trans. Veh. Technol.*, vol. 69, no. 5, pp. 1689–1699, 2020.

[94] Y. Shtessel, C Edwards, L. Fridman, and A. Levant, *Sliding mode control and observation*. Springer, 2014, vol. 10.

[95] K E. Starkov, L N. Coria, and L. T. Aguilar, "On synchronization of chaotic systems based

on the thau observer design," *Commun. Nonlinear Sci. Numer. Simul.*, vol. 17, no. 1, pp. 17–25, 2012.

APPENDIX A

Appendix

A.1 Proof for Proposed Form of Lyapunov Matrix 'P'

For the form of the Lyapunov matrix P as used in [5, 55], for the complete Lyapunov function in Equation (73), substituting complete forms from Equations (74) and (77) in (73)

$$\dot{V}_c = \begin{bmatrix} e_s^T & e_o^T & f^T & \xi^T \end{bmatrix} [M] \begin{bmatrix} e_s \\ e_o \\ f \\ \xi \end{bmatrix} \tag{A.1.1}$$

$$M_1 = \begin{bmatrix} \bar{A_{11}}^T P_1 + P_1 \bar{A_{11}} & P_1 \bar{A_{12}} + \bar{A_{21}} T^T P_o - P_1 G_1 - P_1 L G_2 & P_1 L E_o & P_1 L D_o \\ \bar{A_{12}}^T P_1 + P_o T \bar{A_{21}} & \bar{A_{22}}^T T P_o + P_o T \bar{A_{22}} \quad G_2^T T^T P_o & P_o T G_2 & P_o T E_o & P_o T D_o \\ E_o^T L^T P_1 & E_o^T T^T P_o & 0 & 0 \\ D_o^T L^T P_1 & D_o^T T^T P_o & 0 & \mu I \end{bmatrix},$$

and Considering $P = \begin{bmatrix} P_{11} & P_{12} \\ P_{21} & P_{22} \end{bmatrix} > 0$ (and) $\begin{bmatrix} \bar{A_{11}} & \bar{A_{12}} \\ \bar{A_{21}} & \bar{A_{22}} \end{bmatrix}$ in term $(A_c - GC_c)^T P + P(A - GC) +$ $C_c^T C_c$ and comparing with concerning part of the matrix given in vector Lyapunov equation in (104) implies

$$\bar{P} = \begin{bmatrix} P_1 & 0 \\ 0 & T^T P o T \end{bmatrix} \tag{A.1.2}$$

Because the form of $\bar{P}$ is determined from the T_L transformed system, applying the inverse transformation $T_L^{-1} \bar{P} T_L$ gives

$$P = \begin{bmatrix} P_1 & P_1 L - L P_o T \\ 0 & P_o + T^T P_1 L \end{bmatrix} \tag{A.1.3}$$

Applying the transformation ${T_L}^T P T_L$ on $\bar{P}$ gives:

$$P = \begin{bmatrix} P_1 & P_1 L \\ L^T P_1 & T^T P_o T + L^T P L \end{bmatrix} > 0 \tag{A.1.4}$$

A.2 The Schur Lemma

(i) The Schur complement formula is used in transforming nonlinear inequalities of convex type into LMI. This says that for the LMI

$$\begin{bmatrix} Q(x) & S(x) \\ S(x)^T & R(x) \end{bmatrix} < 0$$

where $Q(x) = Q(x)^T$, $R(x) = R(x)^T$ and $S(x)$ depends affinely on x. Then, it is equivalent to: $R(x) < 0$, $Q(x) \quad S(x)R(x)^{-1}S(x)^T < 0$.

A.3 Schur Complement

The Schur complement is a technique often used to convert NMIs and BMIs to LMIs. By taking the Schur complement, we get the LMIs, which can be optimized by powerful techniques within the above-defined constraints.

$$S \triangleq \begin{bmatrix} A - BD^{-1}C^{-1} & A - BD^{-1}C^{-1}BD^{-1} \\ -D^{-1}CA - BD^{-1}C^{-1} & D^{-1} + D^{-1}CA - BD^{-1}C^{-1}BD^{-1} \end{bmatrix}$$

A.4 Proof For Hamilton–Jacobi–Bellman Equation/Motivation for Using the HJBE Equation

Almost any problem that can be solved using optimal control theory can also be solved by analyzing the appropriate Bellman equation. However, the 'Bellman equation' usually refers to

the dynamic programming equation associated with discrete-time optimization problems. In continuous-time optimization problems, the analogous equation is a partial differential equation that is usually called the Hamilton–Jacobi–Bellman equation. In optimal control theory, the Hamilton–Jacobi–Bellman (HJB) equation gives a necessary and sufficient condition for the optimality of a control with respect to a loss function. It is, in general, a nonlinear partial differential equation in the value function, which means its solution is the value function itself. Once the solution is known, it can be used to obtain optimal control by taking the maximizer/minimizer of the Hamiltonian involved in the HJB equation. A major drawback is that the HJB equation admits classical solutions only for a sufficiently smooth value function, which is not guaranteed in most situations.

For any plant

$$\dot{x} = f(x, u, t)$$

Performance Index

$$J(x(t_o), t_o) = \phi(x(T), T) + \int L(x, u, t)dt$$

Determine a continuous state feedback optimal control u^* on a given interval $[t_o, T]$ that minimizes J and drives a given initial state $x(t_o)$ to a final state that satisfies $\psi(x(T), T) = 0$. Let t be the current time and $x = x(t)$

$$J(x, t) = \phi(x(T), T) + \int_{\tau}^{T} L(x, u, t)d\tau$$

$$= \phi(x(T), T) + \int_{t+\Delta t}^{T} L(x, u, t)d\tau + \int_{\tau}^{t+\Delta t} L(x, u, t)d\tau$$

$$= J(x + \Delta x, t + \Delta t) + \int_{\tau}^{t+\Delta t} L(x, u, t) d\tau$$

Using the first order approximation; $\Delta x \simeq f(x, u, t)\Delta t$ Bellmann Principle of Optimality (on which DP is based)An optimal policy has the property that no matter what is the previous decision, i.e., what controls have been, the remaining decisions must constitute an optimal policy with regard to the state resulting from these previous decisions.

To find the $J^*(x, t)$, let us assume that optimal cost from $(t + \Delta t)$ to T, i.e., $J(x + \Delta x, t + \Delta t)$ is known for possible $x + \Delta x$). Moreover, optimal control has also been determined on this interval Thus, it remains to find the control on the interval $[t, t + \Delta t]$ This is called the principle of optimality for continuous-time systems Let us do Taylor expansion of the second term on the right

$$J^*(x, t) = min_{u(\tau)_{[t \leq \tau \leq t+\Delta t]}} [\int_{t}^{t+\Delta t} L(x, u, \tau) d\tau + (\frac{\partial J^*}{\partial x})^T \Delta x + (\frac{\partial J^*}{\partial t})\Delta t]$$

In this $J^*(x, t)$ and $\frac{\partial J^*}{\partial t} J^*(x, t)\Delta t$ is independent of $u(\tau)$ and $\Delta\tau$ can be taken out, and also using the above defined first order approximation

$$J^*(x, t) = J^*(x, t) + \frac{\partial J^*}{\partial t} J^*(x, t)\Delta t + [\int_{t}^{t+\Delta t} L(x, u, t) d\tau + \frac{\partial J^*(x, t)}{\partial t}^T f(x, u, t)\Delta t]$$

Taking a first-order approximation for the first integral, i.e.,

$$\int_{t}^{t+\Delta t} L(x, u, t) d\tau = \Delta t . L[(t + \alpha\Delta t) x(t + \alpha\Delta t) u(t + \alpha\Delta t)]$$

$$= \Delta t . L$$

(in short)

$$\frac{\partial J^*}{\partial t} J^* \Delta t = min_{u(\tau)}[L.\Delta t + \frac{\partial J^*(x,t)}{\partial t}^T f(x,u,t)\Delta t]$$

Letting $\Delta t \to 0$ gives

$$\frac{\partial J^*}{\partial t} = min_{u(\tau)}(L + (\frac{\partial J^*}{\partial t})^T f)$$

In fact, $V(x,t) \triangleq J^*(x,u,t)$

$$\frac{\partial V(x,t)}{\partial t} = min_{u(t)}[L + \frac{\partial V(x,t)}{\partial t}^T f(x,u,t)] \tag{A.4.1}$$

$$\frac{-\partial V(x,t)}{\partial t} = H_{opt}$$

$$\frac{\partial V(x,t)}{\partial t} + H_{opt} = 0 \tag{A.4.2}$$

This is called the Hamilton–Jacobi–Bellman equation

where

$$H_{opt} == min_{(u \subset \Omega)}[L + (\frac{\partial V}{\partial t})^T f \tag{A.4.3}$$

A.5 LMIs and Solvers

LMIs are matrix inequalities that are linear or affine in a set of matrix variables. They are essentially convex constraints and therefore many optimization problems with convex objective functions and LMI constraints can easily be solved efficiently using existing software. This method has been very popular among control engineers in recent years. This is because a wide

variety of control problems can be formulated as LMI problems. Mainly, we define the LMI problem and the related problems, such as the feasibility problem (FEAS), the minimization of a linear objective under LMI constraints (MINCX), and the generalized eigenvalue minimization problem (GEVP). These solvers solve the given LMIs iteratively to approach the maximum possible sub-optimal solution. The LMI solvers used are .

A.5.1 FEASP (Feasibility Optimization)

$[tmin, xfeas] = feasp(lmisys, options, target)$

computes a solution xfeas (if any) of the system of LMIs described by lmisys. The vector xfeas is a particular value of the decision variables for which all LMIs are satisfied.

For the given LMI system

$N^T L(x) N \leq M^T R(x) M$

xfeas is computed by solving the auxiliary convex program,

Minimize t subject to

$N^T L(x) N - M^T R(x) M \leq t * I$

The global minimum of this program is the scalar value tmin returned as the first output argument by feasp. The LMI constraints are feasible if tmin ≤ 0 and strictly feasible if tmin < 0. If the problem is feasible but not strictly feasible, tmin is positive and very small. Some post-analysis may then be required to decide whether xfeas is close enough to be feasible. The optional argument target sets a target value for tmin. The optimization code terminates as soon as a value of t below this target is reached. The default value is target $= 0$. Solver for LMI

feasibility problems $L(x) < R(x)$ This solver minimizes t subject to $L(x) < R(x) + t * I$ The best value of t should be negative for feasibility

A.5.2 Minimization of a Linear Objective w.r.t LMI Constraint

The minimization of linear objective (Trace) optimization subjected to LMI constraint used in this work is used to compute the H -infinity constrained SMO gains. In Matlab syntax, it uses:

$[copt, xopt] = mincx(lmisys, c, options, xinit, target)$

solves the convex program

minimize $c^T x$ subject to $N^T L(x) N \leq M^T R(x) M$

A.6 Supporting Lemmas

A.6.1 HJIE and Game Theoretic Approach to find G_o^* and ξ^* [2]

According to Theorem 3.1 in [2], considering the augmented system in Equation (11), if V is a continuously differentiable function that satisfies the general HJI equation, as given in Equation (50), is

$$\frac{-\partial V}{\partial t} = min_{u(t)}(H_o + \frac{\partial V}{\partial x}) f(x, u, t)$$

where $u(t)$ is the general input signal Using the cost functional H_o from Equation (24) in the above equation mentioned in (50) (in Appendix 9.5) and using the partial derivative property and

$$\frac{dV(x^*, t)}{dt} = \frac{\partial V(x^*, t)}{\partial t} + \frac{\partial V(x^*, t)}{\partial x^*} \frac{\partial x^*}{\partial t}$$

The HJI equation in this case becomes

$$\Rightarrow \frac{-\partial}{\partial t}V(x,t) = inf_{[G_o]}sup_{[\xi]}[\frac{-\partial V(x^*,t)}{\partial x^*}x^* + {r_K}^T r_K - \alpha\xi^T\xi] \tag{A.6.1}$$

then, by using the concepts of dynamic game theory, the cost functional in Equation (20) gives the pair of strategies (G_o^*, ξ^*) providing a saddle-point solution

$$H_o(G_o, \xi^*) \leq H_o(G_o^*, \xi^*) \leq H_o(G_o^*, \xi)$$

and furthermore, properly choosing the saddle-point value of the game

$$H_o(G_o^*, \xi^*) = V(e(*), *)$$

which ensures $H_o(G_o^*, \xi^*)V(e(*), *) = *$, and guarantees that G_o solves the disturbance attenuation problem (20)

Further, considering the Hamiltonian

$$H_o(G_o, \xi) = V_e\dot{e} + {r_K}^T r_K - \xi^T\xi \tag{A.6.2}$$

and using the derivative $\frac{\partial H_o(G_o, f)}{\partial f}|_{\xi=0} = 0$, G_o^* can be determined and using $\frac{\partial H_o(G_o^*, \xi)}{\partial G_o}|_{G_o=0} = 0$, the critical value of ξ^* can be determined, but this approach is not used in this study.

Remark: Considering the Lemmas 8, 9 in Appendix 9.5, using the HJIE in Equations (A4) and (55), the Hamiltonians in Equations (A5) and ((A7)) and disturbance attenuation/fault sensitivity constraints in Equations (24) and (35), the analytical solution for gain G_o will be dependent

on states, which is undesired (theoretically by Luenberger linear observer theory). However, the inequality version of HJIE will give more freedom in choosing the Lyapunov function $V(e,t)$ and hence more freedom in the design of the sliding mode observer gain G_o being state independent.

A.6.2 HJIE and Game Theoretic Approach to find G_o^* and f^* [2]

According to Theorem 3.2 in [2], considering the augmented system in Equation (11), if V is a continuously differentiable function that satisfies the general HJI Equation (50) mentioned in Appendix 9.5.

$$\frac{-\partial V}{\partial t} = min_{[u]}(H_o + \frac{\partial V}{\partial x})f(x,u,t)$$

Using the cost functional from Equation (35) in Equation (37) and using the partial derivative property

$$\frac{dV(x^*,t)}{dt} = \frac{\partial V(x^*,t)}{\partial t} + \frac{\partial V(x^*,t)}{\partial x^*}\frac{\partial x^*}{\partial t}$$

HJI in this case becomes

$$\Rightarrow \frac{-\partial}{\partial t}V(x,t) = max_{[G_o]}min_{[f]}[\frac{-\partial}{\partial x^*}V(x^*,t)\dot{x^*} + {r_K}^T r_K - \beta f^T f] \tag{A.6.3}$$

then, using the concepts of dynamic game theory, the cost functional in Equation (35) gives the pair of strategies (H^*, f^*) providing a saddle-point solution, i.e ,

$$H_o(G_o, f^*) \leq H_o(G_o^*, f^*) \leq H_o(G_o^*, f)$$

Furthermore, the saddle-point value of the game is

$$H_o(G_o^*, f^*) = V(e(*), *)$$

This ensures $H_o(G_o^*, f^*) \geq V(e(*), *) = 0$, which guarantees that G_o solves the minimum fault sensitivity problem in (35) Considering the Hamiltoman

$$H_n(G_o, f) = V_e\dot{e} + r_K{}^T r_K - f^T f \tag{A.6.4}$$

and using the derivative $\frac{\partial H_n(G_o, f)}{\partial f}|_{f=0} = 0$, G_o^* is determined, and using $\frac{\partial H(G_o^*, f)}{\partial G_o}|_{G_o=0} = 0$ the critical value of f^* is determined

A.6.3 Inequality Version of HJIE with $H\infty$ Constraint:

$$\int_0^t r^T r dt - \alpha^2 \int_0^t \xi^T \xi dt \geq 0$$

$$\int_0^t r^T r dt - \alpha^2 \int_0^t \xi^T \xi dt + V(x^*, t) \geq 0$$

$$\int_0^t r^T r dt - \alpha^2 \int_0^t \xi^T \xi dt + \int_0^t \frac{d}{dt} V(x^*, t) \geq 0$$

Since

$$\frac{dV(x^*, t)}{dt} = \frac{\partial V(x^*, t)}{\partial t} + \frac{\partial V(x^*, t)}{\partial x^*} \frac{\partial x^*}{\partial t}$$

The inequality version of the above equation is :

$$\frac{\partial V(x^*(t), t)}{\partial t} \geq \frac{-\partial V(x^*, t)}{\partial x^*} \dot{x}^* + r^T r - \alpha^2 \xi^T \xi$$

The disturbance attenuation problem is satisfied if:

$$inf)_{[G_o]} sup_{[\xi \neq 0]} H(G_o, \xi) \leq 0$$

Since (G_o^*, ξ^*) provides the saddle point

$$H(G_o, \xi) \leq H(G_o^*, \xi^*) \leq H(G_o^*, \xi)$$

$$H((G_o^*, \xi^*) = V(x^*, 0)$$

This will mean that $(G_o^*, \xi) \leq V(x^*, 0) = 0$, which guarantees that G_o^* will solve disturbance attenuation problem.

The SMO system will be dissipative if

$$\alpha^2 \|\xi^2\|_2 + \|r^2\|_2$$

if there exists a positive definite function Y which satisfies $\frac{\partial Y}{\partial t} + \frac{\partial Y}{\partial \epsilon}\dot{\epsilon} - \xi^T \xi + r^T r \leq 0$ and from the definition of dissipativity, it follows that

$$\|r^2\|_2 < \alpha^2 \|\xi^2\|_2$$

The problem can be studied in detail from [2, 33, 38]

A.6.4 Inequality Version of HJIE with H_∞ Constraint

Considering $V(x^*(t_1), t_1)$ with $V(x^*(0), 0) = 0$; the following inequality holds

$$\int_0^t r^T r dt - \beta^2 \int_0^t f^T f dt \geq 0$$

$$\int_0^t r^T r dt - \beta^2 \int_0^t f^T f dt + V(x^*(t), t) \geq 0$$

$$\int_0^t r^T r dt - \beta^2 \int_0^t f^T f dt + \int_0^t \frac{d}{dt} V(x^*(t), t) \geq 0$$

Since

$$\frac{dV(x^*, t)}{dt} = \frac{\partial V(x^*, t)}{\partial t} + \frac{\partial V(x^*, t)}{\partial x^*} \frac{\partial V(x^*)}{\partial t}$$

So the inequality version of this equation is.

$$\frac{-\partial V(x^*(t), t)}{\partial t} \leq \frac{\partial V(x^*, t)}{\partial x^*} \dot{x}^* + r^T r - \beta^2 f^T f$$

$$H(G_o, f^*) \leq H(G_o^*, f^*) \leq H(G_o^*, f)$$

Since (G_o^*, f^*) provides saddle point

$$H(G_o, f^*) \leq H(G_o^*, f^*) \leq H(G_o^*, f)$$

$$H((G_o^*, f^*) = V(x^*, 0)$$

This will mean that $(G_o^*, f) \leq V(x^*, 0) = 0$, which guarantees that G_o^* will solve the disturbance

attenuation problem

The problem can be studied in detail in [2, 33, 38]

A.7 Definitions

A.7.1 Riccati and Lyapunov Equation

The constrained vector algebraic equations, such as Riccati equations and the other similar ones arising from the LQR and LQG problems, (having their roots in optimal control) are often transformed into inequality versions. The inequality version is utilized to achieve better control on design parameter matrices and the factors, which are optimized using the convex optimization tools. It gets to determine unknown parameters including the SMO gains, and then ensures the stability as well. The Schur complement helps the constrained matrix inequalities and corresponding algebraic forms to be inconvertible Solving such equations is a vital step in designing such controllers and state estimators. For generally system matrices (A,B) and symmetric (parametric and Lyapunov) matrices (P,Q,R), the convex algebraic Riccati equation is given by

$$A^T P + PA + PBR^{-1}B^T P + Q < 0, P > 0, R > 0$$

where the term $PBR^{-1}B^T P$ is an additional quadratic term in basic Lyapunov equation, and is convex in nature. Its inequality version gives more design freedom to find the unknown parameter matrices in it to ensure stability and other required constraints. The determined unknown parameters, including the SM observer gains, would then ensure stability as well. The Schur complement helps the constrained matrix inequalities and corresponding algebraic forms

to be convertible to LMIs.

A.7.2 Hamiltonian

The Hamiltonian function gives a correct description of physical reality to make the connection between energy and rates of change. The Hamiltonian has dimensions of energy and represents the time evolution dynamics directly. So, it can be predicted what state the system will evolve into after an infinitesimal interval of time elapses. The Hamiltonian of the control theory from [2, 33] is used, which here comprises a sum of energy of the output error estimation, fault or disturbance signal, and product of Lyapunov function with rate of change of error vector, where Lyapunov matrix scaled energy of complete estimation error vector.

A.8 Clark, Park, and abc-dq0 Transformation

The abc-dq0 transformation is a combination of Park and Clark transformations and it is used to convert the three-phase voltages and currents to two-phase ones, to give a simplified system without loss of any information of the system, providing easy handling, transformations, and control of the system being of lesser dimensions.

If

$$Kc = \sqrt{2/3}\begin{bmatrix} 1 & -1/2 & -1/2 \\ \sqrt{3}/2 & \sqrt{3}/2 & -\sqrt{3}/2 \\ 1/\sqrt{2} & 1/\sqrt{2} & 1/\sqrt{2} \end{bmatrix}$$

The Clark transformation converts the ABC vector frame-to-frame. The transformation isolates a part of the ABC-reference vector that is common to all three parts of the vector. It is right-

handed, power invariant, and uniformly scaled. It is defined by:

$$\sqrt{2/3}\begin{bmatrix} 1 & -1/2 & -1/2 \\ \sqrt{3}/2 & \sqrt{3}/2 & -\sqrt{3}/2 \\ 1/\sqrt{2} & 1/\sqrt{2} & 1/\sqrt{2} \end{bmatrix}\begin{bmatrix} A \\ B \\ C \end{bmatrix} = \begin{bmatrix} \alpha \\ \beta \\ \gamma \end{bmatrix}$$

If

$$kp = \begin{bmatrix} cos\theta & sin\theta & 0 \\ -sin\theta & cos\theta & 0 \\ 0 & 0 & 1 \end{bmatrix}$$

The Park transformation rotates the reference frame of the vector at an arbitrary frequency. It shifts the frequency spectrum of the reference signal such that the arbitrary frequency serves as dc frequency, and the old dc appears as a negative of the arbitrary frequency. It is defined by:

$$\begin{bmatrix} cos\theta & sin\theta & 0 \\ -sin\theta & cos\theta & 0 \\ 0 & 0 & 1 \end{bmatrix}\begin{bmatrix} \alpha \\ \beta \\ \gamma \end{bmatrix} = \begin{bmatrix} d \\ q \\ 0 \end{bmatrix}$$

The abc-dq0 transformation is defined by:

$$\sqrt{2/3}\begin{bmatrix} cos\theta & cos(\theta - 2\pi/3) & cos(\theta + 2\pi/3) \\ sin\theta & sin(\theta - 2\pi/3) & -sin(\theta + 2\pi/3) \\ \sqrt{2}/2 & \sqrt{2}/2 & \sqrt{2}/2 \end{bmatrix}\begin{bmatrix} A \\ B \\ C \end{bmatrix} = \begin{bmatrix} d \\ q \\ 0 \end{bmatrix}$$

where the combined form of Clark and Park transformation is given by the matrix:

$$KcKp = \sqrt{2/3}\begin{bmatrix} cos\theta & cos(\theta - 2\pi/3) & cos(\theta + 2\pi/3) \\ -sin\theta & -sin(\theta - 2\pi/3) & -sin(\theta + 2\pi/3) \\ \sqrt{2}/2 & \sqrt{2}/2 & \sqrt{2}/2 \end{bmatrix}$$